Continuous Spaces of Low Dimensional Lattices

Thesis submitted in accordance with the requirements of the University of Liverpool for the degree of Doctor in Philosophy
by

Matthew Bright

September 2023

Dedication

The Open University is one of the UK's more unsung assets - without their expertise in building high quality undergraduate courses around complex adult lives it would not have been remotely possible for me to begin the journey which ended here.

I therefore dedicate this thesis to the OU in general, the tutors and support staff of its Mathematics department in particular, and to anyone, whatever their circumstances and whatever their subject, who is embarking on a journey into higher education in later life. It can be done.

We're remnants of a superb explosion
every step choreographed

by a universe so distant
so full of care.

from *galaxies and nothing at all* by Jazz Money

Acknowledgements

First and foremost, I would like to acknowledge the support of my supervisors. I began working with Professor Vitaliy Kurlin as an MSc student, and he has not only provided strong guidance throughout my postgraduate academic journey, but has also been concerned to involve me in a wide range of experiences of academic life, including the rare opportunity to spend a year teaching full time at the University which has cemented my interest in remaining in academia and pursuing a path that involves pedagogy as well as research. My secondary supervisor Professor Andy Cooper has provided a regular grounding in the physical and chemical realities which drive our mathematical work, and meetings with him have stimulated a lot of the empirical questions I have attempted to answer. For this final draft I would also like to thank my external examiners, Professors Marjorie Senechal and Gregory McColm, whose detailed reading of and commentary on my work has helped to improve it greatly - and my internal examiner Professor Leszek Gaseniec, for his support throughout these final steps of the process.

On a more personal level my family have been unfailingly supportive, even when my own enthusiasm has sometimes flagged. I have been lucky enough, also, to have good friends who helped me think through my decision to take the path I've taken, and to have made great new ones on that path who have inspired me professionally and personally. My oldest and closest friend, Professor John Le Quesne, has been there for me in ways large and small throughout my whole adult life. Various members and associates of the Kurlin group have provided productive avenues for both discussion and diversion - I will single out Dr Milo Torda, for his friendship, for his musical recommendations and in particular for choosing me during the COVID lockdowns as the temporary guardian of his cat, Hobbes, whose presence brightened that difficult period considerably. I would finally like to thank Dr Linda Amos, for reasons both personal and professional.

If your primary working tool is your brain, mental health is an essential hygiene factor. Without some alternative activity with which to forget entirely the intellectual and emotional intensities of research, one risks burnout and worse. To this end I would like to thank the various people who have gradually got me increasingly involved in Liverpool's musical community, and in particular the Oriel Singers, one of the city's oldest extant chamber choirs. Whatever else was happening, I was always singing on a Tuesday night.

Abstract

Crystal structures are typically classified discretely by their symmetry groups - however, given the huge growth in deposited crystal structures, and the ability of crystal structure prediction methods (CSP) to generate thousands of potential structures, many of which may be nearly identical in a geometric sense, for a given set of input molecules classification of this nature is potentially too coarse to allow careful exploration of the space of existing or potential structures. Our research aim is therefore to develop a *continuous* classification of periodic structures.

In this work we focus on the simplest of these structures- the two dimensional *lattice*, defined as the infinite set of integer combinations of a basis of $\mathbb{R}^2$. Our approach in this work is to consider any two lattices lattices identical if they are related by *isometry* - or, if we wish to distinguish such structures which are related by reflection, by a *rigid motion*. We seek to map any given lattice to some mathematical object which is the same for any pair of lattices related by these transformations, and different otherwise - a *complete invariant*. We want this invariant to vary continuously, in the mathematical sense, under perturbations of the lattice, such that we may map lattices to a *metric space* in which their geometric similarity may be rigorously compared.

The key contribution of this thesis is a full solution of this problem for two dimensional lattices and the development as a result of a visualisation of all possible lattice configurations as a compact space. We have implemented this solution and applied it to large datasets of actually existing lattices from the Cambridge Structural Database and elsewhere. To our knowledge the various maps shown in this thesis give the first visualisations of the set of real world periodic structures in a continuous space.

List of Publications

The work in this thesis is based on the following pair of published works.

1. Bright, M.J., Cooper A.I., Kurlin,V. (2023). Geographic-style maps of $2D$ lattices. *Acta Cryst A*, 79(1) pp 1-13

2. Bright, M.J., Cooper A.I., Kurlin,V. (2023). Continuous G-chiral distances for $2D$ Lattices, *Chirality*, 35(12) pp 920-936

The Python code necessary for efficiently generating two dimensional lattice invariants defined in this thesis, and for inverse computation of lattices from their invariants may be found at:

3. `https://github.com/MattB-242/Lattice_Invariance`

We close this thesis by discussing extension of our methodology to the three dimensional case. This work is currently incomplete - an early pre-print draft of our ideas can be found on arXiv:

4. Bright, M.J., Cooper A.I., Kurlin,V. (2021) A complete and continuous map of the Lattice Isometry Space for all 3-dimensional lattices.
   arXiv preprint at `https://arxiv.org/abs/2109.11538`

A number of alternative models of periodic structures were investigated and implemented by the author, leading to successful publications that did not contribute to the central research question discussed in the thesis itself. For the sake of completeness we list these below.

5. Bright, M.J., Kurlin,V. (2020). Encoding and Topological Computation on Textile Structures. *Computers and Graphics*, 90, pp. 51-61

6. Bright, M.J., Anosova, O., Kurlin,V. (2022). A Formula for the Linking Number in Terms of Isometry Invariants of Straight Line Segments *Computational Mathematics and Mathematical Physics*, 62(8) pp.1217-1233

Contents

List of Tables

List of Figures

Notation

Existing Notation Used in this Thesis

$(X, \sim)$ A Set X partitioned by the equivalence relation denoted by $\sim$
$\mathbb{R}^+$ The set of *non-negative* real numbers (including 0)
$|x|$ The absolute value of a real number
$\lfloor x \rceil$ The value of a real number rounded to the nearest integer
$\mathbb{R}^n$ The $n-$ dimensional vector space of tuples of real numbers
$L_q(x, y)$ The family of Minkowski metrics on $\mathbb{R}^n$, see Example 1.2.7
$||u - v||$ Distance between two vectors u, v in the L_2 Minkowski metric
$u \cdot v$ Inner product of two vectors u, v
$GL_n(\mathbb{R}), GL_n(\mathbb{Z})$ The set of linear transformations with nonzero determinant in $\mathbb{R}^n$ (resp. $\mathbb{Z}^n$)
$O_n(\mathbb{R}), O_n(\mathbb{Z})$ The *Orthogonal Group* of linear transformations in $\mathbb{R}^n$ (resp. $\mathbb{Z}^n$)
$SO_n(\mathbb{R}), SO_n(\mathbb{Z})$ The set of linear transformations with determinant $+1$ in $\mathbb{R}^n$ (resp. $\mathbb{Z}^n$) that have determinant ± 1 and preserve inner products
$\det A$ The determinant of the matrix A
Λ Any lattice, as defined in Definition 1.3.1
$\Lambda/p\Lambda$ Quotient lattice (Definition 3.2.7)
$V(\Lambda)$ The volume of a lattice Λ (Definition 1.3.4)
$Q(x_1, \ldots x_n)$ Quadratic form in n variables (Definition 2.1.1)
$\theta(\Lambda)$ Theta series of a lattice (Definition 2.3.1)
v_i^2, v_{ij}^2 Lattice Vonorm (Definition 3.3.1)
p_{ij} Lattice Coform (Definition 3.3.1)
r_{ij} Lattice Root Product (Definition 3.3.3)

Notation Defined in this Thesis

LIS Lattice isometry invariance space (Definition 1.3.11)
LIS^o Orientation-aware lattice isometry invariance space (Definition 1.3.11)
$\mathrm{RI}(\Lambda)$ Root Invariant (Definition 3.3.3)
$sign(\Lambda)$ The sign of a lattice (Definition 3.3.7)
$\mathrm{RI}^o(\Lambda)$ The orientation-aware Root Invariant (Definition 3.3.7)
σ The size of the lattice Λ (Defnition 3.3.12)
$\mathrm{PI}(\Lambda), \mathrm{PI}^o(\Lambda)$ Orientation-unaware and orientation-aware projected invariant (Definition 3.3.14)
$\mathrm{SIM}, \mathrm{SIM}^o$ (Orientation aware) superbase isometry metric (Definition 3.3.18)
$\mathrm{SSM}, \mathrm{SSM}^o$ (Orientation-aware) superbase similarity metric (Definition 3.3.18)
$\mathrm{OSI}, \mathrm{OSI}^o$ (Orientation aware) superbase isometry space (Definition 3.3.18)
$\mathrm{RIS}, \mathrm{RIS}^o$ (Orientation aware) Root Invariant Space (Definition 3.3.22
TC Triangular Cone visualisation of RIS (Definition 3.4.1)
∂^i_{TC} ith boundary of the TC (Definition 3.4.1)
DC Doubled Cone visualisation of RIS^o (Definition 3.4.2)
∂^i_{DC} ith boundary of the DC (Definition 3.4.2)
QT Quotient Triangle visualisation of projected invariant (Definition 3.3.14)
∂^i_{QT} ith boundary of the QT (Definition 3.3.14)
QS Quotient Square visualisation of orientation-aware projected invariant (Definition 3.4.5)
∂^i_{QS} ith boundary of the QS (Definition 3.4.5)
$\mathrm{SPI}(\Lambda)$ Spherical Projected Invariant of a lattice (Definition 3.4.6)
$\mu(\Lambda))$ Longitude of the SPI of a lattice
$\varphi(\Lambda)$ Latitude of the SPI of a lattice
$\mathrm{RM}_q, \mathrm{PM}_q$ Root and Projected Metrics induced by the L_q distance (Definition 4.3.1)
$\mathrm{RM}^o_q, \mathrm{PM}^o_q$ Orientation-aware Root and Projected Metrics induced by the L_q distance (Definition 4.3.3)
$\mathrm{RC}_2[G]$ Root G-chiral distance (Definition 4.4.1)
$\mathrm{PC}_2[G]$ Projected G-chiral distance (Definition 4.4.1)
SRM Spherical Root Metric (Definition 4.3.11)
SPM Spherical Projected Metric (Definition 4.3.11)
$\mathrm{SRC}[G]$ Spherical Root G-chiral distance (Definition 4.4.3)
$\mathrm{SPC}[G]$ Spherical Projected G-chiral distance (Definition 4.4.3)

Chapter 1

Introduction

The aim of this first chapter of the thesis is to formalise the research problem that we address. It is divided into four sections. The first discusses the general motivation behind our research approach and states our goal in an informal sense, the second states the basic mathematical tools that we use in that approach, and the final section applies those tools to the mathematical objects under consideration, closing with a formalised statement of the research aim which applies specifically to those objects.

1.1 Motivation: Exploring Structural Space

The work in this thesis is motivated by the explosive growth in the number of structures of solid crystalline materials available in recent years. Even before the tools to fully understand their structure were built, crystals were being used as detectors of EM radiation [5], and indeed it was that property, applied to X-rays, that led to the discovery of the key methodology for understanding their structure [6]. This in turn has led to a growing understanding of how the periodic nature of crystal structures can give rise to their physical properties, resulting in their widespread employment in the generation of solar power [7], for the storage of energy [8]] and for carbon capture [9], among a plethora of other applications.

The increasing accuracy and effectiveness of structure determination methods, and the analysis of their output to determine the atomic structure of a material means that that the determination of crystal structures has become a routine element not just of materials science, but also of the biosciences, where the Protein Data Bank [10] currently holds structural data on $200,000$ biomolecules, with over $10,000$ new structures deposited in any given year.

Beyond this growing repository of experimentally determined structures, improvements in computing power allow for sufficiently accurate simulation of the atomic forces both within and between molecules [11] to explore the possible crystal structures that those molecules may form entirely *in silico*. This approach to Crystal Structure Prediction (CSP), is computationally expensive and relies on a random sampling of initial configurations from which the simulation can develop. It can give rise to tens of thousands of potential structures (see for example [12]).

As a result, several large and growing databases of both real and simulated structures now exist - as well as the aforementioned Protein Data Bank, the Crystallography Open Database [13] holds over half a million crystal structures ranging across many types of molecule, while the Inorganic Crystal Structure Database (ICSD) [14] contains nearly $300,000$ entries which are a mixture of both real and simulated structures. The c.$170,000$ structures in the Materials Project [15], by contrast, are entirely simulated.

In this thesis we use as a test dataset the Cambridge Structural Database (informally known as the CSD) [16], which largely contains crystals derived from organic molecules and which as of the current time of writing contains 1.2 million deposited CIF files (the standard format for crystallographic structural data [17]), ranging from simple to extremely complex arrangements of organic and inorganic molecules (see Figure 1.1).

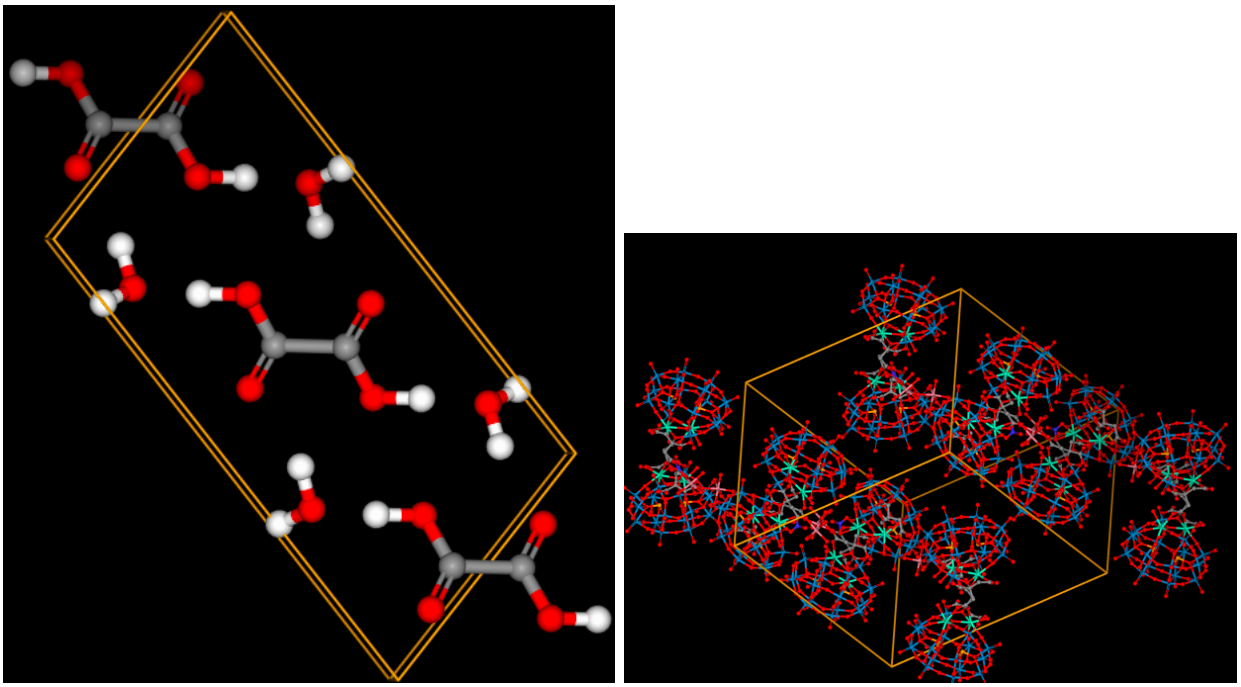

Figure 1.1: Diversity of structures deposited in the CSD. **Left**: one of multiple depositions of the structure of Oxalic Acid crystals with a water solvent- a simple organic molecule used in the testing of structure determination. **Right**: Complex crystalline structure formed of rare earth metals bound to small organic molecules in a ribbon formation [1].

In CSP, many simulated structures can immediately be ruled out by looking at the modelled values of global structural properties such as lattice density and energy and excluding anything known to be unphysical - for example, with lattice energies too high to be compatible with stability under feasible physical conditions, and densities (in terms of atomic mass per unit cell of the lattice) above those normally observed in solid state material [2] (see Figure 1.2). A harder problem is identifying (in an informal sense) genuinely 'different' structures among the remaining data from those related by just a small geometric perturbation of the structure (e.g. a small rotation about a bond).

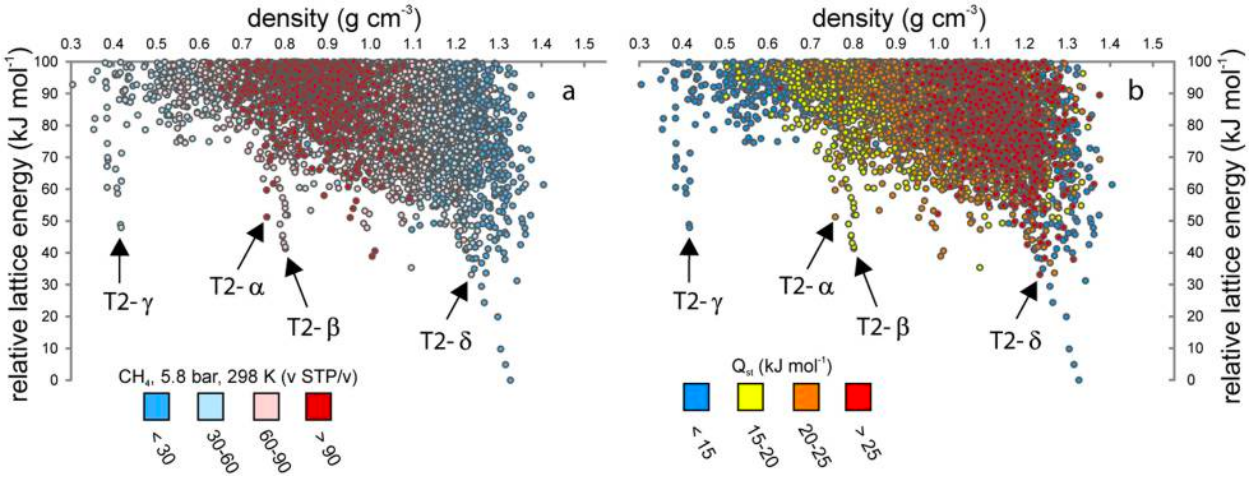

Figure 1.2: Energy/density maps for thousands of simulated crystalline structures of a simulated molecule, taken from [2]. Marked structures have been successfully synthesised.

The extent to which CSP explores all possible - or indeed physically feasible - solid state periodic structures that a molecule could form is unknown, as is the larger question of whether the millions of existing structures represent a full exploration of *all* possible configurations, or whether they are confined to some particular subset of them. Indeed, this informally posed question leads us to consider what a rigorous 'exploration of structures' might mean. In the late 19th century Dimitri Mendeleev noted that certain groups of atomic elements had shared physical properties which suggested an informative spatial arrangement - a positioning of each element in a two dimensional plane such that elements sharing chemical properties occupy the same column (that is, have the same x co-ordinate). The resulting *periodic table of elements* persists to this day as the primary organising principle of the totality of the chemical elements. In highlighting 'gaps' where predicted elements with certain properties should exist, and in driving the search for physical reasons that elements might share particular properties, the key insight that using a spatial arrangement to classify materials can create a framework for explanation and discovery has driven significant advances in physics, chemistry and materials science.

The overall aim of our research is to contribute to the development of a similar spatial arrangement for periodic structures, greatly simplifying the search for model materials with desired properties and providing a tool for designing structures with specific geometries (for example, large pores for gas absorption). To do this with effective mathematical rigour, we will need to work with an idealised model of crystal structures. The representation of molecular and crystal structures has been driven to some extent by the need to use these structures as inputs to machine learning models - see [18] for a recent example. They include to some extent aspects of the physical modelling of molecular structures, in particular the forces governing atomic interactions. A recent review of these approaches can be found in [19] - this illustrates that the mathematics which ensures that such representations are invariant under transformations which are known not to affect the physics of atomic interactions (including the *isometries* defined formally later in this chapter) can become quite complex. Many such representations are also best adapted to finite molecular structures and in the periodic setting are approximated by simply choosing an arbitrary cut-off radius beyond which interatomic forces from the structure are not computed.

The notion of a *periodic graph* [20] abstracts away the physics of atomic interactions completely and represents atoms and their interactions as a purely topological object: the nodes and edges, respectively, of a graph. Periodicity can be accurately represented by appropriate edge labelling and atom identities (if required) by the labelling of nodes. This representation still captures a large amount of structural information, and allows for rigorous investigations of a crystal structure's topology via well-developed software tools such as TopCryst [21]. However, in this case comparison of structures for similarity is equivalent to deciding whether or not two (potentially labelled) graphs have the same topological structure. Algorithms which efficiently solve this *graph isomorphism problem* remain an open problem (see [22] for a recent overview).

A further simplification - the one employed in our research - is to ignore any information about bonds, and not to incorporate any physical modelling at all into our view of periodic structures. Our general model for a crystal is the *periodic point set* defined below and illustrated with an example in figure 1.3:

Definition 1.1.1 (see for example [23], Section 1)**.** *Given a linearly independent* $\{v_1, \dots v_n\}$ *in* $\mathbb{R}^n$*, the* lattice *is the set*

$$\Lambda = \left\{ x : x = \sum_{i=1}^{n} a_i v_i, a_i \in \mathbb{Z} \right\}$$

of all integer combinations of the basis vectors. A motif *is a set of points*

$$M = \left\{ p_1, \dots p_k : p_i = \sum_{i=1}^{n} c_i v_i, c_i \in [0,1] \right\}$$

finite in number and lying within, or on the boundaries, of the closed parallelepiped determined by the basis vectors.

A periodic point set *is the* Minkowski sum *of* $\Lambda + M$ *- that is, the infinite discrete set of points given by applying translations of the points in* M *by the vectors in* Λ.

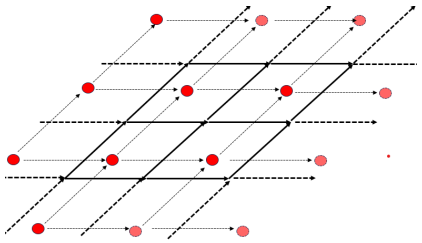

Figure 1.3: A periodic point set consisting of Minkowski sum of the lattice generated by $v_1 = (1, 0), v_2 = (0.3, 0.7)$ (thick black lines) with a motif consisting of a single point $p_1 = (0.3, 0.2)$ (the red dot)

Our justification in choosing this simplified representation of chemical structures is founded in the *crystal isometry principle* (CRISP) discussed in Section 7 of [23]. If an atom of an element in a crystal or molecular structure is replaced by one of a different element, the geometry of the structure will always be perturbed to some extent, since any interatomic forces governed by the replaced atom will not be identical. Several complete characterisations of periodic point sets of this nature exist for different applications. A recent development for general periodic point sets is the continuous Pointwise Distance Distributions ([24], Definition 3.3) which has detected unexpected duplicates in the CSD and which has been used to predict new materials [25].

In this thesis, we will develop and apply an approach to exploring the space of simpler structures - periodic *lattices* - essentially crystalline structures where the motif consists of a single atom. The study of lattices as mathematical objects has spanned centuries. Quite apart from their inherent geometric interest, they have links to mathematical fields as disparate as number theory [26] and cryptography [27] - see [28] for a thorough overview of the many topics where lattices have played a part and [29] for a comprehensive introduction to the surprisingly subtle and complex mathematics that arise from these apparently simple structures.

For the rest of this chapter we will develop the formal mathematical machinery involved in determining whether any two objects - whether geometric structures like lattices or more complex mathematical entities, are 'the same', and if they are different formally quantifying 'how different' they are. We will give formal and rigorous definitions of these high level concepts ,which will allow us to close the chapter by posing the question outlined informally above in more formal, rigorous manner which allows us to make mathematical progress in answering it.

In Chapter 2 we will provide a general survey on past work in the categorisation of lattices and attempts to quantify lattice similarity. Chapters 3 and 4 represent the key contributions of this thesis. In Chapter 3 we will go into further detail of our approach for two dimensional lattices, resulting in a development of the first known *isometry invariant* for these simple structures, which is the key step on the path to situating them in an explorable space. Even in two dimensions the non-trivial nature of the mathematics behind this is clear. Having implemented the algorithm for computing the invariant, we demonstrate its power by applying it to a very large database of lattices generated from the CSD, giving

the first continuous map of real-world periodic structures. In Chapter 4 we actually use this invariant not only to situate two dimensional lattices in a *metric space*, but to develop *continuous chirality distances* - essentially quantifying 'how asymmetric' a two dimensional lattice is. Again, the code for computing these distances is implemented, and we apply it both to the large CSD lattice database and two publicly available databases of monolayer materials. Finally in Chapter 5 we discuss the implications of our work and potential future directions.

1.2 Invariance, Metric Spaces and Isometry

The question of how to determine when any two crystal structures are the same or different is one that involves surprising subtleties -indeed it remains a subject of active discussion in mathematical crystallography [30]. One way to address the challenge is to adhere to some formally rigorous mathematical notion of 'sameness', which we define below.

Definition 1.2.1 (Equivalence)**.** *An* equivalence relation $\sim$ *on a set* X *is a binary relation between pairs of objects in the set satisfying the following axioms:*

1. Identity*:* $x \sim x$ *for all* $x, \in X$
2. Symmetry*:* $x \sim y \iff y \sim x$ *for all* $x, y \in X$
3. Transitivity*:* $x \sim y, y \sim z \implies x \sim z$ *for all* $x, y, z \in Y$*.*

The usefulness of an equivalence relation is that it separates objects in the set into discrete non-disjoint *equivalence classes* - any $x \in X$ is in one unique discrete class. This follows directly from the transitivity axiom: if some object x is in the intersection of classes $Y, Z, \subset X$ then $y \sim x$ for all $y \in Y$ and $x \sim z$ for all $z \in Z$ implies $y \sim z$ or all $y \in Y, z \in Z$.

We illustrate this principle with a classical example::

Example 1.2.2. *Let* d *be an integer, and for integers* z_1, z_2*. If the remainder of* z_1 *when divided by* d *is the same as the remainder of* z_2 *is divided by* d *- that is, if* $z_1 = r + qd$ *and* $z_2 = r + q'd$ *for integers* r, q, q'*, then we write* $z_1 \equiv z_2 \mod d$*.*

This is clearly an equivalence relation - identity is obvious since if $z_1 = z_2$ *then* $q = q'$ *while symmetry and transitivity arise directly from the definition. The relation partitions the integers into a set of* d *distinct classes.*

Often equivalence relations can be defined in ways which do not make it immediately explicit whether or not any two objects are the same. An *invariant* is a mathematical tool for probing the equivalence classes of a set.

Definition 1.2.3 (Invariant)**.** *Let* $(X, \sim)$ *be a set* X *partitioned by the equivalence relation* $\sim$ *and* Y *be some arbitrary set. An* invariant *on* X *is some function* $I : X \to Y$*, such that for any* $x, y \in X, x \sim y \implies I(x) = I(y)$*. An invariant is* complete *if the converse relation also holds.*

A function f_d which maps any integer to its remainder f when divided by d is, for example, a complete invariant of the equivalence relation of Example 1.2.2 by definition.

If we are interesting in comparing equivalence classes then ideally the set Y is equipped with some additional mathematical structure which allows for such comparisons - for example, a *metric*. A set equipped with a metric is a *metric space*.

Definition 1.2.4 (Metric Space)**.** *A* metric space *is a pair (X, d) where X is a set and $d : X \times X \to \mathbb{R}^+$ is a function from pairs of elements of the set to the non-negative real numbers satisfying the following axioms:*

1. Identity*: $d(x, y) = 0$ if and only if $x = y$*
2. Symmetry*: $d(x, y) = d(y, x)$ for all $x, y \in X$*
3. Triangle Inequality*: For all $x, y, z \in X$, $d(x, z) \leq d(x, y) + d(y, z)$.*

The axioms replicate the behaviour of the familiar straight line distance between objects in the plane as illustrated in Figure 1.4.

The simplest example of a metric space is given by the *discrete metric*:

Example 1.2.5 (Discrete Metric)**.** *For any set X, define $d : X \times X \to \mathbb{R}^+$ as follows:*

$$d_0(x, y) = \begin{cases} 0 & x = y \\ 1 & x \neq y \end{cases}$$

Satisfaction of the identity axiom is immediate from the definition, symmetry is guaranteed by the symmetric nature of the equality relation, while the triangle inequality can be verified simply by computing all possible cases.

Metrics can however be defined on any sort of set

Example 1.2.6 (Hamming)**.** *Let B_n be the set of all binary sequences of length n (for example $101 \in B_3$). The* Hamming distance *d_H between any two such sequences in the set is given by the number of positions in which they differ - again, as an example $d_H(101, 011) = 2$.*

The identity and symmetry axioms arise obviously from the definition, and as with the discrete metric the triangle inequality is easily checked by considering the limited number of possible cases that can arise at each position in any three sequences.

Obviously, the discrete metric is not particularly useful if we wish to use a metric as a criterion to determine the similarity of objects in a set, and the Hamming distance applies only to a specific set of objects which are not the topic of this thesis. A more practical example, and the one used throughout this thesis, is defined specifically on $\mathbb{R}^n$:

Example 1.2.7 (Minkowski Metrics)**.** *For two vectors $u = (u_1, \dots u_n), v = (v_1, \dots v_n) \in \mathbb{R}^n$ and $q \in \mathbb{N}$, define the q-Minkowski metric $L_q : \mathbb{R}^n \times \mathbb{R}^n \to \mathbb{R}^+$ as:*

$$L_q(x, y) = \left(\sum_{i=1}^{n} |v_i - u_i|^q \right)^{\frac{1}{q}}$$

For $q = \infty$ we formally define the Chebyshev metric

$$L_\infty = \max_{i \in \{1, \dots n\}} |v_i - u_i|$$

Let $u = (3, 0), v = (0, 4)$ be two vectors in $\mathbb{R}^2$, then

$$L_2(u, v) = \sqrt{(-3)^2 + 4^2} = 5.$$

We may similarly compute $L_1(u, v) = 7$ and $L_\infty(u, v) = 4$.

The satisfication of metric axioms for Minkowski metrics is a classical result, with the triangle inequality following from Cauchy's inequality. Clearly for $q = 2$ we have recovered the standard Euclidean distance in the plane illustrated in Figure 1.4, and indeed Minkowski developed this formulation as the sort of generalisation of the Euclidean notion of distance required to handle computations in special relativity.

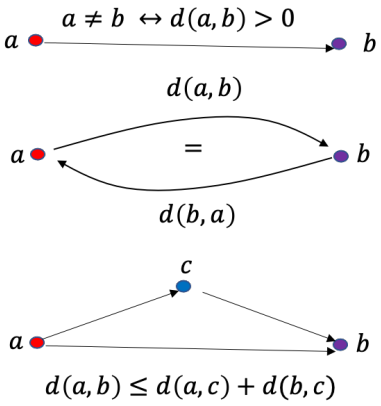

Figure 1.4: The metric axioms for straight line distances in the plane

Definition 1.2.8 (Isometry on a general metric space)**.** *Let (X, d), $(Y.d')$ be metric spaces and $f : X \to Y$ a function between them. The function f is an* isometry *if it preserves the metric structure of the space - that is, for all $x, y \in X$, $d(x, y) = d'(f(x), f(y))$.*

Example 1.2.9. *For any vector in $\mathbb{R}_2$ equipped with any of the Minkowski metrics, let $t_\uparrow$ be the function such that for $u = (u_1, u_2)$, $t_\uparrow(u) = (u_1, u_2 + 1)$. Since for any pair of vectors u, v*

$$v_1 - u_1 + v_2 - u_2 = v_1 - u_1 + v_2 + 1 - u_2 - 1,$$

the map $t_\uparrow$ is an isometry

One key concept we will discuss throughout this thesis is *continuity*. There are many formal definitions of continuity that apply in different circumstances, but all of them capture the fundamental notion that if we have some function $f : X \to Y$ between metric spaces then a small perturbation of some $x \in X$ should results in a small (or at least bounded) perturbation in the value of $f(x) \in Y$. In relation to the spaces and metrics we are using the following formal definition is particularly relevant:

Definition 1.2.10 (Hölder continuity)**.** *Let (X, d) be a metric space and $f : (X, d) \to (Y, d')$ a map to another metric space. The map f is* Hölder continuous *if whenever $d(x, y) = \delta$, $d'(f(x), f(y)) \leq C\delta^\alpha$ for some real-valued constants $C, \alpha > 0$.*

1.3 Lattices

We now define the objects to which we will apply these mathematical ideas - as mentioned in the previous section these are the periodic point sets of Definition 1.1.1 with just a single point in the motif. However, since we may without loss of generality place this point at the origin of $\mathbb{R}^n$ it is clearer to do away with the notion of motif in the definition altogether.

Definition 1.3.1 (Lattice Λ, Unit Cell U)**.** *Let $B = \{v_1, \dots v_k\}$ be a set of linearly independent vectors in $\mathbb{R}^n, k \leq n$. The* lattice $\Lambda(B)$ generated *by B is the set of all integer combinations of vectors in B:*

$$\Lambda(B) = \left\{ \sum_{i=1}^{k} a_i v_i | a_i \in \mathbb{Z} \right\}$$

The value k is the rank *of the lattice in $\mathbb{R}^n$. The lattice is of* full rank *if $k = n$.*

The parallelipiped enclosed by the vectors $v_1, \dots v_k$, given by the set of vectors

$$U = \left\{ \sum_{i=1}^{k} c_i v_i | c_i \in [0, 1] \right\}$$

is a primitive unit cell *of the lattice*

The following notational and terminological conventions relating to lattices will be used throughout this thesis:

- All lattices are of full rank unless otherwise stated.
- Unless we are comparing two bases of a lattice, the presence of a basis will be assumed - we will use Λ rather than $\Lambda(B)$ to denote a general lattice.
- Since we may equally consider a lattice as a discrete periodic point set with a single point or an infinite set of lattice vectors that translate that point from the origin, for ease of readability we will not distinguish between the two. A lattice vector will be denoted by v rather than using strict notation such as $\vec{v}$ or $\mathbf{v}$.
- Unless otherwise stated, $\mathbb{R}^n$ is equipped with the L_2 metric as given in Example 1.2.7 and the standard inner product $u \cdot v$. The distance between two vectors u, v denoted by $||u - v|| := \sqrt{(u - v) \cdot (u - v)}$, and the Euclidean length of a particular vector will be given by $||v|| := \sqrt{v \cdot v}$.
- When referring to isometry-invariant parameters of a lattice (lengths and angles) we will adopt crystallographic conventions. In three dimensions the lengths of vectors are given a, b, c. The angle between a and b is denoted by γ, between a and c by β and between b and c by α. For two dimensional lattices we will use vector lengths a, b and angle γ.

From the general notion of isometry in Definition 1.2.8, we may construct a specific definition in the lattice case, which allows us to distinguish two specific types of lattice transformation which will be important in later sections of the thesis.

Definition 1.3.2 (Lattice isometry, rigid motion)**.** *Let Λ be a lattice in $\mathbb{R}^n$. A* lattice isometry *is a function $f : \mathbb{R}^n \to \mathbb{R}^n$ such that for any pair of vectors u, v in Λ, $|u - v| = |f(u) - f(v)|$.*

Two lattices Λ, Λ' are isometric *if they are related by an isometry - we write $\Lambda \simeq \Lambda$. They are related by a* rigid motion *if there is a continuous family of functions $f_t, t \in [0, 1]$ such that $f_0 = \Lambda$, $f_1 = \Lambda'$ and f_t is an isometry for all t.*

A rigid motion is any combination of translations and rotations, while isometry also allows refections. Figure 1.5 shows a two dimensional example of lattices related by isometries and rigid motions.

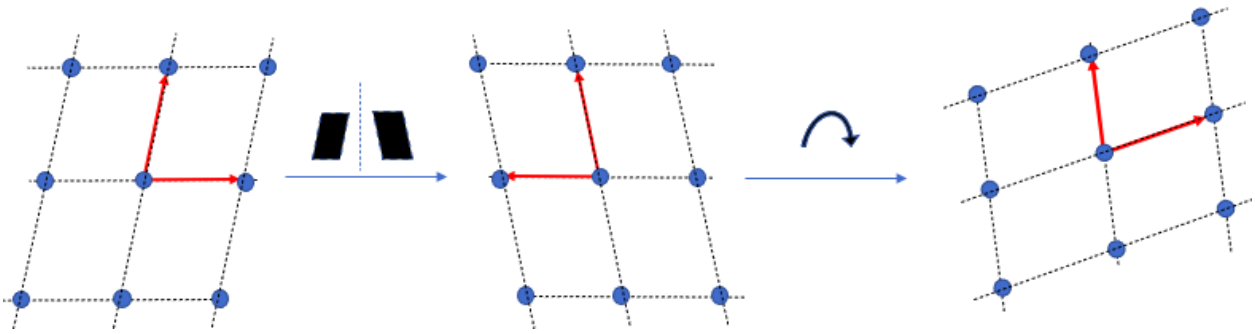

Figure 1.5: Illustration of isometries and rigid motions. The third lattice is related to the second by a rigid motion (a rotation) but to the first only by an isometry, since a reflection is required.

Since an isometry is a linear transformation of the basis vectors, we may consider it in terms of the group of such linear transformations in $\mathbb{R}^n$.

Definition 1.3.3 (Matrix Groups GL_n, O_n, SO_n)**.** *The* general linear group *of real-valued linear transformations $GL_n(\mathbb{R})$ is the group (under matrix multiplication) of real valued $n \times n$ matrices with nonzero determinant. The subgroup $O_n(\mathbb{R})$ is the* orthogonal group *of real valued linear transformations which have determinant ± 1, and which preserve inner products between all vectors. The* special orthogonal group *$SO_n(\mathbb{R})$ is the subgroup of those matrices with determinant 1.*

The fact that these are indeed groups is obvious from the property $\det(AB) = \det A \det B$ for any matrices A, B, the fact that linear transformations are composed by matrix multiplication and the invertibility of any matrix if its determinant is nonzero. We may similarly define groups $GL_n(\mathbb{Z}), O_n(\mathbb{Z})$ and $SO_n(\mathbb{Z})$ for the integers. An isometry is then any application of an element of $O_n(\mathbb{R})$ to the lattice, and a rigid motion the application of an element from $SO_n(\mathbb{R})$ only.

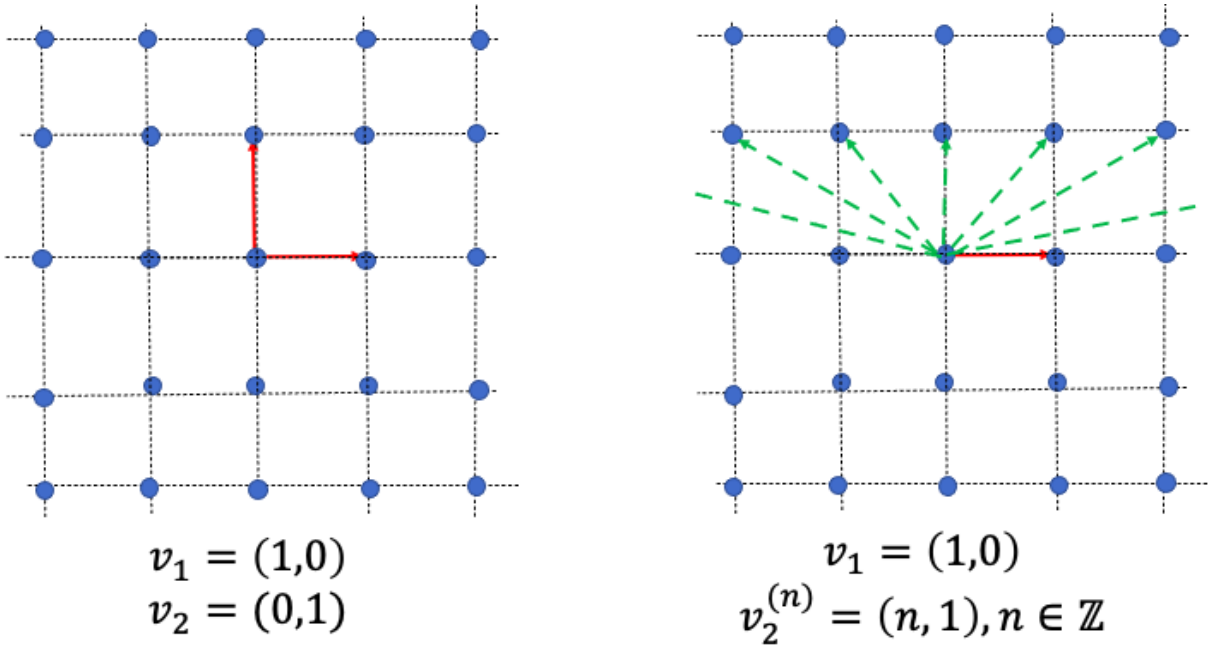

Figure 1.6: Multiple alternate basis choices for the square lattice generated by the basis $v_1 = (1, 0), v_2 = (0, 1)$.

Since $\det(A)^{-1}(A) = 1/\det(A)$ the only invertible matrices in $\mathrm{GL}_n(\mathbb{Z})$ with inverses have determinant ± 1, and so in fact $\mathrm{GL}_n(\mathbb{Z}) = O_n(\mathbb{Z})$, and the only proper subgroup is $\mathrm{SO}_n(\mathbb{Z})$.

From this it follows that isometry and rigid motions are equivalence relations on the set of lattices - the identity matrix is in both the orthogonal and special orthogonal groups, the inverse of any matrix in each group exists and has determinant ± 1, or determinant 1 in the case of $SO_n(\mathbb{R})$.

We have been careful to speak of 'a' unit cell because the choice of cell is not unique. If we consider for example the simple square two dimensional lattice given by $v_1 = (1, 0), v_2 = (0, 1)$ then the same lattice could be generated by a basis given by $v_1 = (1, 0), v_2^{(n)} = (n, 1)$ for any $n \in \mathbb{Z}$. As with isometry and rigid motion, we may express this change of basis in terms of a linear transformation represented by the matrix $\begin{pmatrix} 1 & n \\ 0 & 1 \end{pmatrix}$. Indeed, any basis transformation in the group $GL_n(\mathbb{Z})$ of integer matrices with determinant 1 gives the same lattice, as illustrated in Figure 1.6.

A transformation of this nature is not an isometry of the lattice *basis*, which we can see by noting that $||v_2^{(k)}|| \neq ||v_2^{(k+1)}||$ in the above family of bases for the square lattice. It is, however, an isometry of the *lattice* in the sense of definition 1.3.2, since the distance between any pair of points remains the same. A simple invariant which addresses all isometries is the *volume*.

Definition 1.3.4 (Lattice volume $V(\Lambda)$)**.** *The* volume $V(\Lambda)$ *of a two dimensional lattice is the absolute value of the determinant of the matrix whose columns are the vectors v_1, v_2 of a primitive unit cell.*

Example 1.3.5. *The lattice of figure 1.3 has volume*

$$\begin{vmatrix} 1 & 0.3 \\ 0 & 0.7 \end{vmatrix} = 1 \times 0.7 = 0.7$$

Since isometries and change of basis matrices have determinant ± 1, and transform the matrix of Definition 1.3.4 by multiplication, the volume is invariant under any isometry and any change of basis (including permutation of the basis vectors, which only changes the sign of a determinant). It is not, however, *complete* in the sense of Definition 1.2.3 - the lattices given by $v_1 = (2, 0), v_2 = (0, 2)$ and $v_1 = (1, 0), v_2 = (0, 4)$ are clearly non-isometric but have the same volume.

An appropriate choice of 'canonical' basis vectors is known as a lattice *reduction*. The choice of reduction is crucial to the results in this thesis, and the development of reduction theory (including the reason that 'reduction' is an appropriate description for a canonical basis choice) will be addressed in more detail in Chapter 2 . However, to understand the nature of the problem this thesis addresses we will in this chapter simply state an important example of a reduction specifically for two dimensional lattices, defined by Niggli in his foundational work on lattice geometry [31].

Definition 1.3.6 (Niggli Reduction for 2D Lattices)**.** *A basis v_1, v_2 of a two dimensional lattice is* reduced *if the following two inequalities hold:*

1. $||v_1|| \leq ||v_2||$
2. $-\frac{1}{2}||v_1|| \leq v_1 \cdot v_2 \leq 0$

Example 1.3.7. *The lattice in figure 1.3 is not described with a Niggli reduced basis since $||v_2|| \approx 0.76 < ||v_1||$ and $v_1 \cdot v_2 = 0.3 > 0$. However if we let $u_1 = v_2$ and $u_2 = -v_2 = (-1, 0)$ then $||v_1|| < ||v_2|| = 1$, $v_1 \cdot v_2 = -0.3$ and $-\frac{1}{2}||v_1|| \approx -0.38$ and all conditions are satisfied for Niggli reduction.*

This reduction gives a unique basis up to isometry in two dimensions, but *not* up to rigid motion. If the lattice basis is 'general' in terms of the reduction inequalities and (that is, $||v_1|| < ||v_2||$ and $v_1 \cdot v_2 < 0$) then the only two possible basis choices are $\pm v_1, \pm v_2$, which can be transformed into each other through a rotation of π about any lattice point. However, the two bases of a rectangular lattice given by $v_1 = (a, 0)$ and $v_2 = \pm(0, b)$ are both reduced, but can only be transformed into each other by reflection in the x axis.

If we are not interested in the scale of a lattice, but only its geometry, we may classify lattices up to a 'coarser' equivalence class as below:

Definition 1.3.8 (Lattice similarity)**.** *Two lattices Λ, Λ', generated by v_1, v_2 and u_1, u_2 respectively are* similar up to isometry (resp.rigid motion) *if for some $\lambda > 0 \in \mathbb{R}$ the lattice $\lambda\Lambda$ generated by $\lambda v_1, \lambda v_2$ is isometric to Λ' (resp. related to Λ' by rigid motion).*

Example 1.3.9. *The square lattice generated by $u_1 = (1, 0), u_2 = (0, 1)$ is isometric to the lattice*

$$u_1' = \left(\frac{1}{\sqrt{2}}, -\frac{1}{\sqrt{2}}\right), u_2' = \left(\frac{1}{\sqrt{2}}, \frac{1}{\sqrt{2}}\right)$$

since one can be derived from the other by a clockwise rotation of $45°$ about the origin.

The lattice of Figure 1.3 generated by the Niggli reduced basis $v_1 = (-1, 0), v_2 = (0.7, 0.3)$ is related to the lattice generated by the basis $v_1, v_2' = (0.7, -0.3)$ by an isometry, but they are not related by a similarity, since one may only be transformed into the other by a reflection in the y axis

In general, to avoid ugly and confusing grammatical constructions such as 'invariant up to similarity up to isometry', where it is clear that the non-scaling part of this relation is isometry or rigid motion, we will simply refer to 'similarity'.

If we wish to select a unique basis up to rigid motion we can, of course, add special conditions until we have dealt with every conceivable case (for example, one might additionally insist for a rectangular lattice as described above that $a, b > 0$). Ultimately if we want to classify lattices up to isometry (or rigid motion), a unique selection of basis vectors will give rise to a unique selection of isometry-invariant lattice parameters (lengths and angles) from which we may derive some quantity which allows for classification.

However, such a selection leads to an difficulty in describing the mathematical space of all possible lattices, even in two dimensions, as elegantly as we would like - we encounter the issue of *continuity*, as defined in Definition 1.2.10.

The reason we might be interested in a *continuous* deformation is encapsulated in the following proposition:

Proposition 1.3.10 (see for example Figure 1 in [32].)**.** *Any two lattices in different isometry classes (or classes up to rigid motion) can be continuously deformed into each other.*

Proof. Suppose Λ is generated by the basis $\{u_1, \dots u_n\}$ and Λ' by the basis $\{v_1, \dots v_n\}$. Since the two lattices are in their isometry class, we may assume that they are rotated so that u_1, v_1 share an axis and $u_1 = \lambda v_1$ for some $\lambda \in \mathbb{R}, \lambda > 0$.

We may continuously deform u_1 until its length matches v_1. For any $i \geq 2$ we can continuously rotate v_i until it is parallel to u_i and rescale it in the same way $\square$

This justifies formally defining the set of all lattices in any given dimension as a *space*:

Definition 1.3.11 (Lattice Isometry Space)**.** *The* lattice isometry invariance space $\mathrm{LIS}(\mathbb{R}^n)$ *is the space of all isometry classes of lattices of dimension* n*. The* orientation-aware lattice isometry invariance space $\mathrm{LIS}^o(\mathbb{R}^n)$ *is the space of all classes of lattices of dimension* n *equivalent under rigid motion.*

Where the dimension is either obvious from context or not relevant, we will omit the $\mathbb{R}^n$ for ease of reading and simply refer to LIS or LIS^o.

We may consider deriving an invariant from LIS by computing some quantity related to isometry invariant parameters of the reduced bases of a lattice - vector lengths or angles. However, the following counterexample illustrates how such an invariant may be discontinuous under a continuous deformation of the lattice itself.

Example 1.3.12 (Discontinuity of a Reduced Basis)**.** *Consider a family of lattices initially described by the basis vectors* $v_1 = (1, 0), v_2 = (t, 1)$ *for* $t \in [0, 1]$ *- the lattices where* $t = 0$ *and* $t = 1$*. Each lattice in this family is related to the other by a continuous deformation parameterised by* t*.*

At $t = 0$ *or* $t = 1$*. In the interval* $t \in (0, \frac{1}{2}]$ *the reduced basis vectors (in the reduction of Definition 1.3.6) are* v_1 *itself and* $u_2 = -v_2 = (-t, -1)$*. At* $t = 1/2$ *there is an ambiguity in that we may select* $u_2 = \pm v_2 = (-1/2, \pm 1)$*.*

However, for some small ε*, where* $t = \frac{1}{2} + \varepsilon$*, the reduced basis vector becomes* $u_2 = v_2 - v_1 = (t - 1, 1)$*.*

Figure 1.7 illustrates Example 1.3.12 - if I derive some isometry invariant $I(\Lambda)$ of the lattice purely from the isometry invariant parameters (lengths and angles) of its reduced basis, the value of that invariant will be subject to a discontinuity, even though the lattice itself is being deformed continuously.

1.4 Problem Statement

All of the above leads us to the specific problem that is addressed for 2 and 3 dimensional lattices in this thesis, and then applied to real materials databases.

Problem 1.4.1. *Find an invariant* $I(\Lambda)$ *of lattices up to basis change and isometry (or rigid motion) with the following properties:*

1. Completeness*: I should be a complete invariant in the sense of Definition 1.2.3.*
2. Metric Space*: I should map lattices to a space equipped with a metric obeying all axioms given in Definition 1.2.4.*
3. *Continuity: If two lattices* Λ, Λ' *differ from each other by a small geometric perturbation* δ*, then* $d(I(\Lambda), I(\Lambda')$ *should satisfy some formal continuity requirement as in Definition 1.2.10*

4. *Invertibility: It should be possible to recover* Λ *(up to isometry/rigid motion) from* $I(\Lambda)$.

5. *Computability: Both the computation of the invariant and its inverse should be achievable with modest resources, ideally via a direct analytic computation from the input lattice parameters.*

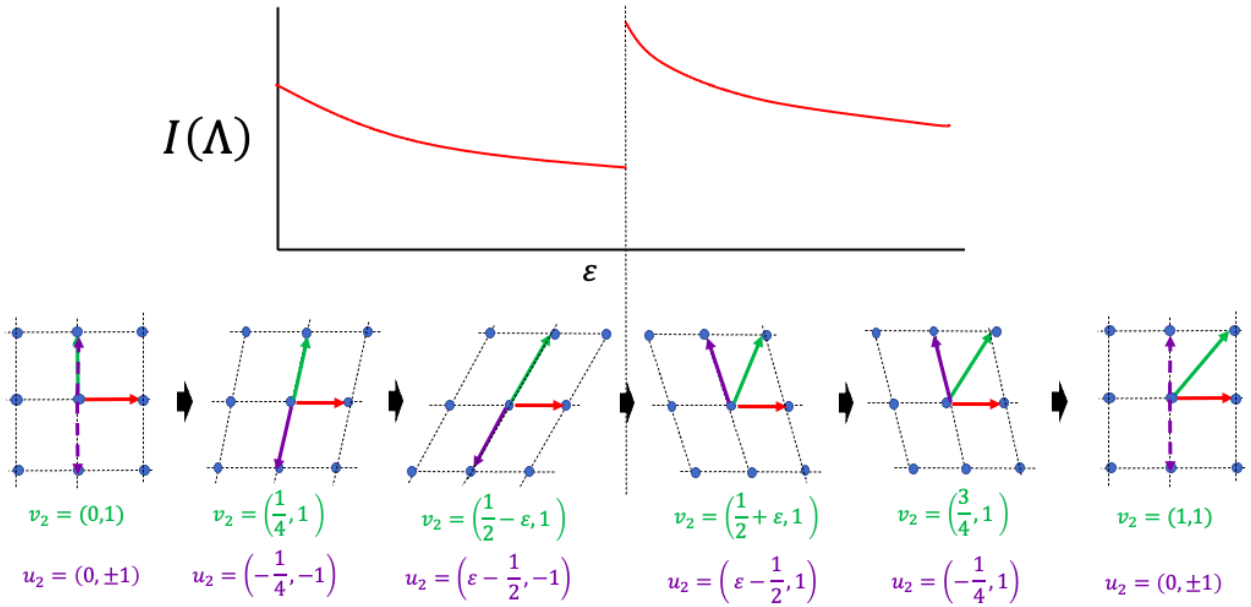

Figure 1.7: Reduced bases in the sense of Definition 1.3.6 of the family of lattices $v_1 = (1,0), v_2 = (t,1)$ for $t \in [0,1]$. For some small ϵ, v_2 continuously deforms from $(1/2-\epsilon,1)$ to $(1/2+\epsilon,1)$ there is a discontinuous change in the lattice basis.

One approach to Problem 1.4.1 is to consider lattices as a special case of the periodic point sets of Definition 1.1.1. The *density function* of such a set is described in [33], and an algorithm exists for its computation [34] which has been applied in the investigation of one-dimensional periodic structures [35, 36]. It is not, however, provably invertible. The *isoset* of a periodic point set [37], is provably a complete invariant, but is not easily computable.

Provided some canonical choice of unit cell can be made it is not difficult to find isometry invariants of lattices - any quantity constructed from the lengths of lattice vectors and the angles between them will suffice. Indeed, the volume of Definition 1.3.4 is one such invariant. However, it is certainly not complete in the sense of Definition 1.2.3 - one can make a continuous non-isometric deformation of a unit cell which preserves its volume.

The primary focus of this thesis is on lattices as the fundamental building blocks of crystallographic structures. Throughout this thesis, we will therefore focus on full rank lattices in 2 dimensions, although we will indicate where particular methodologies may apply more generally.

Chapter 2

Previous Work on Lattices

There has to our knowledge been no work which successfully addresses Problem 1.4.1 in its totality for lattices. A possible reason for this is that the study of lattices touches, as mentioned in Chapter 1, on disparate topics where some aspects of the problem - and indeed some types of lattice - have been more important than others. That range of topics also means that a complete survey of the mathematics of lattices would go far beyond the scope of the original research conducted in this thesis. In analysing past work , we will therefore concentrate on three different research areas which are particularly relevant to our own approach.

A canonical lattice basis is more commonly known as a *reduction* for reasons we will discuss below. The theory of lattice reductions has given rise to a selection of different but related approaches as well as a rich field of algorithmics dedicated to computing (or approximating) a particular reduction given an input set of lattice parameters or some arbitrary linearly independent basis in $\mathbb{R}^n$, which we will survey in section 2.1 of this chapter. Ultimately, as we will discuss in Chapter 3, we address the the problem of basis selection by picking a reduction which is not widely used in traditional crystallography, but which is algorithmically computable and from which continuous invariants which address Problem 1.4.1 can be derived.

The traditional approach to classification of lattices has focussed on at discrete symmetries of lattice geometry rather than isometry equivalence. This has given rise to the 'standard' crystallographic approach of distinguishing lattices by the set of non-translational symmetries (the 'crystallographic systems') as well as a number of finer and coarser classifications. In section 2.2 we will give details of this classification approach, and in particular the development of the Bravais types which are perhaps the best known discrete lattice classifications. In the development of the invariants and metrics discussed in Chapters 3 and 4, these discrete lattice classifications will arise as subspaces in the continuous lattice space.

Attempts to quantify lattice similarity via comparison of some quantity or set of quantities derived from lattice parameters have usually fallen short in some way from a solution to Problem 1.4.1 - typically the similarity fails to satisfy the metric axioms, or the invariant chosen is discontinuous with respect to the chosen canonical ('reduced') basis. In section 2.3 we will look at these attempts, highlighting the non-triviality of Problem 1.4.1 even for simple two dimensional lattices.

2.1 Lattice Bases and Reduction Algorithms

In this section, we consider some of the more widely used approaches to choosing a 'canonical' lattice basis from the infinite number of possible selection discussed in Chapter 1. We will focus in particular on the approaches most commonly used in mathematical crystallography. We will briefly mention the particular reduction we use for our own work at the end of this section, although it will be given a more thorough exposition in Chapter 3, where we prove various results which demonstrates its suitability for our purposes.

The description of a canonical lattice basis as 'reduced' comes from the fact that early work on the question was viewed as a particular kind of minimisation problem in number theory. It arose from the work of Gauss [38] and Lagrange [39] on *quadratic forms* (see Chapters 3 and 4 of [40] for a recent English language review).

Definition 2.1.1 (Quadratic Form)**.** *An n-ary integral* quadratic form *is a polynomial equation with integer coefficients in variables $x_1, \dots x_n$ where all terms are of degree two - that is, an equation of the form.*

$$Q(x_1, \dots x_n) = \sum_{i,j=1}^{n} a_{ij} x_i x_j$$

with all $a_{ij} \in \mathbb{Z}$. The form is positive *if for any n-tuple $p = (p_1, \dots p_n)$ of integers $Q(p) \geq 0$*

Two such quadratic forms Q_1, Q_2 can be considered equivalent if for all $p = (p_1, \dots p_n)$, $Q_1(p_n) = Q_2(p_n)$ - it is immediate that this is an equivalence relation in the formal sense of Definition 1.2.1. Both Lagrange and Gauss were interested in finding the particular form in each equivalence class that minimised the coefficients of $x_i x_j$. Lagrange in [39] proved the following result for a form of two variables x, y.

Theorem 2.1.2 (Reduced Quadratic Form)**.** *Let*

$$Q(x, y) = q_{11}x^2 + q_{12}xy + q_{22}y^2$$

be a positive integral binary quadratic form. Then there is a equivalent reduced *form Q' with coefficients $q'_{11}, q'_{12}, q'_{22}$ such that $0 < q_{11} \leq q_{22}$ and $-q'_{11} \leq q'_{12} \leq 0$. If Q is positive, then the reduced form is unique.*

Lagrange and Gauss considered this question to be of a purely number-theoretic nature, but its connection to the geometry of lattices can be expressed through the notion of the *Gram matrix*.

Definition 2.1.3 (Gram matrix)**.** *Let $v_1, \dots v_n$ be a linearly independent basis of $\mathbb{R}^n$. The* Gram matrix *of the basis is the matrix A whose entries are given by $a_{ij} = v_i \cdot v_j$.*

If the basis is being considered as generating a lattice, then its Gram matrix is sometimes referred to as the *metric tensor* of the lattice. The diagonal entries of the metric tensor are thus the squared lengths of lattice basis vectors, while the symmetry of the inner product (i.e. $v_i \cdot v_j = v_j \cdot v_i$) means that the matrix is symmetric about this diagonal.

Example 2.1.4. *The gram matrix of the Niggli reduced bases $v_1 = (0.3, 0.7), v_2' = (-1, 0)$ of figure 1.3 is* $\begin{pmatrix} 1 & -0.3 \\ -0.3 & 0.58 \end{pmatrix}$

Any $n \times n$ gram matrix A can be written as the quadratic form $x^T A x$ where $x = (x_1, \dots x_n)$ are the n variables of the form, resulting in the polynomial $\sum_{i=1}^{n} a_{ii} x_i^2 + 2 \sum_{i,j=1}^{n} a_{ij} x_{ij}$. If the Gram matrix is that of a lattice, then minimising the coefficients of this quadratic form is equivalent to finding basis vectors of that lattice which are both as short as possible (to minimise the a_{ii}) and as close to orthogonal as possible (that is, with minmial a_{ij}). The problem of finding short lattice vectors is thus strongly connected to the problem of finding minimal quadratic forms as defined by Gauss and Lagrange.

Definition 2.1.5 (Successive minima, Minkowski reduction)**.** *The* successive minima *of a lattice Λ of rank n are the lengths of the shortest vectors fully spanning the lattice - more formally, the lengths $\lambda_1, \dots \lambda_n$ of lattice vectors such that any vectors $v \in \Lambda$ such that $||v|| \leq \lambda_k$ span a lattice of rank k.*

A lattice basis consisting of vectors whose lengths are $\lambda_1, \dots \lambda_n$ is Minkowski reduced*.*

Example 2.1.6. *The lattice presented in Figure 1.3 with the basis given in its caption is Minkowski reduced. The alternative basis $v_1 = (1, 0), u_2 = v_2 - v_1 = (-0.7, 0.7)$ is not Minkowski reduced since $||u_2||^2 = 0.98 \leq ||v_2||^2$. Note that the alternative Niggli reduced bases for this lattice given in example 1.3.7 is also Minkowski reduced.*

In considering the possible lengths of the first minimum λ_1 (that is, the length of the shortest vector in any lattice) Hermite derived a lattice isometry invariant which he showed has an upper bound for all lattices of a particular dimension.

Theorem 2.1.7 ([41], p265)**.** *Let $\lambda_1(\Lambda)$ and $V(\Lambda)$ denote the first successive minimum and volume (see definition 1.3.4) of a lattice Λ of rank d .* Hermite's invariant *is given by:*

$$H(\Lambda) := \frac{\lambda_1(\Lambda)^2}{|V(\Lambda)|^{2/d}}$$

Hermite's Constant *is the maximal value of $H(\Lambda)$ over all lattices of rank d: $\gamma_d := \sup_{\Lambda \subset \mathbb{R}^d} H(\Lambda)$. This maximal value exists and has an upper bound:*

$$\gamma_d \leq \left(\frac{4}{3}\right)^{(d-1)/2}.$$

Precise values of Hermite's constant are known for dimensions 1 to 8 [42], and for dimension 24 [43]. In particular, $\gamma_2 = 2/\sqrt{3}$.

Example 2.1.8. *For the Minkowski reduced basis in example 2.1.6 of the lattice Λ in figure 1.3,*

$$H(\Lambda) = \frac{0.58}{0.7} \approx 0.83 < \frac{2}{\sqrt{3}} \approx 1.15$$

In dimensions 2 and 3, any set of 2 (resp. 3) non-parallel vectors which achieve the successive minima of the lattice also form a basis for that lattice. In four dimensions, however, this is no longer necessarily the case - the classical example being the lattice whose co-ordinates sum to an even number. This lattice can have vectors of norm no less than $\sqrt{2}$. It is spanned by the basis $v_1 = (1,-1,0,0), v_2 = (1,0,1,0), v_3 = (1,0,0,1), v_4 = (1,0,1,0)$, all with $|v_i| = 2$. The four vectors $u_1 = (1,-1,0,0), u_2 = (1,1,0,0), u_3 = (0,0,1,-1), u_4 = (0,0,1,1)$ also achieve four successive minima and do not span the lattice. In $n \geq 5$ dimensions Korkine and Zolotareff proved [44] (see paragraph 14, p.270) that in fact any set of vectors in a lattice achieving n successive minima will not span that lattice.

Minkowski described and explored the connection between successive minima and quadratic forms.

Theorem 2.1.9 ([45] (p.247))**.** *Let Λ be a lattice of full rank in $\mathbb{R}^n$ with determinant $d(\Lambda)$, in the sense of Definition 1.3.4, and let S be a convex subset of $\mathbb{R}^n$ which is symmetric about the origin and whose interior volume is at least $2^n|d(\Lambda)|$. Then there exists at least one point of Λ other than the origin in the interior of S.*

In two dimensions, it can be derived from this theorem that a Minkowski-reduced basis is not only unique, but precisely the one whose Gram matrix gives the coefficients of a unique reduced quadratic form. Unfortunately this does not hold for lattices of dimension three and above - three dimensional lattices can have several Minkowski reduced bases, only one of which gives rise to the Lagrange-reduced quadratic form, while in dimensions $n \geq 4$ and above the fact that n successive minima may not be the lengths of vectors which span the lattice effectively 'decouples' the Minkowski and Lagrange reductions completely.

The development of X-ray crystallography generated interest in the geometry of lattices in 2 and 3 dimensions themselves , rather than as objects which facilitated proofs in number theory, giving rise to an increased interest in the field of *mathematical crystallography*. In the 1920s the mathematician Paul Niggli explored lattices directly from their geometry, and in the second of his trilogy of papers on the topic [31], he recovered the Lagrange reduction in this way - it transpires that in those terms it is exactly the reduction of Definition 1.3.6, which we reiterate here for ease of reference.

Definition 2.1.10 (Niggli Reduction in 2D)**.** *Let Λ be a lattice in $\mathbb{R}^2$ with basis v_1, v_2. The lattice is (obtuse)* Niggli Reduced *if $||v_1|| \leq ||v_2||$ and $-\frac{1}{2}|v_1| \leq v_1 \cdot v_2 \leq 0$.*

Note that it is also possible to select an acute Niggli reduction by reversing the signs in the second condition of Definition 2.1.10. In two dimensions a Niggli reduced basis is also reduced in the terms of Lagrange and Minkowski. Niggli showed that the geometric meaning of this reduction could be expressed as the selection of the two vectors whose (obtuse) angle was closest to 90°.

Figure 2.1 illustrates this geometric meaning more clearly - if we apply an isometry to place v_1 along the x-axis then v_2 is constrained to occupy a narrow strip of the plane above the circle of radius $||v_1||$.

Niggli's extension of this reduction to three dimensions [46] is the standard approach to stating reduced lattice bases for crystallographic structures. While the inequalities of the Niggli reduction are a straightforward extension of the two dimensional case for pairwise combinations of each of the three vectors, the 'special conditions' handling various equalities expand considerably. In addition, the Niggli reduction can give rise to two 'types' of lattice.

Definition 2.1.11 (Niggli Reduction in 3D - see for example [47], Section 3)**.** *Let G be the gram matrix of a lattice given by a basis v_1, v_2, v_3, whose entries $g_{ij} = v_i \cdot v_j$ (see Definition 2.1.3) have absolute values $|g_{ij}|$.*

The basis is Niggli-reduced *of* type 1 *(acute) if the following conditions hold:*

$$g_{11} \leq g_{22} \leq g_{23} \tag{2.1}$$

$$g_{12} \leq g_{13} \leq \frac{1}{2} g_{11} \tag{2.2}$$

$$g_{23} \leq \frac{1}{2} g_{22} \tag{2.3}$$

$$g_{ij} > 0 \text{ for all } i \neq j \tag{2.4}$$

$$\text{If } g_{11} = g_{22} \text{ then } g_{23} \leq g_{13} \tag{2.5}$$

$$\text{If } g_{22} = g_{33} \text{ then } g_{13} \leq g_{12} \tag{2.6}$$

$$\text{If } g_{12} = \frac{1}{2} g_{11} \text{ then } g_{13} \leq 2g_{23} \tag{2.7}$$

$$\text{If } g_{13} = \frac{1}{2} g_{11} \text{ then } g_{12} \leq 2g_{23} \tag{2.8}$$

$$\text{If } g_{23} = \frac{1}{2} g_{22} \text{ then } g_{12} \leq 2g_{13} \tag{2.9}$$

It is Niggli-reduced of type 2 *(obtuse) if the following conditions hold:*

$$\textit{Conditions } 2.1, 2.2 \textit{ for type } 1 \textit{ lattices.} \tag{2.10}$$

$$(|g_{12}| + |g_{13}| + |g_{23}|) \leq \frac{1}{2}(g_{11} + g_{12}) \tag{2.11}$$

$$g_{ij} \leq 0 \textit{ for all } i \neq j \tag{2.12}$$

$$\textit{If } g_{11} = g_{22} \textit{ then } |g_{23}| \leq |g_{13}| \tag{2.13}$$

$$\textit{If } g_{22} = g_{23} \textit{ then } |g_{13}| \leq |g_{12}| \tag{2.14}$$

$$\textit{If } g_{12} = \frac{1}{2}g_{11} \textit{ then } g_{13} = 0 \tag{2.15}$$

$$\textit{If } g_{13} = \frac{1}{2}g_{11} \textit{ then } g_{12} = 0 \tag{2.16}$$

$$\textit{If } g_{23} = \frac{1}{2}g_{22} \textit{ then } g_{12} = 0 \tag{2.17}$$

$$\textit{If } (|g_{12}| + |g_{13}| + |g_{23}|) = \frac{1}{2}(g_{11} + g_{12}) \textit{ then } g_{11} \leq 2|g_{13}| + |g_{12}| \tag{2.18}$$

The complexity of these conditions arises from the need to ensure that the resulting reduced basis is unique to any lattice. Buerger defined a reduced lattice which can be stated rather more simply in terms of extremal conditions on vector lengths:

Definition 2.1.12 (Buerger cell [48])**.** *A* Buerger cell *of a lattice is given by a basis v_1, v_2, v_3 of the lattice such that $||v_1|| + ||v_2|| + ||v_3||$ is minimal among all basis selections.*

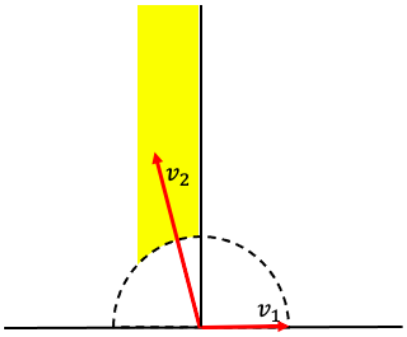

Figure 2.1: Constraints on vectors for an (obtuse) Niggli reduction in $2D$

Unfortunately, this simple definition does not give a unique cell - in three dimensions a lattice can have up to five possible Buerger cells [49], although Gruber [50] proved that the unique Niggli cell can be recovered by imposing the additional conditions on the angles α, β, γ between the basis vectors such that $|\cos\alpha| + |\cos\beta| + |\cos\gamma|$ and $|\cos\alpha\cos\beta\cos\gamma|$ are maximal among all possible selections of Buerger cell. The definition is also not necessarily constructive - as we will see in the next section, finding efficient algorithms that minimise lattice basis vector lengths is a topic of open research.

Our final example of lattice reduction is one which will be foundational for the work of this thesis - we therefore give only a brief definition here.

Definition 2.1.13 (Selling Reduction)**.** *Let $v_1, \ldots v_n$ be a lattice basis and define*

$$v_0 = -\left(\sum_{i=1}^{n} v_i\right)$$

The basis is Selling reduced *if for all pairs v_i, v_j with $i \neq j \in \{0, \ldots, n\}$ the inner product $v_i \cdot v_j$ is negative.*

Note that the Selling reduction condition does not, unlike the Niggli reduction condition, impose an ordering on the lengths of vectors in the basis.

Example 2.1.14. *The Niggli reduced basis of the lattice given in figure 1.3 is* $v_1 = (-1, 0), v_2 = (0.3, 0.7)$. *We compute the* v_0 *of definition 2.1.13 as* $(0.7, -0.7)$ *and thus*

$$v_1 \cdot v_2 = -0.3$$
$$v_0 \cdot v_1 = -0.7$$
$$v_0 \cdot v_2 = -0.28$$

and the basis is also Niggli reduced.

The lattice basis $v_1 = (1, 0), v_2 = (0, 2)$ *is* not *Niggli reduced since* $||v_1|| < ||v_2||$, *but is Selling reduced since in this case* $v_1 \cdot v_2 = 0$ *and since* $v_0 = (-1, -2)$ *all of the other inner products of definition 2.1.13 are negative.*

Selling reduction can be simply defined, but it is not immediately clear from the definition whether or not a Selling reduced basis exists for any particular lattice. The answer to these questions is dependent on lattice dimension, and we will focus on it in Chapter 3.

Example 2.1.14 also shows that if a reduced basis does exist, it is not, in some sense, unique. In the first example, we may simply multiply all vectors by -1 and the reduction conditions will still hold. The second is even more complex - I can multiply *either* vector by -1 and leave the other fixed and still have a Selling reduced basis. Thus,for a crystallographer seeking a genuinely unique representation of the data of any given lattice, the Selling reduction is not suitable

However, note that all of the possible alternate Selling reduced bases of example 2.1.14 discussed above are related to each other by isometries - to replace each vector by its negative is simply to rotate the basis by 180° about the origin, while the various options for a basis with two orthogonal vectors are related by reflections in the x and y axis. This makes it an attractive target for the solution of problem 1.4.1.

2.1.1 Reduction Algorithms

Given a definition of a reduced basis, a key problem is to practically derive such a basis from any arbitrary set of linearly independent input vectors. This has typically been done using *reduction algorithms* - each v_i in a lattice basis is subjected to stepwise subtractions of some appropriate linear combination of the remaining basis vectors (which by the original Definition 1.3.1 will result in some other lattice vector) until some set of conditions are reached which are either exactly those of the reduction or satisfy some criterion which is proven to hold for a basis which approximates the reduction conditions.

The first such algorithm for two dimensional lattices was proposed by Lagrange [39], and can be simply stated below in the form of modern pseudocode (adapted here from [51], p.42).

The vector $v_1 - \frac{v_1 \cdot v_2}{|v_2|^2} v_2$, which is not necessarily a lattice vector unless the scalar quantity happens to be integral, is the projection of the vector v_2 on to the line orthogonal to v_1. Line

Algorithm 1 Lagrange Reduction in 2 Dimensions

Input: Any linearly independent vectors v_1, v_2

Output: A Lagrange-reduced basis for the lattice generated by v_1, v_2.

1: **repeat**
2: **if** $|v_1|^2 > |v_2|^2$ **then** swap v_1 and v_2
3: **end if**
4: $u \leftarrow v_1 - \left\lfloor \frac{v_1 \cdot v_2}{|v_2|^2} \right\rceil v_2$
5: $v_1 \leftarrow v_2$
6: $v_2 \leftarrow u$
7: **until** $|v_1|^2 \leq |v_2|^2$

4 of Algorithm 1 selects a vector which is 'as close to orthogonal' as possible. The algorithm is guaranteed to terminate since it decreases the length of one of the input vectors at every iteration, and since a lattice is discrete eventually some finite lower bound in length must be reached. The resulting lattice is reduced in all the senses discussed above, since they are equivalent in $2D$.

Because of their applicability to real world crystal structures, reductions for three dimensional lattices have been of particular interest. Kŕivý and Gruber's algorithm for finding the Niggli reduced cell [52] modifies Gruber's initial reduction algorithm to the Buerger cell [49], and relies on a specific presentation of the parameters of a basis - the Niggli form [46, 53] - which is related to the invariant we will discuss in Chapter 3.

Definition 2.1.15 (Niggli form)**.** *Let Λ be a Niggli reduced lattice basis $\{v_1, v_2, v_3\}$, with gram matrix G (see Definition 2.1.3) The 2×3 matrix*

$$\begin{pmatrix} g_{11} & g_{22} & g_{33} \\ 2g_{23} & 2g_{13} & 2g_{12} \end{pmatrix}$$

is the Niggli form *of the lattice.*

Kŕivý and Gruber's algorithm begins with the parameters of a Niggli form for an arbitrary basis, reordering them so that $a^2 \leq b^2 \leq c^2$. It then reduces the length of input vectors whenever the various conditions of Definition 2.1.11 are not satisfied for either positive or negative inner products. A pseudocode implementation is shown as algorithm 2.

Algorithm 2 Křivý-Gruber Niggli Reduction Algorithm (adapted from [52])

Input: an arbitrary basis v_1, v_2, v_3

Output: the Niggli form of the lattice generated by the input basis

Compute g_{ij} for $i, j \in \{1, 2, 3\}$
For $i \neq j$, $g_{ij} \leftarrow \text{sign}(g_{12}g_{13}g_{23})|g_{ij}|$
while Niggli conditions not fulfilled **do**
    if $g_{11} > g_{22}$ **then**
        Swap v_1, v_2
        Recompute $g_{11}, g_{22}, g_{13}, g_{23}$
    end if
    if $g_{22} > g_{33}$ **then**
        Swap v_2, v_3
        Recompute $g_{22}, g_{33}, g_{12}, g_{13}$
    end if
    for all $i, j, k \in \{1, 2, 3\}$ **do**
        if $g_{ii} > 2g_{ij}$ or ($g_{ii} = 2g_{ij}$ and $g_{ik} > 2g_{jk}$) or ($g_{ii} = -2g_{ij}$ and $g_{ik} < 0$) **then**
            $v_j \leftarrow v_j + \text{sign}(g_{jk})v_k$
            Recompute g_{ij}, g_{jj}, g_{jk}
        end if
    end for
    if $2|g_{12}| + 2|g_{13}| + 2|g_{23}| + g_{11} + g_{12} < 0$ or ($2|g_{12}| + 2|g_{13}| + 2|g_{23}| + g_{11} + g_{12} = 0$ and $g_1 1 > 2|g_{13}| + |g_1 2|$) **then**
        $v_3 \leftarrow v_1 + v_2 + v_3$
        Recompute g_{13}, g_{23}, g_{33}
    end if
end while

Gross-Kunstleve *et al.* noted [54] that this algorithm is not numerically stable - that is, repeated floating point calculation errors can cause the algorithm to fail to terminate. They proposed a simplified version in which termination occurs if the the updated lengths after a cycle of the algorithm differ from the input lengths by less than 10^{-5} Ångstroms.

The most recent modification to the Křivý and Gruber algorithm is by Shi and Li [55], which is intended to deal with the slightly different problem of measurement errors. Unlike floating point calculation errors, these can be magnified at each step of a reduction - thus, after each step of the reduction process, parameters are updated with actual measured vectors of the lattice within some defined error tolerance of the theoretical Niggli-reduced cell before the next step.

For our purposes, however, such approaches are incompatible with constructing a formal equivalence relation under isometry or rigid motion as described in Proposition 1.3.10, since if two lattices are declared to be isometric (or similar) if they can be transformed into each other by some small deformation, then since any lattice can be transformed to any other by a series of such small deformations, all lattices effectively collapse into the same isometry class (see Figure 2.2 for an illustration of this principle).

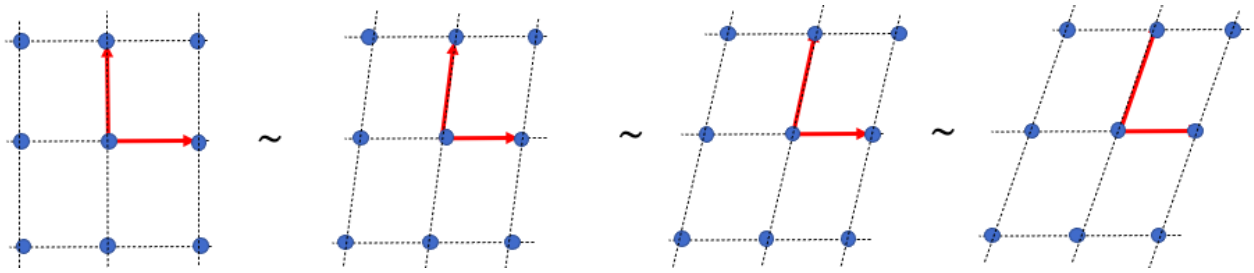

Figure 2.2: Any lattice is equivalent to any other under by a series of small deformations.

To conclude this subsection, we will briefly discuss generalised reduction algorithms for higher dimensions - a more detailed overview, and in particular the reasoning and proofs behind the application of the LLL-algorithm whose description closes this section, can be found in [51]. The challenge in higher dimensions is that only an upper bound on the length of the shortest set of spanning vectors can be found.

The challenge of extending Křivý-Gruber type algorithms into higher dimensions is one of mounting computational complexity - the number of conditions needed to specify a reduced cell grow rapidly with dimension. Approaches extending the Lagrange algorithm (Algorithm 1) to higher dimensions are more common. Here the barrier is that in higher dimensions the order in which the input basis vectors are selected can affect the output basis, and the output is therefore not unique. Higher dimensional extensions use the weaker notion of *size reduced* lattices, where the lengths of all vectors in the basis have lengths below some upper bound.

The *Lenstra-Lenstra-Lovasz (LLL) algorithm* [56], with various modifications, adds an additional condition on the *relative* lengths of vectors, and is the most widely used approach in current practice. The algorithm relies on the well-known process of *Gram-Schmidt orthogonalisation*, which derives an orthogonal output basis from any given input basis:

Definition 2.1.16. *(Gram-Schmidt orthogonalisation) Let $v_1, \dots v_n$ be a full rank lattice in $\mathbb{R}^n$. The* Gram-Schmidt orthogonalisation *$u_1, \dots u_n$ is given by the vectors*

$$u_i = v_i - \sum_{j=1}^{i-1} \mu_{i,j} u_j$$

where $\mu_{i,j} = \frac{v_i \cdot u_j}{|u_j|^2}$.

The LLL algorithm generates a basis of any lattice in any dimension which satisfies the following condition:

Definition 2.1.17 (LLL condition [56]). *Let $v_1, \dots v_n$ be a basis of a lattice Λ and $u_1, \dots u_n$ be its Gram-Schmidt orthogonalisation with constants $\mu_{i,j}$ of Definition 2.1.16. The basis is* LLL-reduced *if $|\mu_{i,j}| \leq \frac{1}{2}$, and for all u_i, u_{i+1} and some $\delta \in [\frac{1}{4}, 1]$:*

$$||u_i + \mu_{i+1,i}u_{i+1}||^2 \leq \frac{4\delta}{3}||u_i||^2$$

Briefly, the Lovasz condition ensures that the difference between vectors v_i and v_{i+1} in any basis is not 'too large'. At any step of the LLL algorithm if any pair of vectors u_i, u_{i+1} do not satisfy the Lovasz condition, the vectors v_i, v_{i+1} are and the algorithm repeated until the condition is satisfied.

The bases arising from all of these reduction algorithms do not satsify the continuity condition of Problem 1.4.1. The Niggli reduced cell has long been known to behave discontinuously under continuous lattice deformation [57], and indeed it is proved in [23] that any reduced basis changes discontinuously under a continuous deformation of the lattice itself.

Our own work relies on the less well-known approach of *Selling reduction* - this still results in discontinuous bases but 'keeps track' of a third lattice vector, from which continuity can be recovered. The nature of and algorithm for Selling reduction, and a proof that it always terminates and outputs a Selling reduced basis for $n = 2$, will be discussed in Chapter 3.

2.2 Discrete Lattice Classification

Recall that our aim in Problem 1.4.1 is to classify lattices *continuously*. However, the general classification of lattices has been discrete - placing them in some finite set of classes. We provide an outline of the more important classification approaches in two and three dimensions in this section- a more detailed introduction which extends these ideas to higher dimensions can be found in [29]. The approaches used in mathematical crystallography are definitively codified in section A of the International Tables of Crystallography, which also includes a detailed mathematical exposition of the topic [58].

We have so far described lattices as purely geometric entities - sets of vectors in $\mathbb{R}^n$. However, they can also be described in rather more abstract mathematical terms as finite sets of *group actions* (considered as translations, rotations etc.) in $\mathbb{R}^n$. Indeed, since these actions remain the same regardless of the relative orientation of the lattice in the plane they will prove useful in addressing the 'isometry' element of Problem 1.4.1

Lattices can be described by considering their set of *automorphisms* - that is, the set of isometries which map any lattice to itself. We will begin Section 2.2 by describing these automorphisms in more formal terms. This will enable us to discuss those discrete lattice classifications which are based in one way or another on distinguishing two lattices by some subset of their automorphism group. We will consider the most well-known of these to

crystallographers: the *Bravais types*, of which there are five in 2 dimensions and 14 in three - we will discuss the former in some detail as an illustrative case and summarise the latter. We will explore how these interact with other classification systems, and giving rise to a variety of lesser known (but also discrete) classification system based on parameters of the Niggli reduced lattice basis.

To understand the construction of the Bravais classes, we recall from chapter 1 Definition 1.3.3 of the matrix groups representing isometries in $\mathbb{R}^n$. We will also require some notions from group theory - that of the *conjugacy class* and of a *group action*:

Definition 2.2.1. *(Conjugacy class) Let G be a group. Elements $g, k \in G$ are* conjugate *if $k = hgh^{-1}$ for some $h \in G$. The* conjugacy class *of an element g is the set $K \leq G$ of all k that are conjugate to g.*

Conjugacy is an equivalence relation: any group has an identity element e which is its own inverse, g is conjugate to itself through $ege = g$, all group elements have an inverse so if $g = hkh^{-1}$ then $k = h^{-1}gh$. Finally if $g = hkh^{-1}$ and $k = ala^{-1}$ for some $a, l \in G$ then $g = hala^{-1}h^{-1} = (ha)l(ha)^{-1}$, which confirms transitivity.

Definition 2.2.2. *(Group Action, Orbit, Stabilizer - see Chapter 2 of [29]) Let X be an arbitrary set and let H be the group of its* automorphisms *(that is, the set of all functions $f : X \to X$. An* action *of a group G on X is a group homomorphism $\rho : G \to H$. To avoid unnecessary brackets the automorphism given by $\rho(g)(x)$ is generally written as gx if the specific group homomorphism is understood. The* orbit *x_G of $x \in X$ is the set of all elements of X under the action of all g in G. The* stabiliser *G_x of an element $x \in X$ is the set $\{g \in G | gx = x\}$ of elements in g which leave x fixed. A group action is* effective *if the only element of g which stabilises every element of x is the identity.*

Extending the notation above, we consider the stabiliser of a group action G_{gx}. Now if $h \in G_{gx}$ then $hgx = gx$, and thus $(g^{-1}hg)x = x$ showing that the stabiliser of a group action on an element $x \in X$ is in the same conjugacy class as the stabiliser of x. Since the group itself is partitioned into its conjugacy classes, this gives a natural classification of X with respect to the action of G.

Definition 2.2.3. *(Orbifold - see Chapter 2 of [29]) Let G be a group acting on the set X. Two orbits x_G, y_G are of the same* type *if the stabilisers of x_G, y_G are in the same conjugacy class. A* stratum *$X||G$ of X with respect to G is a set of orbits of the same type. An* orbifold *of X with respect to G consists of a single representative of each stratum of X with respect to G.*

This rather technical set of definitions can be illustrated with a simple but pertinent example:

Example 2.2.4. *(See Figs 2.1, 2.5, 2.7 of [29]) Denote by D_3 the group of six symmetries of an equilateral triangle, consisting of the identity element, the anticlockwise rotations r_1, r_2 by $2\pi/3$ and $4\pi/3$ respectively, and the reflections s_1, s_2, s_3 through the bisectors at each vertex of the triangle.*

We define the group action $\rho : G \to O_2(\mathbb{R})$ by mapping any symmetry element to linear transformations which preserve the symmetry of an equilateral triangle whose barycentre is at the origin of $\mathbb{R}^2$, so that (for example) r_1 is the anticlockwise rotation element given by $\begin{pmatrix} \cos 2\pi/3 & 0 \\ 0 & -\sin 2\pi/3 \end{pmatrix}$ *and s_1 is the reflection* $\begin{pmatrix} -1 & 0 \\ 0 & 1 \end{pmatrix}$ *in the y axis.*

There are three conjugacy classes of D_3, given by the identity element which is conjugate to itself), the rotations r_1, r_2 (which together with the identity element form a subgroup isomorphic to the cyclic group $\mathbb{Z}_3$) and the reflections s_1, s_2, s_3. Figure 2.3 illustrates how the orbits of points in $\mathbb{R}^2$ are split into different types in the sense of Definition 2.2.3 - any pair of brown and purple points represent the orbit type of the reflection conjugacy class while three identically coloured dots represent the orbit type of the rotation conjugacy class.

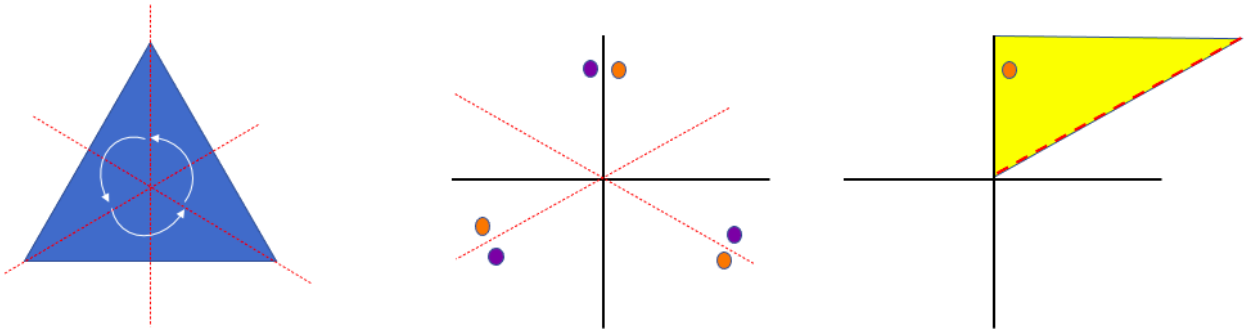

Figure 2.3: **Left:** Symmetry group D_3 of the equilateral triangle. **Centre**: Orbits and strata of the group action of D_3 on $\mathbb{R}^2$. **Right**: Orbifold of the action of D_3 on $\mathbb{R}^2$ - the yellow area contains all points of the same type

The automorphism group of a lattice falls into two types. There is an infinite group of translations mapping any point in the lattice to any other point. No individual point of the lattice is fixed under such translations. There is also some (possibly trivial) set of automorphisms that fix a single lattice point - this latter is the *point group* of the lattice. More formally:

Definition 2.2.5. *(Lattice point group - see for example [59], Definition (5), p.273) The* point group *of a lattice Λ in n dimensions is the subset of O_n which stabilises the orbits of all points in Λ.*

In a crystallographic context, the point group is also called the *crystallographic system* of a lattice. The periodic structure of a lattice places *crystallographic restrictions* on the contents of its crystallographic system - it was proven by Bieberbach ([60], see [61] for a short proof in English) that the cardinality of the point group must be finite for lattices in any dimension.

For a lattice in one dimension, consisting of all values $ka, k \in \mathbb{Z}$ for a fixed real a, it is obvious that any point group can contain only the identity transformation, and the 'centrosymmetric inversion' given multiplication of all values by -1, and indeed that every one dimensional lattice in $\mathbb{R}$ must have this point group, and can have no other.

Indeed for a lattice in any dimension d it is similarly clear that the point group must at least contain the identity transformation given by multiplication of all vectors by the $d \times d$ identity matrix I and also the centrosymmetric inversion given by multiplication by $-I$.

Attempts to compute which point groups are possible in higher dimensions rely on understanding what finite subgroups of $GL_n(\mathbb{R})$ (Definition 1.3.3)may exist (in fact it is sufficient to prove results in the general linear group $GL_n(\mathbb{Q})$ of matrices with rational entries), and the following theorem places limits on which such subgroups of what order may exist in any dimension.

Theorem 2.2.6 ([62], Theorem 2.7)**.** *Let $m = p_1^{x_1} p_2^{x_2} \dots p_m^{x_m}$ with all p_i prime*
The general linear group with rational $GL_n(\mathbb{Q})$ has an element of order m if and only if:

$$\begin{cases} \sum_{i=1}^{n} (p_i - 1)p_i^{x_i} - 1 \leq n & p_1^{x_1} = 2 \\ \sum_{i=1}^{n} (p_i - 1)p_i^{x_i} & p_1^{x_1} \leq m \neq 2 \end{cases}$$

In two dimensions this means that any lattice can only contain elements of order $2, 3, 4$ or 6. We can demonstrate this less formally by considering two points p, q in a lattice such that $||p-q|| = \lambda_1$ is the shortest possible separation distance in a lattice (see Definition 2.1.5). We consider the image q' of q under a rotation by θ about p, and likewise the image q'' of p under a rotation by $-2\pi/n$ about q. We encounter a contradiction if $q' \neq q''$ and $||q' - q''|| \leq \lambda_1$. As shown in Figure 2.4, this limits us to point groups containing elements of order 6 or order ≤ 4.

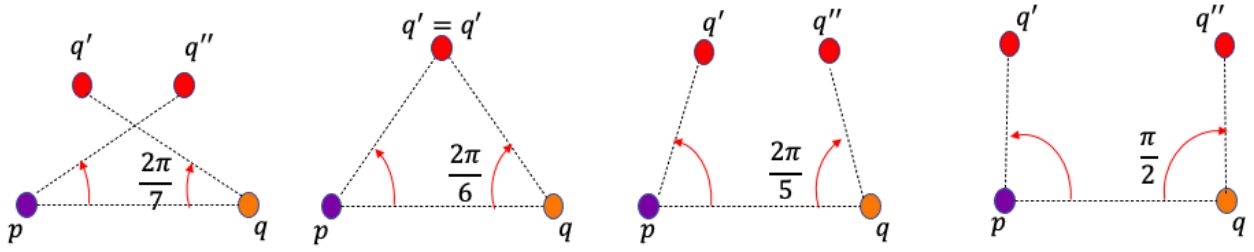

Figure 2.4: A lattice in two dimensions can only map to itself by a rotation about a fixed point of order $2, 3, 4$ or 6.

In Figure 2.5 we show the subsets of $\mathbb{R}^2$ whose points are the orbits of rotations of order $2, 4$ and 6. In addition to the cyclic group of rotations, three of these include a reflection of order 2 that can be combined with these rotations, forming the well known *dihedral groups* D_2, D_4 and D_6. For the rotation group of order 2 it is also possible to build a lattice that excludes the reflection element - in two dimensions the inversion is geometrically equivalent to a rotation by π, and the resulting subset is a rhombus. We omit the rotation of order 3, since a lattice constructed with this symmetry also has a rotation of order 6.

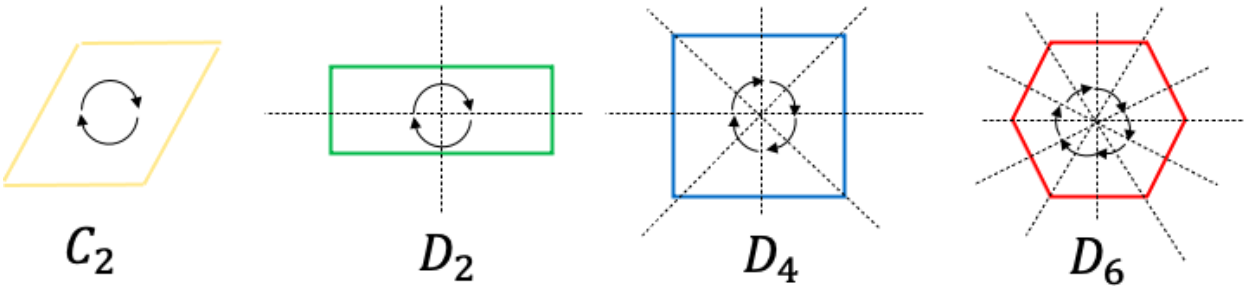

Figure 2.5: The four crystallographic systems in 2 dimensions.

When constructing lattices with the different crystallographic systems, we find as in Figure 2.6 that there is only one way of constructing a lattice with rotational symmetry order 4 (as a primitive square) and one way in which we can construct a lattice with rotational symmetry of order 6 (as a hexagonal lattice). There are two ways in which we may construct a lattice with D_2 symmetry. These differ geometrically in terms of the unit cell encompassed by their (Niggli) reduced basis - in one case the cell is rhomboid, in the other it is rectangular. The latter unit cell is referred to as *primitive*, the former as *centred*. Figure 2.6 illustrates the intuition behind this terminology - a centred lattice can be constructed from a primitive one by adding a lattice point at the centre of its unit cell.

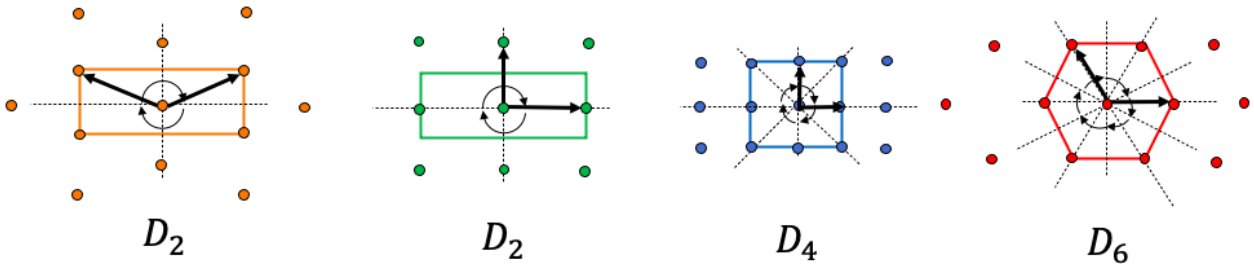

Figure 2.6: Lattices constructed with the permitted crystallographic symmetries

A more formal way of distinguishing these two lattice geometries is in terms of their automorphism groups. We consider the change of basis matrices in $GL_2(\mathbb{Z})$ that are also automorphisms of the lattice. If the two D_2 point group lattices have the bases shown in Figure 2.6, then a reflection through the vertical axis in Figure 2.5 in the primitive case can be represented by the matrix $M_p = \begin{pmatrix} 1 & 0 \\ 0 & -1 \end{pmatrix}$, in the centered case by $M_c = \begin{pmatrix} 0 & 1 \\ 1 & 0 \end{pmatrix}$. If it were possible to convert the symmetries of the primitive lattice into those of the centered lattice by some change of basis , then these reflections should be in the same conjugacy class in $GL_2(\mathbb{Z})$ - that is, there should exist some $B \in GL_2(\mathbb{Z})$ such that $BM_pB^{-1} = M_c$ and vice versa. It can be discovered either by direct computation or by noting that this amounts to the primitive and centred versions of the lattice being isometric (since otherwise B would not be invertible at all) that there can be no such B. This distinction was first explored by Auguste Bravais [63], and the classification based on it is thus named after him.

Definition 2.2.7 (Bravais Class - see [59], Definition (7) p.274)**.** *The* Bravais class *of a lattice in* $\mathbb{R}^n$ *is the conjugacy class of its crystallographic system in* $GL_n(\mathbb{Z})$.

Bravais classes are typically denoted in 2 and 3 dimensions, as shown in Figure 2.7, by *Hermann-Mauguinn notation* [64]. The symbol opens with a p or c which indicates whether we are in the primitive or centered case. The point group is then in this notation by a number indicating the order of any rotation symmetries followed in the 2 dimensional case by a number of ms which indicate the presence of orthogonal mirror planes along different axes. Primitive and centered cases (with the former a 'default') are distinguished by a lower case prefix.

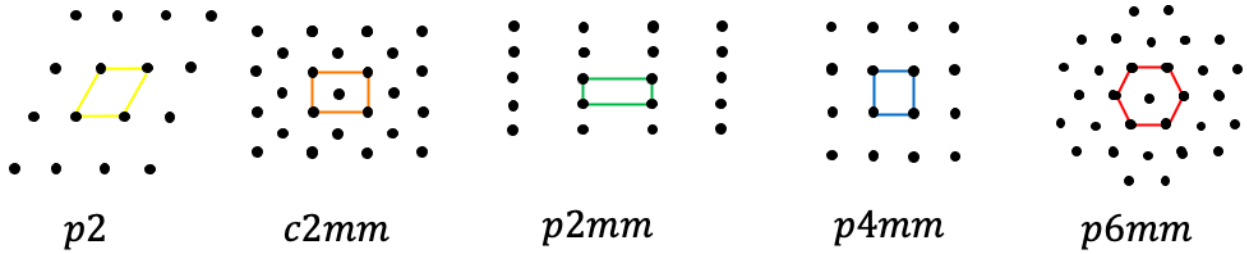

Figure 2.7: The five distinct Bravais lattice types in 2 dimensions. The two systems with Hermann-Mauginn symbol $p2mm$ and $c2mm$ have the same crystallographic system, but one cannot be transformed into the other by a change of basis.

The Bravais types are in fact related by continuous deformations - from a general Niggli reduced lattice basis (see Definition 1.3.6) given by $v_1 = (a, 0), v_2 = (-b, c)$ with $a, b, c > 0$, we may continuously deform the parameter value b in the range $[-a/2, 0]$ whose extremes produce, respectively, a centered and a primitive rectangular lattice. The primitive rectangular lattice $(a, 0), (0, c)$ may further have c deformed continuously until it is equal to a, giving a square lattice. From a centered rectangular lattice , we may continuously scale v_1

until $||v_1|| = ||v_2||$, giving rise to a hexagonal lattice in which all lattice vectors are of equal length, or continuously change the angle between the two vectors to recover a square lattice. These relationships are summarised in Figure 2.8.

We have illustrated in detail the construction of point groups and Bravais classes in two dimensions. The approach to the three dimensional case is similar - since the main results of this thesis involve the two dimensional case (and in any case we aim to replace all discrete classifications with a continuous one), we will only briefly summarise the results. Explicit computation of point and Bravais groups in three dimensions can be found in rigorous technical detail in Louis Michel's exposition of the topic [59].

While we can compute the crystallographic restrictions for lattices in $\mathbb{R}^3$ directly, the process is simplified by the following theorem, which is proved for the rational numbers but extends to the reals:

Theorem 2.2.8 ([62], Corollary 2.9)**.** *For $k \in \{1, 2, \ldots\}$, $GL_{2k}(\mathbb{Q})$ has an element of order n if and only if $GL_{2k+1}(\mathbb{Q})$ also has an element of that order.*

Setting $k = 1$ this means that the construction of point groups can begin with the assumption that just as in dimension 2, point groups in dimension 3 can contain only elements of orders $2, 3, 4$ and 6. We consider the number of elements of order 2 in the lattice. If there are none then the lattice is *triclinic* and inversion (multiplication by $-I$, where I is the 3×3 identity matrix) is the only lattice symmetry If there is only one then the lattice is *monoclinic* If there is more than one, then it is either a plane of reflection, or by the restriction on rotation orders it must be a rotation of π/k where $k = 2$ (an *orthorhombic* lattice) , 3, 4 (a *tetragonal* lattice) or 6 (a *hexagonal* lattice). In the case of $k = 3$ it is possible for there to be either just a single set of three order 2 elements (a *trigonal* lattice) or two such sets lying in orthogonal planes (the lattice is then *cubic*).

For each of these seven crystallographic systems, Bravais classes may be constructed by 'centering' in the same way as for the 2 dimensional case - that is, for any lattice where an orthogonal pair of basis vectors exist (and thus there is a D_2 symmetry about the lattice in that plane) we may place an additional lattice point at the centre of the 2 dimensional 'unit cell'. As with 2 dimensional lattices, if no centering occurs then the lattice is of *primitive* Bravais subtype. We may thus enumerate Bravais types by considering what centerings may give rise to distinct conjugacy classes of lattice in $GL_3(\mathbb{Z})$.

For monoclinic and orthorhombic lattices, we may centre at a single unique pair of orthogonal vectors to give the *base-centered* subtype. For cubic, tetragonal and orthorhombic lattices all basis vectors are orthogonal, and thus all unit cell faces may be centred, giving rise to a *face centred* Bravais subtype for each. Cubic, orthogonal and tetragonal systems also admit points at the centre of their unit cells, giving rise to a *body centered* lattice. Thus, of the 7 crystallographic systems, the monoclinic admits only two distinct centerings (primitive and base-centered), tetragonal and cubic admit three and orthorhombic four. The total count of possible centerings is thus 15. However, the 'face-centered tetragonal lattice' is conjugationally equivalent by a change of basis in $GL_3(\mathbb{Z})$ to a body-centered orthogonal lattice and so in fact there are only 14 distinct Bravais classes.

Table 2.1 lists these in full, along with the common crystallographic reference system used in the International Tables to denote them [58], and their Hermann-Mauguinn symbol. The latter requires expansion from the 2 dimensional version - since inversion and rotation are distinct in three dimensions if a number is barred (as in $Fm\bar{3}m$ for a face centered cubic lattice) it indicates that an axis of rotation also has an inversion centre at the lattice point it fixes. (a 'rotoinversion'). The slash in N/m, where N is the order of a rotation element, indicates that the plane of reflection denoted by m is orthogonal to the rotational element of order N denoted in the symbol. Finally, a capital letter prefix denotes the particular type of centering present.

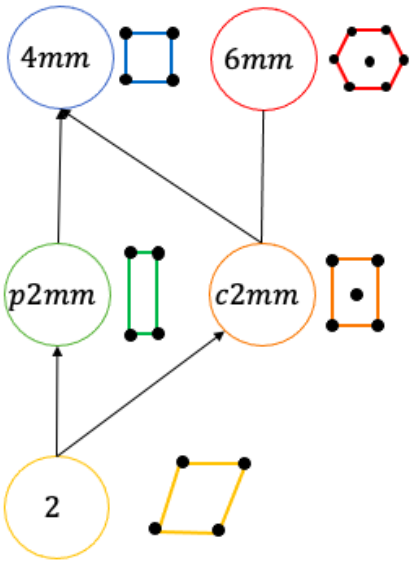

Figure 2.8: Bravais classes of two dimensional lattices, related by continuous deformations.

Similar computations can and have been made in higher dimensions showing the number of classes to grow rapidly - there are 64 known Bravais classes of in 4 dimension [65], while in 5 and 6 dimensions there are 189 and 826 respectively [66]. We have not been able to find any explicit computations for Bravais classes of higher dimension done since, possibly because alternative approaches to discrete classification in dimension ≥ 4 have since been suggested [66].

A more granular, although less rigorously defined, classification of lattices was developed initially by Niggli [67], and is based on what he described (without further rigorous definition) as 'essential geometric relations' within a lattice. In two dimensions, Niggli subdivided centered rectangular lattices into two separate *characters*, depending on whether the two shortest vectors in the lattice were of equal or unequal lengths, as illustrated in Figure 2.9.

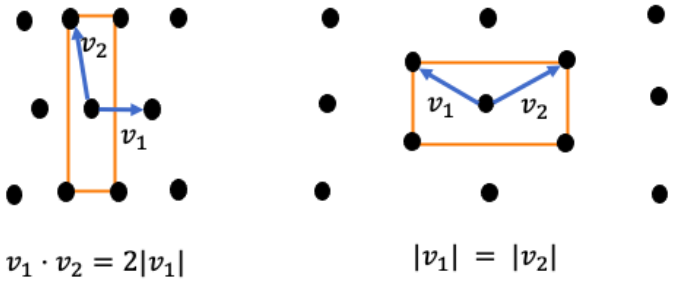

Figure 2.9: Niggli's two characters for centered rectangular lattices in $2D$.

In three dimensions, Niggli defined 41 characters through direct computation, although later careful analysis by Mighell [68] increased this to 44. However, it was not until much later that the lattice characters were rigorously defined in terms of all possible relations (within a particular Bravais class) of reduced basis lengths and inner products [69].

The relationships between crystallographic systems, Bravais types and lattice characters are summarised in Figure 2.10.

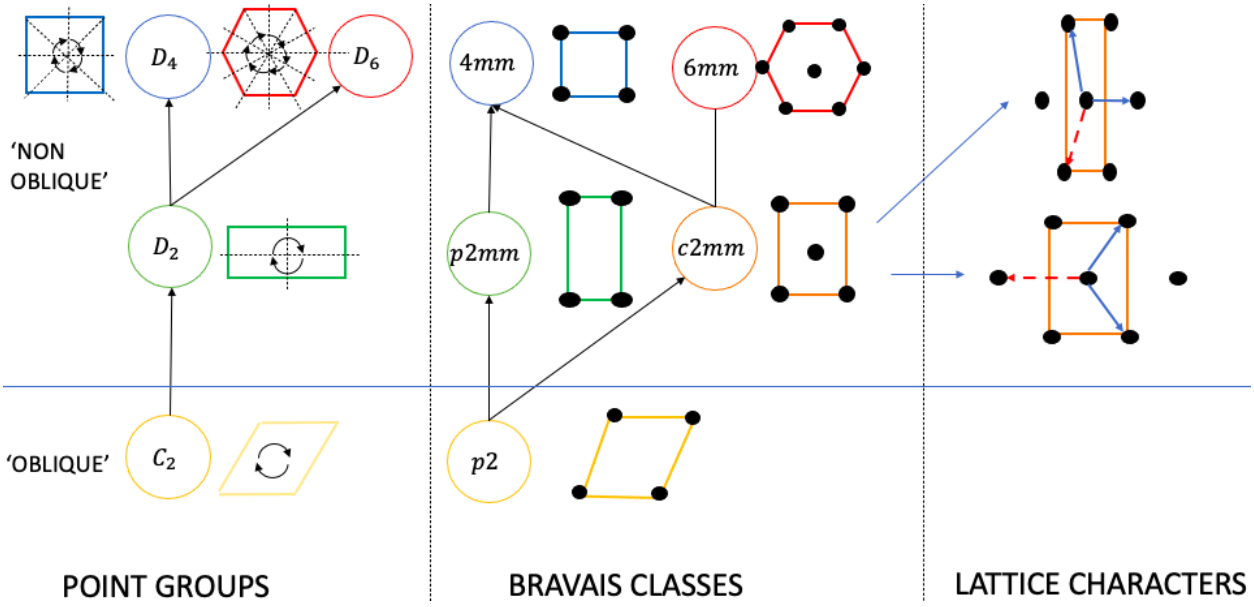

Figure 2.10: Summary of discrete lattice classifications discussed in this chapter for two dimensional lattices.

The Selling reduction discussed in the previous section gives rise to a different discrete classification based on the *Voronoi cells* of the lattice. Again, we will reserve detailed discussion of these to the next chapter, where they contribute to our new work and its results.

System	Bravais Class	Crystallographic Symbol	H-M Symbol
Triclinic	Primitive	aP	$\bar{1}$
Monoclinic	Primitive	mP	$P2/m$
Monoclinic	Base-Centered	mS	$C2/m$
Orthorhombic	Primitive	oP	$Pmmm$
Orthorhombic	Base-Centered	oS	$Cmmm$
Orthorhombic	Face-Centered	oF	$Fmmm$
Orthorhombic	Body-Centered	oI	$Immm$
Rhombohedral	Primitive	rP	$R\bar{3}m$
Tetragonal	Primitive	tP	$P4/mmm$
Tetragonal	Body-Centered	tI	$I4/mmm$
Hexagonal	Primitive	hP	$6/mmm$
Cubic	Primitive	cP	$Pm\bar{3}m$
Cubic	Face Centered	cF	$Fm\bar{3}m$
Cubic	Body Centered	cI	$Im\bar{3}m$

Table 2.1: The 14 distinct Bravais lattice types in three dimensions - their common crystallographic symbol as well as their Hermann-Mauguinn symbol is shown

2.3 Invariants and Similarity Measures on Lattices

All of the classifications of lattices in the previous section have been *discrete*, and therefore cannot be used to devise the continuous metric required by requirements 2 and 3 of Problem 1.4.1, although they should (and indeed do) arise as meaningful subsets of that continuous classification. In this section we will briefly discuss work towards the development of isometry invariants that are intended to support the continuous comparison of two lattice geometries.

The most straightforward isometry invariant of any lattice, if not the most tractable, is simply an ordered list of all distances in a lattice. It is obvious that this is an isometry invariant since it is by definition a collection of precisely those quantities which do not change under an isometry. Is it, however, a *complete* invariant?

The list of distances is usually defined in terms of a series which counts the multiplicity of vectors of a certain length:

Definition 2.3.1 (see [70], Definition 2.1.4)**.** *Let* Λ *be a lattice. The* theta series *of the lattice is defined as*

$$\theta(\Lambda) = \sum_{v \in \Lambda} e^{2\pi i ||v||^2}$$

and its coefficients give the count of lattice vectors with length $||v||$ *for all* $v \in \Lambda$*. Two lattices* Λ, Λ' *are* isospectral *if* $\theta(\Lambda) = \theta(\Lambda')$*.*

In these terms we may frame the question of completeness by asking 'do isospectral, non-isometric lattices exist'?

In one dimension the answer is trivial - the list of distances in any $1D$ lattice will be a multiset of pairs of identical values $\{ka, ka | k \in \mathbb{Z}\}$ where a is the regular distance between points along the real line specifying the lattice. The lattice is clearly uniquely determined by the value a.

In two dimensions it is similarly easy to generate the list of distances (see Figure 2.11), but less clear that no two non-isometric latties will have the same list. In fact, the question was answered positively in 1978 [71], and in four dimensions it was answered negatively by Conway and Sloane [72], who discovered an infinite family of counterexamples. If a counterexample exists in dimension d, then one may generate a counterexample in dimension $d+1$ by embedding some pair of isospectral lattices of rank d into $\mathbb{R}^{d+1}$ and adding the unit vector orthogonal to the basis vectors of each - in each case an equal number of vectors of length 1 will have been added to the lattice. This result thus settled the question for every dimension $d \neq 3$.

The problem proved surprisingly non-trivial in three dimensions. Schiemann developed a proof in 1990 (published in English at [73] - a excellent detailed exposition can be found in [70]). The proof is based on the construction of an algorithm which would terminate (in any dimension) if and only if no isospectral, non-isometric lattices existed. On being run for dimension 3, the algorithm did indeed terminate after 14 steps.

Since the theta series for a lattice is infinite, it is obviously rather unwieldy to work with - certainly not fulfilling the computability requirement of Problem 1.4.1. It is possible to induce a metric on the space of any two power series - for two theta series θ_1, θ_2 a classical approach would be to define $d(\theta_1, \theta_2) = 2^{-k}$ where k is the first position in the series at which the coefficients differ. This may require computation of many terms of each series. However, it is possible that there is some length at which one may truncate the series - some minimal set of lattice distances which are sufficient to completely recreate a lattice of dimension less than 4. Indeed, as we will show in the next chapter, in two dimensions just three lattice vectors are sufficient to uniquely reconstruct a lattice.

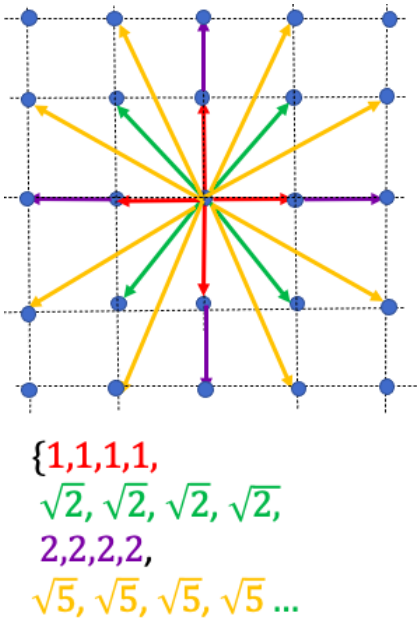

Figure 2.11: An ordered list of distances for the square lattice with orthogonal basis $v_1 = (1, 0), v_2 = (0, 1)$.

Some of the most extensive work on developing a continuous space of lattices in three dimensions has been done by Andrews and Bernstein. Most recently they have proposed an ordered list of lattice distances for a Niggli reduced cell [74], consisting of the three reduced basis vectors, the face diagonals of the unit cell and all body diagonals. They suggested that the seven smallest such distances should be sufficient to reconstruct it completely. However, after a family of counterexamples was found suggesting this was incomplete, this was updated to use a specific *unordered* distance set - the unit cell lengths, the three shortest face diagonals and the shortest body diagonal [75].

Their other approaches have suggested the use of values from the Gram matrix (see Definition 2.1.3) - that is, including both inner products and cell lengths. They have noted that the three vector lengths and three inner products from the Gram matrix of the Niggli cell represent a point in $\mathbb{R}^6$ [76] which they define as the $G6$ *vector*, with the various Bravais types and characters being subspaces. They have conducted an exhaustive analysis of these subspaces [47], and their relation to the various discrete lattice classifications. They have also discussed the use of Selling rather than the Niggli reduced cell has been previously discussed [77], again considering a exhaustive investigation of the subspaces of the $G6$ vector of this reduction. In each case, the discontinuity of the basis has led to highly complex subspaces in which it is not clear how to compute a stable metric that will compare two lattices.

A practical quantification of the the similarity between two lattices is given by the computation of the *strain tensor*, which is a measure of the physical deformation required to convert one cell into the other [78]. It is derived from the length and angle parameters of each of the two lattices involved. Strain tensor computation is implemented in the Bilbao Crystallographic Server [79]. However, the strain tensor can be shown not to be a metric, since it does not satisfy the triangle inequality (a counterexample is computed in Appendix A of [80]), and therefore does not address the metric space requirement of Problem 1.4.1.

Other approaches to determining lattice similarity have been designed specifically to aid in Bravais lattice classification from (possibly erroneous) crystallographic data by determining if the parameters of its reduced form is within some small perturbation of any of of the finite number of possible reduced bases of a 'model' Bravais type - see for example similarity definitions in [81], or the algorithms for determining lattice type from data with errors in [82].

These approaches are highly effective in terms of discrete classification, but as discussed in previous sections, approaches which assign lattices to a particular class if their parameters are within some given tolerance are again not suitable for addressing Problem 1.4.1 - as illustrated in Figure 2.2, such an approach makes a single equivalence class of all lattices.

2.4 Conclusion

In this chapter we have discussed three key foundations to the work in this thesis from the field of lattice geometry. From the various reduced lattice bases investigated, none are (or, as proved in [23], can be) in themselves continuous, but our own work selects one that is less commonly used in crystallography, but may have continuous quantities derived from it.

This same reduction leads to a particular discrete categorisation of lattices which again is not commonly used, since it is less granular that either point groups, Bravais lattices or lattice Characters. As we show in the following chapter, however, that the continuous space we derive from this classification has the Bravais lattices and indeed characters arising 'naturally' arising as subspaces, and thus its parameters are the most suitable for addressing the problem of continuous lattice classification and comparison.

We have, finally, discussed previous approaches to continuous classification and comparison of lattices, and discussed a number of approaches which have proved effective in the practical discrete classification of lattices, but fall short of fully and rigorously addressing all of the requirements of our research problem. In the rest of the thesis we will close this gap.

Chapter 3

Continuous Classification of 2D Lattices

(This chapter is adapted from the paper 'Geographic-style Maps for Two Dimensional Lattices', authored by M.B. A. Cooper and V. Kurlin, published in *Acta Crystallographica A* in 2023).

3.1 Contributions and Chapter Outline

In this section our main contribution is the rigorous solution of sub-problems $1, 4$ and 5 (completeness, invertibility and computibility) of Problem 1.4.1 for two dimensional lattices, and a less formal demonstration of continuity by deriving a complete isometry invariant which can easily be adapted to be invariant under the stronger condition of rigid motion. We show that this invariant is easy to compute, and that a lattice may be uniquely reconstructed from the invariant up to the correct equivalence relation. We have implemented the code to compute this invariant and used it to provide the first view of the continuous space of all existing lattice structures of real crystals, decomposed into a set of three $2D$ lattices. In this work we build on a number of statements made by Conway in his series of papers on lattices [83], which had truncated or incomplete proofs which can be found in expanded and corrected forms in [84], leading to the development of the maps in [32]. We will demonstrate in this chapter that the invariant varies by a small defined amount under small lattice perturbations. In Chapter 4 we will impose explicit metrics and by showing that they have formal continuity properties under lattice perturbation, rigorously demonstrate that the invariant also provides a solution to sub-problems 2 and 4.

We will begin by focussing on the specific view of lattice symmetries and lattice reductions which allow for our continuous approach, which was the Selling reduction outlined in Chapter 2 (see Definition 3.2.9). As promised in chapter 2, we will provide a detailed view of this topic, and the resulting simpler but more geometrically informative - and, crucially, continuous - classification of lattice symmetries.

We will then work through the key proofs that the Selling reduction does in fact lead to a continuous lattice invariant, and explain how this invariant gives rise to a three dimensional space in which we can visualise the space of all equivalence classes of lattices up to isometry (or rigid motion), and define maps for visualising equivalence classes of lattices up to isometry or rigid motion and similarity in two. We will apply two different versions of these maps to a large dataset of crystals from the Cambridge Structural Database [16], and thus demonstratee that real, physical crystals occupy a continuous subset of that space, justifying our continuous classification approach.

All empirical results in this section appear in [32] and arise from computations using the code written by the author of this thesis at
`https://github.com/MattB-242/Lattice_Invariance`.

3.2 Theoretical Background

3.2.1 Voronoi Domains, Voforms and Coforms

We have already encountered two different ways of looking at n-dimensional lattices: as a selection of n linearly independent basis vectors, divided into equivalence classes up to isometry (or rigid motion) and change of basis, and as a discrete subgroup of linear transformations of $\mathbb{R}^n$. We will now consider a third view of lattices, as a specific instance of a more general definition of discrete sets of points in $\mathbb{R}^n$, introduced by Delone (the anglicised spelling is sometimes given as Delauney, although we will use Delone throughout) [85]:

Definition 3.2.1 (Delone Set)**.** *A discrete subset $X \subset \mathbb{R}^n$ is a* Delone Set *if the following two conditions apply:*

1. *There exists some positive real number r such that every open ball in $\mathbb{R}^n$ of radius less than r contains at most one point of X (equivalently, for $x, y \in \mathbb{R}, ||x - y|| < r$)*
2. *There exists some positive real number R such that every closed ball in $\mathbb{R}^n$ of radius greater than R contains at least one point of X.*

Informally, points in a Delone set are separate (the first condition) but never infinitely far apart (the second condition). For every point in a Delone set we define a particular geometric structure:

Definition 3.2.2 (Voronoi Cell)**.** *Let $p \in X \subset \mathbb{R}^n$ be a point in a Delone set. The* Voronoi cell *of p is the set of all points in $\mathbb{R}^n$ that are closer to p than to any other point of X.*

$$V(p) = \{x \in X | ||p - x|| \leq ||p - y||\} \forall y \in X$$

Voronoi cells for a point in a Delone set are constructed by taking the hyperplanes normal to and bisecting line segments of the *star* of the point - the lines between that point and all other points in the set. A subset of these hyperplanes will enclose a polytope surrounding

the point - since that polytope is an intersection of convex sets, it will itself be a convex set. In two dimensions the bisectors are lines, and the polytopes are more usually called *parallelotopes*

Clearly a lattice is an example of a Delone set, since every point is at least at a distance of the first successive minimum (see Definition 2.1.5) λ_1 away from any other, and any closed ball of diameter greater than λ_1 must contain at least one point of the lattice.

Furthermore, since any point in a lattice maps to any other point in the lattice, the set of distances of any point in a lattice to its neighbouring points is identical. Conversely, if the Voronoi cells of any pair of points in a Delone set are identical, then the set of distances between those points and their neighbouring ones must be identical. This proves the following geometrically intuitive theorem, which means we may speak of 'the Voronoi cell' of a lattice:

Theorem 3.2.3 ([86], Lemma A2)**.** *A Delone set is a lattice if and only if all of its Voronoi cells are related to each other by a translation.*

Thus, a lattice can be defined by the configuration of its Voronoi cell. Figure 3.1 shows the Voronoi cells for the five $2D$ Bravais types. The comparison of Voronoi cells is thus another potential continuous classification approach, and indeed such a metric, based on the comparison of two such cells over all of their rotational orientation to each other has been developed [87] - in fact this this represents the first formal approach to Problem 1.4.1. It falls short as a solution only because computability involves comparison over the infinite, continuous set of all rotational orientations. It has been implemented as an approximate algorithm which selects a discrete subset of these orientations, and has successfully used in this case as a descriptor in the prediction of lattice energies via machine learning [88].

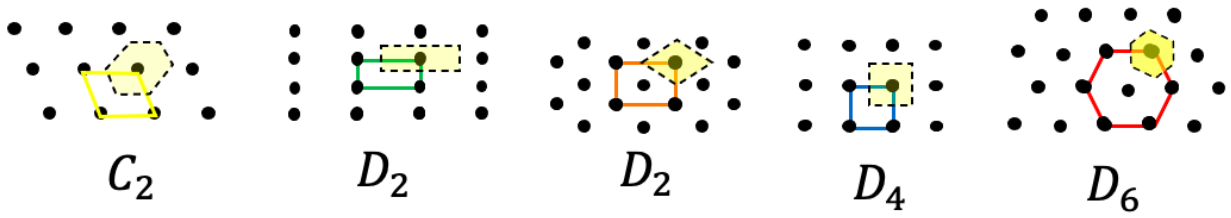

Figure 3.1: Voronoi cells for the five Bravais lattice types in 2 dimensions

If a Delone set is embedded in $\mathbb{R}^n$ then clearly every point in $\mathbb{R}^n$ must be in some Voronoi cell since it is closest to at least one point of the set. From this fact and Theorem 3.2.3 it is immediately clear that some polytope is the Voronoi cell of a lattice if and only if it tiles $\mathbb{R}^n$ - that is, $\mathbb{R}^n$ can be completely covered by translates of the Voronoi cell. In particular, we see that $\mathbb{R}^2$ can be tiled only by a rectangle (of which squares are a special case), a rhombus and a hexagon whose parallel sides are of equal length (of which the regular hexagon is a special case). This is illustrated in Figure 3.1, from which it is visible that the discrete classification of lattices by the *shape* of their Voronoi cells is coarser than any approach discussed in Chaper 2. We can more formally define the notion of 'shape' in the context of a polytope as follows:

Definition 3.2.4 (Combinatorial equivalence of polytopes)**.** *Two $d-$dimensional polytopes P_1, P_2 are* combinatorially equivalent *if there is a one-to-one mapping between every face of every dimension - that is, both P_1 and P_2 have the same number of d-dimensional faces, and for every $k-1$-dimensional face arising from the meeting of n $k-$dimensional faces in P_1 there is a $k-1$-dimensional face arising from the meeting of the same number of k-dimensional faces in P_2*

Example 3.2.5. *The Voronoi cells in the C_2 and D_6 case of Figure 3.1 are combinatorially equivalent - they have six one-dimensional faces (edges), and every pair of such faces meets in a 0-dimensional face (a vertex). They are not combinatorially equivalent to the D_2 and D_4 cases since these have only 4 faces.*

There are thus really only two types of Voronoi cell of a two Dimensional lattice in the sense of definition 3.2.4 - a hexagon and a quadrilateral. As with Bravais types there is a continuous relationship between the two Voronoi types in that one may retrieve the quadrilateral type by continuously shortening a pair of parallel of the hexagonal type. In three dimensions, there only five combinatorial types of Voronoi cell - these were orginally identifed over a century ago by Fedorov [89], and their relation to the continuous classification of crystals, again by continuous deformations of one polytope into another, is still a subject of active discussion [90].

Clearly only a finite subset of the (infinite) set of bisectors of the star of a point in the lattice will actually form the boundaries of its Voronoi cell. The following definition specifically distinguishes vectors which determine these bisectors.

Definition 3.2.6 (Voronoi vector)**.** *A* Voronoi vector *of a lattice in $\mathbb{R}^d$ is any vector v whose bisecting hyperplane $\{x : v \cdot x = \frac{1}{2}||v||\}$ intersects the Voronoi cell (Definition 3.2.2) about the lattice point at the origin. The vector is* strict *if the bisecting hyperplane also intersects a $d-1$ dimensional face of the Voronoi cell, and* non-strict *otherwise.*

To understand why Voronoi vectors are useful in both reduction and continuous classification, we require the following definition:

Definition 3.2.7 (Quotient Lattice)**.** *For a lattice Λ we denote by $n\Lambda$ the sublattice consisting of all lattice vectors of the form nv for $v \in \Lambda$.*

If $u, v \in \Lambda$ and $u - v \in n\Lambda$ then u and v are equivalent in $n\Lambda$*. It is easily checked that this is indeed an equivalence relation, and we denote by $\Lambda/p\Lambda$ the* quotient lattice *whose members are such equivalence classes of lattices.*

Definition 3.2.7 allows us to state the following key theorem.

Theorem 3.2.8 ([83], Theorem 2)**.** *A vector v of a lattice Λ is a Voronoi vector if and only if it is the shortest lattice in its equivalence class in the quotient lattice $\Lambda/2\Lambda$. It is a* strict *Voronoi vector if $\pm v$ are the only two vectors in their equivalence class.*

.

3.2.2 The Obtuse Superbase

The *obtuse superbase* of a lattice was briefly discussed in Chapter 1 (see Definition 3.2.9). As promised, we now give a more detailed mathematical exposition that will enable us to relate it to our new lattice invariant.

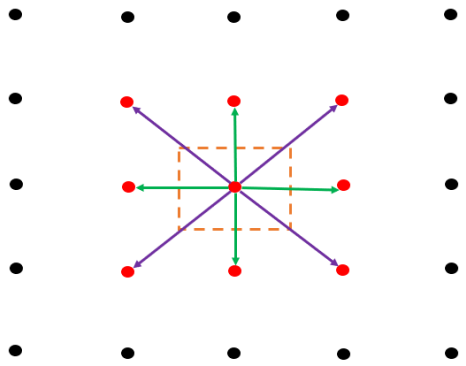

Figure 3.2: A rectangular lattice, with its Voronoi cell (brown) and Voronoi vectors indicated - the green arrows indicate strict vectors, the purple ones are non-strict since they pass through a vertex (0-dimensional face) of the Voronoi cell rather than a face. The red points indicate representative elements of the lattice $\Lambda/2\Lambda$.

Definition 3.2.9. *(Selling Reduction) Let $v_1, \dots v_n$ be the basis of a lattice. The* superbase *is the basis augmented with an additional vector $v_0 = -\sum_{i=1}^{n} v_i$. A basis is* Selling reduced *if the superbase is* obtuse *- that is, for all $i \neq j$ the* Selling parameters *$p_{ij} = -(v_i \cdot v_j) \geq 0$.*

While 'Selling reduction' is the standard nomenclature for this approach in crystallographic literature, it has been proposed separately by not only Selling [91] but also Seeber [92], both of whom considered only three dimensional lattices (in both cases from the point of view of their gram matrices as ternary quadratic forms). Charve [93] extended the idea to four dimensions, and Delone [85] suggested a more general version.

An important theorem of Delone [94] allows us to use the Selling reduction in the analysis of lattices in dimensions 2 and 3.

Theorem 3.2.10 ([94], Theorem 1)**.** *Every lattice of dimension $d \leq 3$ admits an obtuse superbase.*

If a lattice has an obtuse superbase with Selling parameters p_{ij}, then the squared norm of any vector $u \in \Lambda$, can expressed in terms of the Selling parameters using Selling's formula:

Theorem 3.2.11 (Selling [91], p169)**.** *Let Λ have an obtuse superbase $\{v_0, \dots v_n\}$ in $\mathbb{R}^n$. We may express any vector v in Λ as the integer sum $\sum_{i=0}^{d} a_i v_i$ of superbase vectors, and*

$$||v||^2 = \left|\left|\sum_{i=0}^{d} a_i v_i\right|\right|^2 = \sum_{0 \leq i < j}^{n} (a_i - a_j)^2 p_{ij}$$

From this equation, Conway derives the following crucial theorem, which connects the obtuse superbase to the Voronoi vectors.

Theorem 3.2.12. *[[83], Theorem 3] Let $\{v_0, \dots v_n\}$ be an obtuse superbase of a lattice of the first kind. Then for $S \subset \{0, \dots, n\}$,*

$$v_S := \sum_{i \in S} v_i$$

are the Voronoi vectors of the lattice. If U is the complement of S in $\{0, \dots n\}$ then $v_U = -v_S$, otherwise $U \neq S \implies v_U - v_S \notin 2\Lambda$ - that is, v_U, v_S are in different equivalence classes of the quotient lattice $\Lambda/2\Lambda$

Proof. By Theorem 3.2.8 the Voronoi vectors are the shortest vectors in their equivalence class in $\Lambda/2\Lambda$ - these will be the ones where the integer coefficients of all basis vectors are equal to ± 1 or 0. By Selling's formula we minimise the norm of any vector, expressed as a sum of obtuse superbase vectors, by minimising the coefficients $(a_i - a_j)^2$ of Theorem 3.2.11 for any i, j for which $p_{ij} > 0$. Since all the coefficients $(a_i - a_j)^2$ will be in $\mathbb{Z}_2$, they will be exactly the vectors defined in Theorem 3.2.12. □

We can use the above to demonstrate that the obtuse superbase provides a source of isometry invariants for a two dimensional lattice.

Lemma 3.2.13. *[[84], Theorem 3.7] A pair of two dimensional lattices Λ, Λ' are related by isometry if and only all of their obtuse superbases are isometric. If Λ is not of primitive rectangular Bravais type (see Figure 2.7) , then the lemma also holds for rigid motion. If Λ is of primitive rectangular Bravais type then it has two isometry classes of obtuse superbase, related by a reflection.*

Proof. $\implies$ Any isometry between B and B' extends to an isometry between the lattices Λ, Λ' generated by the superbase vectors.

$\impliedby$: By Theorem 3.2.12 the only two superbases of a non-rectangular lattice are given by the vectors $\{v_1, v_2, -v_1 - v_2\}$ and $\{-v_1, -v_2, v_1 + v_2\}$, which are related by a rotation of π about the origin.

Any rectangular lattice with orthogonal reduced basis vectors v_1, v_2 has a superbase related by reflections in the line along v_1 or v_2, so that as well as the two superbases $\{v_1, v_2, -v_1 - v_2\}, \{-v_1, -v_2, v_1 + v_2\}$ related by rigid motion, we also have obtuse superbases $\{v_1, -v_2, v_2 - v_1\}$ and $\{-v_1, v_2, v_1 - v_2\}$. If the lattice is square then $||v_1|| = ||v_2||$ and these bases are once again isometric, related by rotations of $\pi/2$ about the origin. □

Note that as part of the proof of Theorem 3.2.13 we state that any isometry of a lattice extends to an isometry of an obtuse superbase of that lattice. To avoid unnecessary verbiage or notation, unless it is important to point out the multiplicity of possible obtuse superbases, references to 'an obtuse superbase B of a lattice Λ' should be taken to refer to the equivalence classes of both objects up to to isometry.

3.2.3 Finding the Obtuse Superbase

If we are to satisfy the computability requirement of Problem 1.4.1, then there must be some algorithmic way of finding an obtuse superbase. Such an algorithm is outlined, but not fully detailed, for two dimensional lattices in [83]. Geometrically, if any pair of vectors v_i, v_j give rise to a positive inner product, the vector v_i is replaced by $-v_i$

Algorithm 3 Obtuse Superbase in 2 Dimensions (adapted from the description in [83])

Input: Any linearly independent vectors v_1, v_2

Output: An obtuse superbase u_1, u_2, u_0 for the lattice generated by the basi vectors v_1, v_2.

Compute superbase vector $v_0 = -(v_1 + v_2)$
Compute $p_{ij} = -v_i \cdot -v_j$ for all $i < j \in \{0, 1, 2\}$
while $p_{ij} > 0$ for some $i, j \in \{0, 1, 2\}$ **do**
    for $i < j \in \{0, 1, 2\}$
    if $p_{ij} < 0$ **then**
        $u_1 \leftarrow -v_i$
        $u_2 \leftarrow v_j$
        $u_0 \leftarrow v_j - v_i$
        $p_{ij} \leftarrow -u_i \cdot u_j$
    end if
end while

The effectiveness of the algorithm is stated in the following theorem, which was asserted but not formally proved by Conway:

Theorem 3.2.14 ([86], Appendix A)**.** *Algorithm 3 terminates and outputs the unique (up to isometry) superbase of the lattice generated by the input vectors.*

Proof. Suppose $v_1 \cdot v_2 > 0$. In the next step of the algorithm, the vector norms $||u_1||^2 = ||v_1||^2$ and $||u_2||^2 = ||v_2||^2$ unchanged. However, $||u_0||^2 = ||v_2 - v_1||^2 = (v_2 - v_1) \cdot (v_2 - v_1) = ||v_1||^2 + ||v_2||^2 - 2v_1 \cdot v_2 \leq ||v_1||^2 + ||v_2||^2 \leq ||v_1 + v_2||^2 = ||v_0||^2$.

Thus each step of the algorithm shortens one superbase vector, while leaving the rest unchanged. Since the lattice generated by the input vectors is discrete, it cannot contain any vectors of zero length, and the algorithm must therefore terminate when some shortest vector has been reached.

By Theorem 3.2.10 an obtuse superbase exists, so we must reach it at some point prior to the termination of the algorithm, and by Lemma 3.2.13, the resulting obtuse superbase is unique up to isometry (or rigid motion, if the lattice does not have rectangular symmetry). □

3.3 Defining Lattice Invariants

In the previous section, we demonstrated that for two dimensional lattices the obtuse superbase is unique up to isometry, and that an obtuse superbase is in principle computable from any set of input basis vectors. We are now in a position to define invariants under rigid motion, isometry and similarity that solve Problem 1.4.1 for two dimensional lattices. We begin by recalling the terminology and notation used by Conway [83] to define the geometric parameters of the obtuse superbase.

Definition 3.3.1 (see [83], Theorems 4 and 6)**.** *Let Λ be a lattice of Voronoi's first kind and $v_0, \ldots v_n$ an obtuse superbase. For $S \subset \{0, \ldots, n\}$ the* vonorms *are the squared lengths of all Voronoi vectors:*

$$v_S^2 := ||v_S||^2$$

The pairwise Selling parameters

$$p_{ij} = -v_i \cdot v_j$$

of an obtuse superbase of the lattice are its conorms

The removal of the standard notation for norms in this case is simply for ease of reading since we will refer to these quantities repeatedly in the text - in what follows the notation v_S^2 will be used exclusively for the norms of vectors in an obtuse superbase, while the standard notation will be employed for norms of any other kind.

The following simple computation on vonorms in general dimension follows from $v_0 = -\sum_{i=1^n} v_i$:

$$v_S^2 = \left(\sum_{i \in S} v_i\right) \cdot \left(-\sum_{j \notin S} v_j\right) = \sum_{i \in S, j \notin S} p_{ij}$$

and gives us some useful algebraic relationships between the vonorms and conorms of an obtuse superbase of a two dimensional lattice:

$$v_0^2 = p_{01} + p_{02},\ v_1^2 = p_{01} + p_{12},\ v_2^2 = p_{02} + p_{12}$$

and hence

$$p_{12} = \frac{1}{2}(v_1 + v_2 - v_0),\ p_{01} = \frac{1}{2}(v_0 + v_1 - v_2),\ p_{02} = \frac{1}{2}(v_0 + v_2 - v_1)$$

These relationships combined with the Selling formula of Theorem 3.2.11 give rise to a useful theorem regarding the vonorms, proved in [83]:

Theorem 3.3.2 ([83], Theorem 7)**.** *The vonorms v_1^2, v_2^2, v_0^2 of an obtuse superbase of a lattice in $\mathbb{R}^2$ are the squares of the three successive minima of the lattice (see Definition 2.1.5.*

Proof. The Selling formula means that the length of any vector v in the lattice is given by

$$||v|| = \sum_{0 \leq i < j \leq 2} (a_i - a_j)^2 p_{ij}, a_i, a_j \in \mathbb{Z}$$

If $a_0 = a_1 = a_2$ than v is the null vector, so for v to be a superbase vector at least one of the three coefficients must be unequal.

Suppose (without loss of generality) that $a_0 \neq a_1$ and $a_1 = a_2$. Then $v = a_1(v_1 + v_2) - a_0(v_0) = (a_0 - a_1)(v_1 + v_2)$ which is some multiple of v_0 which is minimised for $a_0 = \pm_1, a_1 = 0$or $a_0 = 0, a_1 = \pm 1$ and in either case $v = \pm v_0$.

The final case is $a_0 \neq a_1 \neq a_2$. Then $||v||^2 \geq p_{12} + p_{01} + p_{02}$. But since any $v_i = p_{ij} + p_{ik}$ for $i \neq j \neq k \in \{0, 1, 2\}$, v must be longer than any v_i. □

3.3.1 The Root Invariant

We are now in a position to define the contributions to lattice classification discussed in this work, and to begin the work of proving that they have all of the properties required to address Problem 1.4.1.

Definition 3.3.3 ([84], Definition 3.1)**.** *Let $B = v_0, v_1, v_2$ be the obtuse superbase of a lattice Λ, with lengths ordered such that $v_1^2 \leq v_2^2 \leq v_0^2$*

The root products *of Λ are the roots of the Selling Parameters $r_{ij} = \sqrt{-v_i \cdot v_j}$ for $i, j \in \{0, 1, 2\}$.*
The Root Invariant *is given by*

$$\mathrm{RI}(\Lambda) = (r_{12}, r_{01}, r_{02})$$

.

The relationship between the parameters of an obtuse superbase discussed above means that the ordering of the root products induces an ordering on the lengths of the vectors in the obtuse superbase:

Proposition 3.3.4 (see Appendix A in [80])**.** *For the root invariants of any lattice, if $r_{12} \leq r_{01} \leq r_{02}$ then $v_1^2 \leq v_2^2 \leq v_0^2$.*

Proof. Working for ease of computation with the conorms, we compute:

$$p_{02} = -v_0 \cdot v_2 = -v_0 \cdot v_2 = (v_1 + v_2) \cdot v_2 = |v_2|^2 - p_{12},$$

and similarly $p_{01} = -v_0 \cdot v_1 = (v_1 + v_2) \cdot v_1 = |v_1|^2 - r_{12}^2$. Taking the difference, $p_{02}^2 - p_{01}^2 = |v_2|^2 - |v_1|^2 > 0$ and thus $p_{01} \leq p_{02}$. We can also express

$$p_{01} = -v_0 \cdot v_1 = v_0 \cdot (v_0 + v_2) = |v_0|^2 - p_{02}$$

$$p_{12} = -v_1 \cdot v_2 = (v_0 + v_2) \cdot v_2 = |v_2|^2 - p_{02}$$

Again, taking the difference $p_{01} - p_{12} = |v_0|^2 - |v_2|^2 > 0$ and thus $p_{12} \leq p_{01}$. □

Example 3.3.5. *A primitive rectangular lattice Λ_{p2mm} with basis $v_1 = (a, 0), v_2 = (0, b)$ has an obtuse superbase consisting of these two vectors and $v_0 = (-a, -b)$. It has another obtuse superbase related by reflection, given by $v_1' = (a, 0), v_2' = (0, -b), v_0 = (-a, b)$. The root product of both bases is given by $RI(\Lambda_{p2mm}) = (0, a, b)$.*

Let a centered rectangular lattice Λ_{c2mm} have an obtuse superbase $v_1 = (a, b), v_2 = (a, -b), v_0 = (-2a, 0)$. Its root products are given by $r_{12} = \sqrt{b^2 - a^2}, r_{01} = r_{02} = \sqrt{2}a$. The root invariant is given by

$$\mathrm{RI}(\Lambda_{c2mm}) = \begin{cases} (\sqrt{b^2 - a^2}, \sqrt{2}a, \sqrt{2}a) & b^2 > 3a^2 \\ (\sqrt{2}a, \sqrt{2}a, \sqrt{2}a) & b^2 = 3a^2 \\ (\sqrt{2}a, \sqrt{2}a, \sqrt{b^2 - a^2}) & b^2 > 3a^2 \end{cases}$$

In the second case above, note that the vonorms $v_1^2 = v_2^2 = v_0^2$ and the lattice is in fact hexagonal (that is, all vectors in the lattice are of equal length).

The examples above form part of the proof of the following lemma:

Lemma 3.3.6 ([84], Lemma 3.3)**.** *An obtuse superbase generates a lattice Λ with a mirror symmetry if and only if one of the following conditions for the root invariant hold:*

1. *One of the root products in* $\mathrm{RI}(\Lambda)$ *takes the value zero*
2. *Some pair of the root products in* $\mathrm{RI}(\Lambda)$ *are equal.*

Proof. $\implies$ Suppose there is a zero value in the root product. Then the two vectors which are orthogonal to each other generate a primitive rectangular superbase, which has a mirror symmetry. Suppose two root products are equal, say $p_{01} = p_{02}$. Then

$$v_0^2 + v_1^2 = v_0^2 + v_2^2$$

and thus v_1, v_2 in the obtuse superbase have the same length. We may permute v_1, v_2 through a reflection in their bisector, which will not affect $v_0 = -(v_1 + v_2)$.

$\impliedby$ The only lattices with a mirror symmetry are either primitive rectangular, centred rectangular, square or hexagonal. The computations of Example 3.3.5 show that a primitive rectangular lattice has a zero in its root product, and a square lattice is simply a primitive rectangular lattice with two equal basis vectors. Similarly, a centered rectangular lattice has two equal root products, and a hexagonal lattice is a centered rectangular lattice where the angle between any pair of superbase vectors are equal. □

Definition 3.3.7 ([84], Definition 3.4)**.** *Let $B = v_1, v_2, v_0$ be the obtuse superbase of a lattice such that $||v_1|| \leq ||v_2|| \leq ||v_0||$. The* sign *$sign(B)$ of the superbase is equal to 0 if it has a mirror symmetry, otherwise it is equal to the sign of the determinant of the matrix whose columns (in order) are v_1, v_2.*

The Orientation Aware Root Invariant *is the decorated ordered triple*

$$\mathrm{RI}^o(B) := (r_{12}, r_{01}, r_{02})_\varepsilon$$

where $\varepsilon = \mathrm{sign}(B)$.

For notational clarity the subscript of RI^o is omitted for the ordered triple of a lattice with mirror symmetry, since by Lemma 3.3.6 this will be immediately visible in the root invariant from either $r_{12} = 0$ or some pair of values being equal.

Lemma 3.3.8 ([84], Lemma 3.8)**.** *The sign of an obtuse superbase (Definition 3.3.7 is an invariant of a lattice up to both rigid motion (Definition 1.3.2) and similarity under rigid motion (Definition 1.3.8).*

Proof. If Λ, Λ' have obtuse superbases ordered by length $B = \{v_1, v_2, v_0\}, B' = \{u_1, u_2, u_0\}$ related by a rigid motion, then the matrix M whose columns are v_1, v_2 may be transformed into the matrix M' whose columns are u_1, u_2 via multiplication by some rotation matrix $R \in SO_2(\mathbb{R})$, which has determinant 1, and which therefore will not change the sign of the determinant of M. Similarly, if Λ and Λ' are similar then M may be transformed into M' via multiplication by some scaling matrix λI for $\lambda \in \mathbb{R}^+$, and since $\lambda > 0$ this matrix also has positive determinant and therefore will not change the sign of M. □

In what follows, we may therefore refer to the sign of the obtuse superbase of definition 3.3.7 as the sign of the lattice itself.

Example 3.3.9. *The signs of the lattices in Example 3.3.5 are all zero, since they are mirror symmetric.*

Let $v_1 = (3, 0), v_2 = (-1, 3), v_0 = (-2, -3)$ *be a superbase* B *of a lattice. All inner products are negative so the superbase is obtuse and* $||v_1|| \leq ||v_2|| \leq ||v_0||$.

The root invariant is $\mathrm{RI}(B) = (\sqrt{3}, \sqrt{6}\sqrt{7})$ *- by Lemma 3.3.6 the lattice is not mirror symmetric. Since* $\det \begin{pmatrix} 3 & -1 \\ 0 & 3 \end{pmatrix} = -9$, $\mathrm{sign}(\Lambda) = -1$ *and* $\mathrm{RI}^o(B) = (\sqrt{3}, \sqrt{6}\sqrt{7})_-$.

A mirror reflection in the x axis gives a superbase B' *generated by* $v_1 = (3, 0), v_2 = (-1, -3), v_0 = (-2, 3)$. *The root products remain unchanged, but*

$$\det \begin{pmatrix} 3 & -1 \\ 0 & -3 \end{pmatrix} = 9, \mathrm{sign}(\Lambda') = +1 \text{ and } \mathrm{RI}^o(B') = (\sqrt{3}, \sqrt{6}\sqrt{7})_+$$

Figure 3.3 illustrates the computations of Example 3.3.9, and their geometric meaning. Since we order the length of the superbase vectors the values of root products do not change, but they are ordered 'clockwise' rather than 'anticlockwise'.

The following Theorem shows that all these invariants satisfy the completeness requirement of Problem 1.4.1:

Theorem 3.3.10 ([84], Theorem 4.2)**.** *The Root Invariant is a* complete *invariant of two dimensional lattices up to isometry, and the orientation-aware root invariant is a* complete *invariant of two dimensional lattices up to rigid motion.*

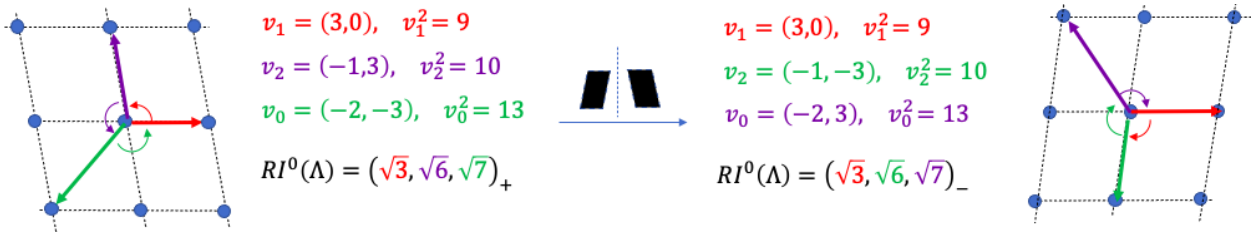

Figure 3.3: Computing the oriented root invariant RI^o for the reflected lattices of example 3.3.9

Proof. By Lemma 3.2.13, the obtuse superbase is an isometry invariant of a lattice, and since an isometry by definition does not change lengths of vectors or the angles between them, the inner products of the superbase will also not change.

To prove completeness, suppose that we have two non-isometric lattices Λ, Λ' such that $\mathrm{RI}(\Lambda) = \mathrm{RI}(\Lambda') = (r_{12}, r_{01}, r_{02})$. Now since the vonorms of the obtuse superbase can be computed directly from the root products, all vectors of the obtuse superbase must have the same length, so if Λ, Λ' are non-isometric then some pair of superbase vectors must have unequal angles. But in this case the inner products (and hence the Selling parameters) of the obtuse superbase must be unequal, leading to a contradiction. □

We have thus have mapped the rather complicated space of isometry classes of two dimensional periodic lattices - the Lattice Invariance Space of Definition 1.3.11 - to a much simpler set which consists simply of ordered triples of positive real numbers (which we can consider as a subset of three dimensional Euclidean space). Theorem 3.3.10 allows us to simplify our notation somewhat - for a given lattice Λ we may speak of the (orientation-aware) root invariants of a *lattice* $\mathrm{RI}(\Lambda)$ and $\mathrm{RI}^o(\Lambda)$.

Theorem 3.3.10 confirms that a lattice most be uniquely determined by its root invariant. However, we may go further and address the *computability* requirement of problem 1.4.1:

Theorem 3.3.11 ([86], Lemma 4.1)**.** *Any two dimensional lattice can be directly reconstructed as a unique basis in $\mathbb{R}^2$ up to isometry from its root invariant, and up to rigid motion from its oriented root invariant*

Proof. We demonstrate the unique computation of a lattice from its (oriented) root invariant $\mathrm{RI}^o(\Lambda) = (r_{12}, r_{01}, r_{02})_\epsilon$. Now $v_1^2 = r_{12}^2 + r_{01}^2$, so we may orient the shortest vector along the x axis of $\mathbb{R}^2$ as

$$v_1 = (\sqrt{r_{12}^2 + r_{01}^2}, 0)$$

Similarly, we may calculate the length of v_2, and the (obtuse) angle between the two vectors is then given by $\theta = \arccos(-r_{12}/||v_1||||v_2||)$. If the root invariant is oriented and $\varepsilon = \mathrm{sign}(\Lambda) \neq 0$ then

$$v_2 = (||v_2|| \cos\theta, \varepsilon ||v_2|| \sin\theta)$$

otherwise the factor ε is omitted in the calculation of v_2. □

3.3.2 Similarity Invariants

If we are interested in lattices only up to similarity as in Definition 1.3.8, then any scaling factor λ on the length of basis vectors mutiplies the root invariants by λ^2 - thus the root invariants of similarity classes of lattices are related by multiplication by some constant factor.

The usual quantity indicating the scale of a lattice is its volume $V(\Lambda)$ (Definition 1.3.4). However, the volume has no theoretical lower bound - scaling a root invariant by $1/V(\Lambda)$ therefore gives the possibility of infinitely large root products in the root invariant. We define the following alternative quantity, which also simplifies computation of the resulting invariant.

Definition 3.3.12. *(Lattice size) The* size $\sigma(\Lambda)$ *of a lattice* Λ *with root invariant* $\mathrm{RI}(\Lambda) = (r_{12}, r_{01}, r_{02})$ *is*

$$\sigma(\Lambda) := r_{12} + r_{01} + r_{02},$$

the sum of all the root products in its root invariant. For any root product r_{ij} *of a two dimensional lattice, we define* $\bar{r}_{ij} := r_{ij}/\sigma$.

Lemma 3.3.13 ([84], Lemma 7.4)**.** *Let a lattice* Λ *have obtuse superbase* $B = \{v_0, v_1, v_2\}$ *such that* $\max_{v \in B} ||v|| = l$. *Then* $\sigma(\Lambda) \geq l$.

Proof. The proof follows from computation using the relationships between vonorms and conorms. Suppose without loss of generality that $|v_1| = l$. Then $v_1^2 = l^2 = p_{01} + p_{12}$. Now $\sigma(\Lambda) = \sqrt{(r_{12} + r_{01} + r_{02})^2} \geq \sqrt{r_{12}^2 + r_{01}^2 + r_{02}^2} = \sqrt{p_{12} + p_{01} + p_{02}} \geq l$. □

The size has an additional benefit in an applied context, in that like the root product it retains the same units as the length parameters of the lattice vectors. In general where it is obvious from context which lattice is being referred to, we will refer to the size of a lattice simply by σ. Using this quantity, we define the following similarity invariant

Definition 3.3.14 ([84], Definition 4.5)**.** *Let a lattice have (oriented) root invariant* $\mathrm{RI}(\Lambda) = (r_{12}, r_{01}, r_{02})$. *The* projected invariant *of the lattice is given by*

$$\mathrm{PI}(\Lambda) := (\bar{r}_{02} - \bar{r}_{01}, 3\bar{r}_{12})$$

Its oriented projected invariant $\mathrm{PI}^o(\Lambda)$ *is defined in the as its projected invariant with a signed subscript matching that of* $\mathrm{RI}^o(\Lambda)$.

We have chosen this particular mapping of the values of the root invariant to assist in visualisation of similarity classes of lattices in a manner that will be discussed in subsequent sections.

Theorem 3.3.15 ([86], Proposition 4.9)**.** *The (oriented) root invariant of any lattice Λ can be uniquely computed up to a scaling factor from an (oriented) projected invariant.*

Proof. Let $PI^o(\Lambda) = (x, y)_\epsilon$. Clearly $r_{12}/\sigma = y/3$. Now recall that by the definition of $\sigma(\Lambda)$, $\bar{r}_{12} + \bar{r}_{01} + \bar{r}_{02} = 1$ and therefore $x + y = 1 - (2r_{01} + 2r_{12}/\sigma \implies r_{01}/\sigma = (3 - 3x - y)/6$, from which we immediately compute $r_{02}/\sigma = 1 - y/3 - r_{01}/\sigma = (3 + 3x - y)/6$. Thus

$$\frac{1}{\sigma}\mathrm{RI}^o(\Lambda) = \left(\frac{3 - 3x - y}{6}, \frac{3 - 3x + y}{6}, y/3\right)_\varepsilon$$

where ε is the sign of the lattice (if nonzero). □

This computation illustrates the following corollary:

Corollary 3.3.16 ([84], Corollary 4.6)**.** *The projected invariant is a complete similarity invariant of a lattice.*

Proof. The computation proving Theorem 3.3.15 shows that a projected invariant is a complete invariant up to scaling of a root invariant, and from Theorem 3.3.10 any root invariant is a complete invariant of a lattice. □

Example 3.3.17. *The isometry class of hexagonal lattices Λ_{p6mm} all have root invariants* $\mathrm{RI}(\Lambda_{p6mm}) = (a, a, a)$ *for $a > 0$, and thus are identical up to a scaling factor. All such lattices have a single projected invariant* $\mathrm{PI}(\Lambda_{p6mm}) = (1, 0)$*. Similarly, square lattices all have root invariants* $\mathrm{RI}(\Lambda_{p4mm}) = (0, a, a)$ *and thus have a single projected invariant* $\mathrm{PI}(\Lambda_{p4mm}) = (0, 0)$*.*

Any primitive rectangular lattice with $\mathrm{RI}(\Lambda_{pmm}) = (0, a, b)$ *has* $\mathrm{PI}(\Lambda_{pmm}) = ((b-a)/(a+b), 0)$*. For centered rectangluar lattices the root invariant is either* $\mathrm{RI}(\Lambda_{cmm}) = (a, a, b)$ *and* $\mathrm{PI}(\Lambda_{cmm}) = ((b - a)/(2a + b), 3a/(2a + b)) = (x, 1 - x)$ *for $x = (b - a)/(2a + b)$, or it is* $\mathrm{RI}(\Lambda_{cmm}) = (a, b, b)$ *and* $\mathrm{PI}(\Lambda_{cmm}) = (0, 3a/(a + 2b))$*.*

3.3.3 Continuity of the Root Invariant

In this section we demonstrate that continuity of the root invariant arises from continuity of the obtuse superbase. To do this, we need to prove that the set of both obtuse superbases and the root invariants that arise from them can be defined as metric spaces and then prove that the continuity property of Definition 1.2.10.

A visually intuitive demonstration of why the obtuse superbase (and thus any invariant derived from its parameters) changes continuously with continuous deformations of a lattice is illustrated in Figure 3.4. We consider the deformation of the square lattice discussed in Example 1.3.12 of Chapter 2 and shown in Figure 1.7 - but now we keep track of the obtuse superbase vectors rather than the Niggli reduced basis (which in fact we see always forms one pair of the obtuse superbase). Where the latter changed discontinuously as the lattice was deformed through the higher symmetry centered rectangular configuration where

$v_2 = (1/2, 0)$, the change is simply a permutation of the vector length ordering. The isometry-invariant parameters of the superbase, including the root products, thus remain the same up to a permutation of vector indices. By forcing an order of vector indices through the ordering of root products (see Proposition 3.3.4) the root invariant changes continuously.

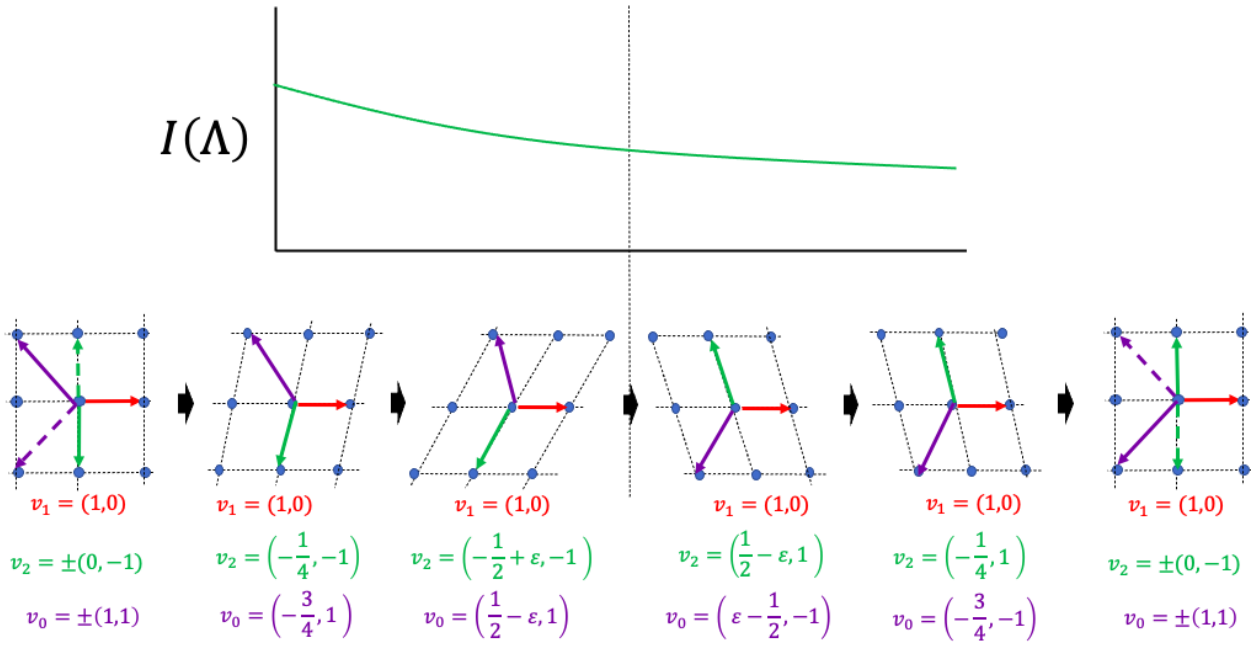

Figure 3.4: Illustration of the continuity property of an obtuse superbase, cf. Figure 1.7. Superbase vectors are shown ordered according by length. Two superbases related by a reflection appear in the square lattice. Continuous deformation through the higher symmetry point results in a permutation of vectors, but all parameters remain continuous

.

To prove this property formally, we need to define a continuous space of obtuse superbases.

Definition 3.3.18 ([84][Definitions 7.1, 7.2)**.**] *Let* $B = \{u_0, u_1, u_2\}, B' = \{v_0, v_1, v_2\}$ *be two obtuse superbases. The* Superbase Similarity Metric $\mathrm{SIM}(B, B')$ *is defined as*

$$\min_{f \ in SO_2(\mathbb{R})} \max_{i=0,1,2} ||f(u_i) - v_i||$$

that is, the minimal distance between all vectors over all possible relative isometries of one lattice with relation to the other. We extend this to the orientation-aware SIM^o *by replacing* $O_2(\mathbb{R})$ *with* $SO_2(\mathbb{R})$*, so that distances are minimised only over rotations. We may also extend this to an (oriented)* Superbase Similarity Metric $\mathrm{SSM}, \mathrm{SSM}^o$ *by adding a continuous scaling of lattice by some factor* $\lambda \in \mathbb{R}^+$*. In this case the relevant groups replacing* $O_2(\mathbb{R})$ *in the definition of* SIM *are the direct products* $O_2(\mathbb{R}) \times \mathbb{R}^+, SO_2(\mathbb{R}) \times \mathbb{R}^+$*.*

The (orientation-aware) Obtuse Superbase Isometry Space OSI *(resp.* OSI^o*) is the space of isometry (resp.rigid motion) classes of obtuse superbases equipped with the metric* SIM *(resp.* SIM^o*). The (orientation aware)* Obtuse Superbase Similarity Space *is the space of similarity classes of obtuse superbases up to rigid motion, equipped with the metric* SSM *(resp.* SSM^o*).*

Lemma 3.3.19 ([84], Lemma 7.2)**.** *The metrics in Definition 3.3.18 satisfy all metric axioms.*

Proof. We give an explicit proof for $\mathrm{SIM}(B, B')$:

Identity: Suppose $\mathrm{SIM}(B, B') = 0$. Then there exists some isometry $f \in O_2(\mathbb{R})$ such that $\max_{i\in\{0,1,2\}} |f(u_i) - v_i| = 0$. Thus B, B' are isometric.

Symmetry: Let f be the isometry in $O_2(\mathbb{R})$ which achieves $\mathrm{SIM}(B, B')$ - that is, $\max_{i=0,1,2} |f(u_i) - v_i|$ is minimised by the action of f Any isometry is invertible (since it has nonzero determinant) and so f^{-1} exists, and furthermore $\max_{i=0,1,2} |f(u_i) - v_i| = \max_{i=0,1,2} |u_i - f^{-1}(v_i)|$ also minimises all vector differences

Triangle Inequality Let $B, B', B'' = (w_0, w_1, w_2)$ be three obtuse superbases, and let f be the isometry achieving $\mathrm{SIM}(B, B')$ and g the one achieving $\mathrm{SIM}(B', B'')$ Now by the definition of SIM and the properties of the Euclidean norm,

$$\begin{aligned}\mathrm{SIM}(B, B'') &\leq \max_{i=0,1,2} |g(f(u_i)) - w_i| \\ &\leq \max_{i=0,1,2} |g(f(u_i)) - g(v_i)| + \max_{i=0,1,2} |g(v_i)) - w_i| \\ &= \mathrm{SIM}(B, B') + \mathrm{SIM}(B', B'').\end{aligned}$$

This proof is applicable across all of the groups involved in the other metrics of Definition 3.3.18 □

This leads us to a demonstration of the continuity of Root Invariants:

Lemma 3.3.20 ([84], Theorem 7.5)**.** *Let B, B' be obtuse superbases of vectors Λ, Λ', and let l be vector of maximum length among the six vectors of these superbases, and suppose $SIM(B, B') = \delta$. Then the maximum absolute difference between any pair of root products in* RIS *is $\sqrt{2l\delta}$.*

Proof. The proof is by a computation involving Cauchy's inequality:

$$\begin{aligned}|u_1 \cdot u_2 - v_1 \cdot v_2| &= |(u_1 - v_1) \cdot v_2 + (u_2 - v_2) \cdot (v_1)| \\ &\leq |(u_1 - v_1) \cdot u_2| + |(u_2 - v_2) \cdot u_1| \\ &\leq |u_1 - v_1||v_2| + |u_2 - v_2||u_1| \\ &\leq \delta(|u_1| + |v_2|) \leq 2l\delta\end{aligned}$$

□

From this the following general statement of continuity can be made for the lattice isometry space.

Theorem 3.3.21 ([84], Theorem 7.7)**.** *Let Λ, Λ' be two lattices of with obtuse superbases B, B', differing by a slight perturbation such that* $\mathrm{SIM}(B, B') = \delta$*. Then as $\delta \to 0$,* $\mathrm{RI}(\Lambda') \to \mathrm{RI}(\Lambda)$ *and* $\mathrm{PI}(\Lambda) \to \mathrm{PI}(\Lambda')$

Proof. For the root invariant, the statement follows immediately from Lemma 3.3.20, the upper bound on the absolute difference between any two root products is $\sqrt{2l\delta}$, which clearly vanishes as $\delta \to 0$.

For the projected invariant, let $\mathrm{RI}(\Lambda) = (r_{12}, r_{01}, r_{02})$ and $\mathrm{RI}(\Lambda') = (s_{12}, s_{01}, s_{02})$ with sizes σ, τ respectively and suppose without loss of generality that $\sigma \leq \tau$. From Lemma 3.3.13 $\sigma \geq l$, and so the difference between values in the projected invariants can be computed as

$$|3(\bar{r}_{12} - \bar{s}_{12)}| \leq \frac{3}{\sigma}\sqrt{2\delta l} \leq \frac{3}{l}\sqrt{2l} = 3\sqrt{\frac{2\delta}{l}}$$

and similarly

$$|(\bar{r}_{02} - \bar{r}_{01}) - (\bar{s}_{02} - \bar{s}_{01})| = |(\bar{r}_{02} - \bar{s}_{02} - (\bar{s}_{01} - \bar{r}_{01})| \leq \frac{4}{\sigma}\sqrt{\delta l} = 4\sqrt{\frac{2\delta}{l}}$$

□

We are therefore justified, via Theorem 3.3.10, in mapping the Lattice Isometry Space LIS defined in Chapter 1 to a continuous space of both root invariants and projected invariants.

Definition 3.3.22 (Root Invariant Space)**.** *The* Root Invariant Space RIS*. is the set of all triples (r_{12}, r_{01}, r_{02}) of non-negative real numbers realisable as root invariants of two dimesional lattices (that is, $r_{12} \leq r_{01} \leq r_{02}$ and $r_{01} > 0$). The* Orientation-Aware Root Invariant Space RIS^o *is the set of orientation-aware root invariants $(r_{12}, r_{01}, r_{02})_\varepsilon$ with $\varepsilon \in \{+, -\}$ if $r_{12} > 0$ and no pair of root products are equal, and $\varepsilon = 0$ otherwise.*

In Chapter 3 we will impose explicit metrics on RIS and thus demonstrate formal continuity between LIS and RIS as invariant spaces. In the next section we discuss explicit visualisations of RIS and RIS^o.

3.4 Mapping Isometry and Similarity Classes of 2D Lattices

3.4.1 The Doubled Cone and Quotient Triangle

The most straightforward way of visualising RIS is as an embedding of all root invariants as points in $\mathbb{R}^3$. Since the root products are ordered, the resulting subset of $\mathbb{R}^3$ will be a cone, although with a one dimensional subspace removed as described below.

Definition 3.4.1 (Triangular Cone, adapted from [84] Definition 4.4)**.** *Let* $f : \text{RIS} \to \mathbb{R}^3$ *be such that* $f : (r_{12}, r_{01}, r_{02}) = (r_{01}, r_{02}, r_{12})$*. The resulting subset of* $\mathbb{R}_3$ *is the* Triangular Cone TC*, in which each point represents an isometry class of a two dimensional lattice. It is defined by the following set of inequalities:*

$$TC := \{x, y, z \in \mathbb{R}^3 | 0 \leq z \leq x \leq y\}$$

The boundaries of TC are given by the following intersections:

$$\partial^0_{TC} = \text{TC} \cap \{(x, y, z \in \mathbb{R}^3 | z = 0\}$$
$$\partial^1_{TC} = \text{TC} \cap \{(x, y, z \in \mathbb{R}^3 | x = y\}$$
$$\partial^2_{TC} = \text{TC} \cap \{(x, y, z \in \mathbb{R}^3 | x = z\}$$

By Lemma 3.3.6, any Root Invariant mapped to a point in these boundaries is that of a mirror-symmetric two dimensional lattice. From Lemma 3.3.6 we see that a root invariant maps to a point in the interior of the boundary ∂^0_{TC} if and only if it represents a primitive rectangular lattices, and to a point in the disjoint interiors of ∂^1_{TC} and ∂^2_{TC} if it represents an rectangular centered lattice.

In the interior of ∂^2_{TC} are all lattices where $r_{12} = r_{01}$, implying that $v_1^2 < v_2^2 = v_0^2$, while in the interior of ∂^1_{TC} are all lattices where $r_{01} = r_{02} \implies v_1^2 = v_2^2 < v_0^2$. By Theorem 3.2.8 v_1, v_2 are the first two successive minima of the lattice (Definition 2.1.5) . These two disjoint boundaries thus represent the two distinct lattice characters of centered rectangular lattices discussed in Chapter 2.

At the intersection $\partial^0_{TC} \cap \partial^2_{TC}$ are rectangular lattices with two equal nonzero root products. We can use the computation of vonorms from conorms in this case to show $v_1^2 = p_{01} + p_{12} = p_{01} = p_{02} = v_2^2$. At the intersection $\partial^1_{TC} \cap \partial^2_{TC}$ all root products are equal and the lattice is hexagonal since all vonorms are of equal length.

Any lattice whose root invariant maps to the interior of the cone is *oblique*, having no mirror symmetries. No root invariant of a lattice maps to the intersection $\partial^0_{TC} \cap \partial^1_{TC}$, since if $p_{12} = p_{01} = 0$ then $v_1^2 = 0$, and the resulting structure is not a lattice.

To visualise RIS^o we create two copies of this cone and glue them together along the boundary ∂_1:

Definition 3.4.2 (Doubled Cone)**.** *Let* $f : \mathrm{RIS}^o \to \mathbb{R}^3$ *be such that:*

$$f(r_{12}, r_{01}, r_{02})_\epsilon = \begin{cases} (r_{01}, r_{02}, r_{12}) & \epsilon \in \{0, +\} \\ (r_{02}, r_{01}, r_{12}) & \epsilon = - \end{cases}$$

The resulting subset of $\mathbb{R}^3$ *is the* doubled cone DC*, described by the set of inequalities*

$$DC := \begin{cases} \{x, y, z \in \mathbb{R}^3 | 0 \leq z \leq y\} & x \leq y \\ \{x, y, z \in \mathbb{R}^3 | 0 \leq z, y < z\} & x > y \end{cases}$$

in which each point represents the equivalence class of a lattice up to rigid motion.

DC is a partially closed set with boundaries given by the intersections

$$\partial^0_{DC} = \mathrm{DC} \cap \{(x, y, z \in \mathbb{R}^3 | z = 0\}$$
$$\partial^1_{DC} = \mathrm{DC} \cap \{(x, y, z \in \mathbb{R}^3 | y = z\}$$

Again by Lemma 3.3.6 the boundary ∂^1_{DC} contains only centered rectangular lattices where $r_{01} = r_{02}$. The intersection of the plane $x = y$ with the DC is not a boundary as it is for the TC, but still represents all centered rectangular lattices where $v_1^2 = v_2^2$.

If we wish to represent lattices up to similarity, we may simply select all lattices of the same size. Figure 3.5 illustrates this by showing the intersection of a triangular and doubled cone with a hyperplane given by $r_{12} + r_{01} + r_{02} = c$. Any line through the origin passing through a particular point in this intersection represents a similarity class of lattices.

The specific form of the projected invariant allows for a highly intuitive visualisation of similarity classes of lattices within a two dimensional simplex as follows:

Definition 3.4.3 (see Definition 4.5 in [84])**.** *The* projected invariant $\mathrm{PI}(\Lambda)$ *of a lattice with root invariant* $\mathrm{RI}(\Lambda) = (r_{12}, r_{01}, r_{02})$ *is given by*

$$\mathrm{PI}(\Lambda) := \frac{1}{\sigma}(3r_{12}, r_{02} - r_{01})$$

where σ *is the size of the lattice as given in definition 3.3.12.*

Proposition 3.4.4. *The projected invariants of all lattices lie within, or on the boundary of, the triangle* $\mathbb{R}^2$ *bounded by the vertices* $(0, 0), (0, 1), (1, 0)$*. No isometry class of any lattice has a projected invariant at the vertex* $(1, 0)$*.*

Proof. Since $\bar{r}_{12} + \bar{r}_{01} + \bar{r}_{02} = 1$ and r_{12} is the minimum root product, $\bar{r}_{12} \leq 1/3 \implies 3\bar{r}_{12} \in [0, 1]$. From the root product ordering, $0 \leq \bar{r}_{02} - \bar{r}_{01}$, and since $0 < r_{01}, \bar{r}_{02} - \bar{r}_{01} < 1$), $\bar{r}_{02} - \bar{r}_{01} \in [0, 1)$. □

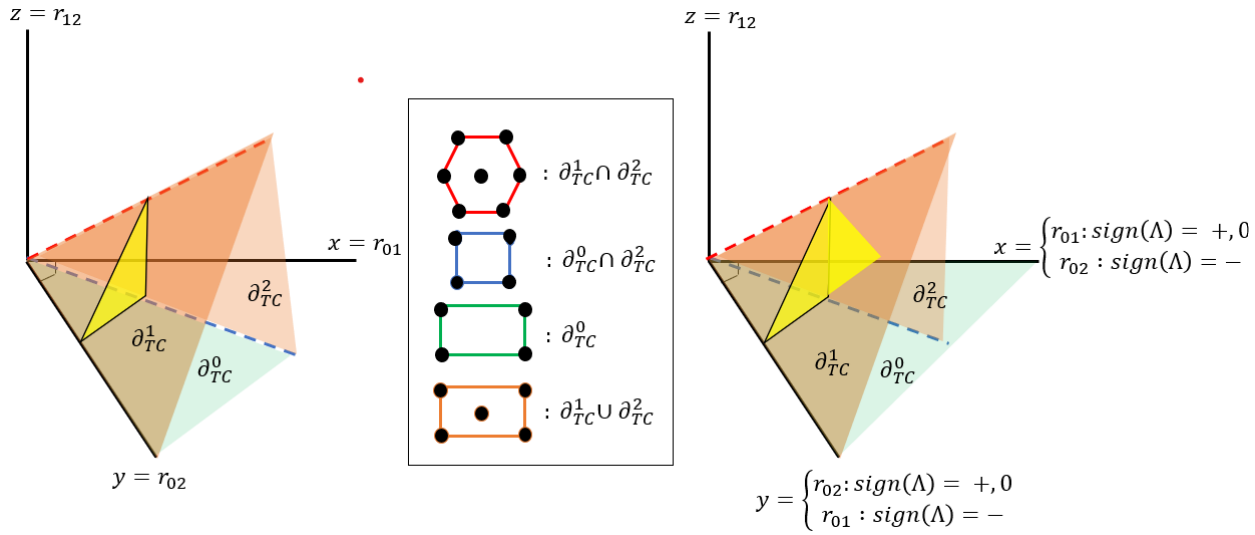

Figure 3.5: The triangular cone (TC) and the doubled cone (DC) are embeddings of RIS and RIS^o respectively in $\mathbb{R}^3$ with subspaces which represent represent root invariants of lattices with $sign(\Lambda) = 0$. The intersection of TC and DC with a hyperplane $r_{12} + r_{01} + r_{02} = c$ where $c \in \mathbb{R}^+$ is a right (resp. isosceles) triangle is shown.
. The yellow triangles show the intersection of each space a plane $x + y + z = \sigma, \sigma \in \mathbb{R}$, where all lattices have the same size.

We define this space as the *quotient triangle*:

$$\text{QT} := \{(x, y) \in \mathbb{R}^2 : x \geq 0, y \geq 0, x + y \leq 1\}$$

It is illustrated on the left of figure 3.6. As with the TC of Definition 3.4.1, the boundaries of this space are intersections with various linear subspaces:

$$\begin{aligned}
\partial^0_{QT} &= \text{QT} \cap \{(x, y) \in \mathbb{R}^2 | y = 0\} \\
\partial^1_{QT} &= \text{QT} \cap \{(x, y) \in \mathbb{R}^3 | x = 0\} \\
\partial^2_{QT} &= \text{QT} \cap \{(x, y) \in \mathbb{R}^3 | x + y = 1\}
\end{aligned}$$

In this case, ∂^0_{QT} represents all similarity classes of lattices where $r_{12} = 0$ (that is, primitive rectangular lattices) while for any similarity class of lattice represented by a point in ∂^1_{QT}, $\bar{r}_{01} = \bar{r}_{02} \implies r_{01} = r_{02} v_1^2 = v_2^2$. Recalling that $\bar{r}_{12} + \bar{r}_{01} + \bar{r}_{02} = 1$, for any point in ∂^2_{QT}:

$$\begin{aligned}
3\bar{r}_{12} - \bar{r}_{01} + \bar{r}_{02} &= \bar{r}_{12} + \bar{r}_{01} + \bar{r}_{02} \\
&\implies 2\bar{r}_{12} = 2\bar{r}_{01} \\
&\implies r_{12} = r_{01}
\end{aligned}$$

and thus $v_2^2 = v_0^2$, so that the disjoint interiors of ∂^1_{QT} and ∂^2_{QT} again represent the two separate characters of a centered rectangular lattice.

The intersection of ∂^1_{QT} and ∂^0_{QT}, $r_{12} = 0$ and $v_1^2 = v_2^2$, and so the vertex $(0, 0)$ represents the one similarity class of square lattices, at the intersection of ∂^1_{QT} and ∂^2_{QT} all root products are equal and thus the vertex at $(0, 1)$ represents the one similarity class of hexagonal lattices (see Example 3.3.17). The intersection of ∂^2_{QT} and ∂^0_{QT} at the vertex $(1, 0)$ is empty, since at that point all root product values are equal to zero and this triple is not realisable by any lattice and is thus not in the root invariant space (see Definition 3.3.22).

For the orientation-aware projected invariant, we may glue another copy of the QT along any boundary as we did with the triangular cone. We chose the following mapping:

Definition 3.4.5 (see [84], Fig 12)**.** *Let Λ be a lattice with orientation-aware root invariant $\mathrm{RI}^o(\Lambda) = (r_{12}, r_{01}, r_{02})_\epsilon, \epsilon \in \{-, 0, +\}$. The orientation-aware projected invariant is given by*

$$\mathrm{PI}^o(\Lambda) = \begin{cases} \frac{1}{\sigma}(3r_{12}, r_{02} - r_{01}) & \epsilon \in \{0, +\} \\ (1 - (r_{02} - r_{01}), 1 - 3r_{12}) & \epsilon = - \end{cases}.$$

All invariance classes of lattices up to similarity under rigid motion map to *quotient square* QS, defined as

$$\mathrm{QS} = \{(x, y) \in \mathbb{R}^2 | x \in [0, 1), y \in [0, 1)]\}$$

and illustrated on the right of figure 3.6.This is a partially closed square, with sides of length 1 and vertices at $(0, 0), (0, 1), (1, 1)$. Its boundaries are

$$\partial^0_{QS} = \mathrm{QS} \cap \{(x, y) \in \mathbb{R}^2 | y = 0\}$$
$$\partial^1_{QS} = \mathrm{QS} \cap \{(x, y) \in \mathbb{R}^3 | x = 0\}$$

Any lattice with sign 0 will map to the intersection $\mathrm{QS} \cap \{(x, y) | x + y = 1\}$ in the interior of the quotient square if $r_{12} = r_{01}$ or to the boundaries ∂^0_{QS} or ∂^1_{QS}, whose interiors represent the same subset of similarity classes of lattices as ∂^0_{QT} or ∂^1_{QS}.

If a lattice Λ_+ has $\mathrm{PI}^o(\Lambda_+) = (x, y)_+$ then the lattice Λ_- with $\mathrm{PI}^o(\Lambda_+) = (x, y)_-$ maps to the reflection of the point (x, y) in the line $x + y = 1$. Both the QT and the QS are illustrated in Figure 3.6.

One could glue along any of the quotient triangle boundaries with a different maps. The map discussed in the next section tackles this ambiguity and uniquely identifies a two dimensional lattice up to rigid motion with a single point in a compact surface.

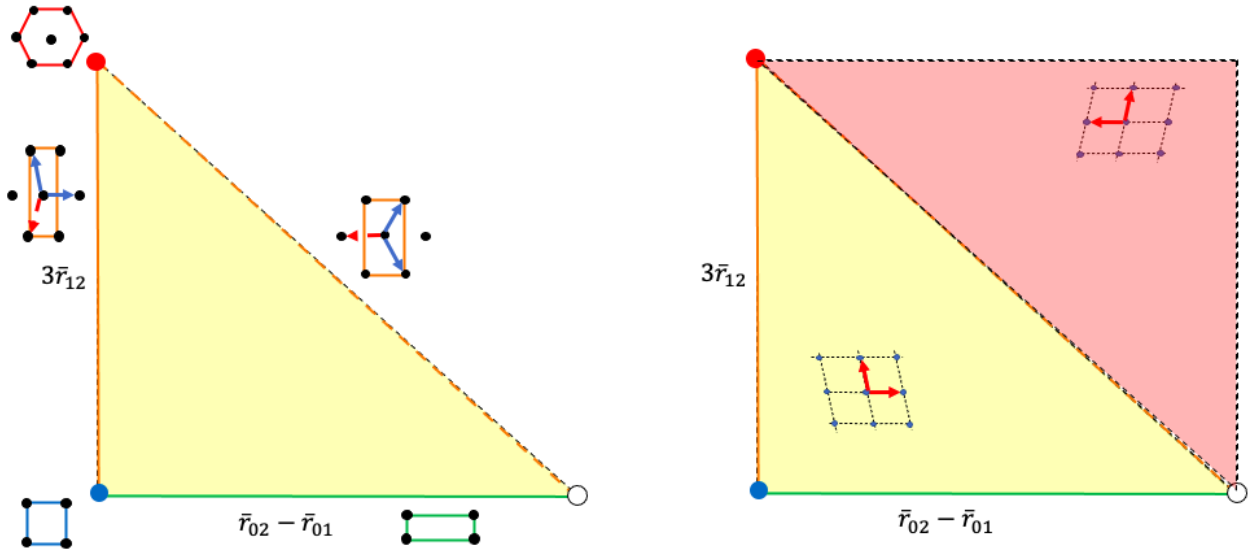

Figure 3.6: The quotient triangle (QT) and the quotient square (QS) are embeddings of (oriented) projected invariants of lattices in $\mathbb{R}^3$. Their boundaries represent projected invariants of lattices with $sign(\Lambda) = 0$. The geometry of lattices on the boundaries are shown, as well as a pair of lattices with the same projected invariant and opposite signs.

3.4.2 The Quotient Sphere

In the quotient square, each lattice mapping to a point of the of the oriented piecewise linear curve running from the vertex $(0,1) \to (0,0) \to (1,0)$ can be identified with the oriented piecewise linear curve running from the vertex $(0,1) \to (1,1) \to (1,0)$. Thus, the quotient square has the topology of a *punctured sphere* (punctured because the point $(1,0)$ itself is missing).

Our aim is to create a continuous homeomorphism from the QS to a punctured sphere. The most 'geographically natural' way to do this is to place the boundaries representing lattices with mirror symmetry on a distinguished line, with some distinguished point on that line representing the missing point. Since crystallographers are more used to stating angles in degrees, we calculate using these units in what follows rather than the more mathematically usual radians.

Definition 3.4.6 ([32], Definition 5.1)**.** *Let P be the incentre of the quotient triangle, that is, the centre of the unique inscribed circle tangent to all three of its sides. Let ℓ_G be the line originating at P and the vertex $(1,0)$. Denote the* latitude μ *of the vertex $(1,0)$ to be $0°$ and its* longitude φ *to be $180°$.*

Let $PI^o(\Lambda) = (x,y)_\epsilon$ be a general oriented projected invariant. Let ℓ be the line through P and (x,y), which goes on to meet the boundary of the QT *at some point (χ,ν).*

The longitude $\mu(\Lambda) \in (-180^o, 180^o]$ *is the anticlockwise angle $\theta \in (-180, 180]$ between ℓ_G and ℓ. The* latitude $\psi(\Lambda)$ *is given by $\frac{\epsilon}{90}\varphi$ where φ is the ratio $|P-(x,y)/|P-(\chi,\nu)|$*

of the distance between the incentre and (x, y) *and the distance between the incentre and the point after passing through* (x, y) *where it meets the boundary of the* QT.

The spherical projected invariant SPI(Λ) *of a lattice is the pair* $(\mu(\Lambda), \psi(\Lambda))$.

We illustrate the mapping of Definition 3.4.6 in Figure 3.7.

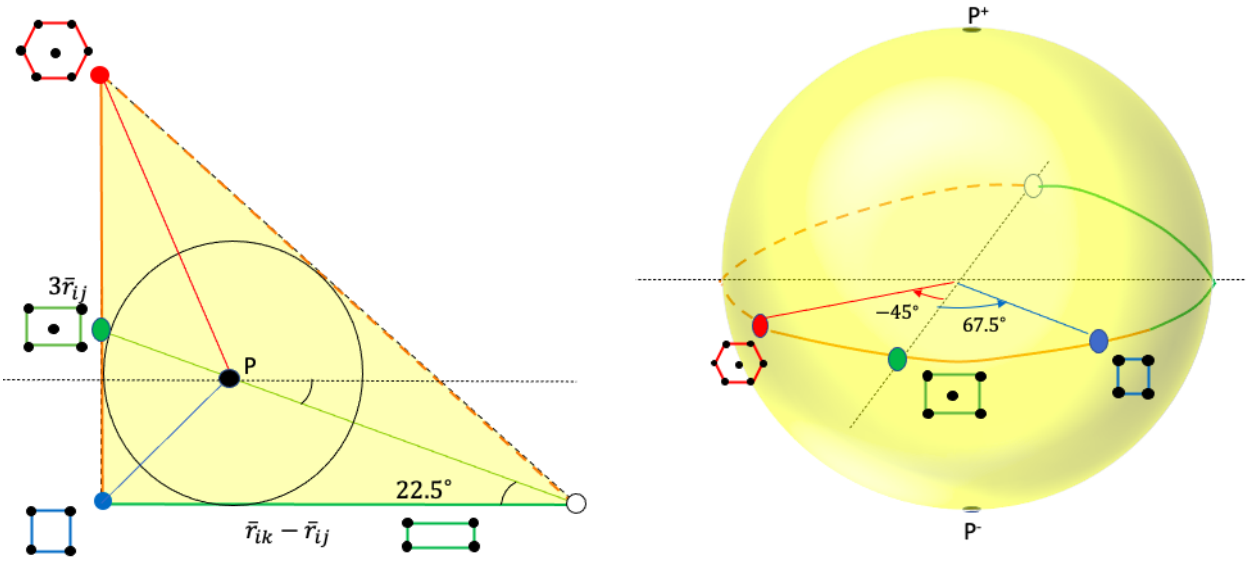

Figure 3.7: Mapping from the quotient triangle to the quotient sphere. **Left**: P is the centre of the incircle of the QT. The lattice whose projected invariant is at the green point maps to longitude $\mu(\Lambda) = 0$. **Right** The Spherical Projected Invariant of Definition 3.4.6 maps all lattices with sign 0 to the intersection of the sphere given by $\{(x, y, z) \in \mathbb{R}^3 | x^2 + y^2 + z^2 = 1\}$and the the plane $z = 0$ in $\mathbb{R}^3$. Lattices with negative sign map to the hemisphere below this plane, with positives sign to the hemisphere above it.

For lattices with PI(Λ) in the straight-line segment between the excluded vertex $(1, 0)$ and the incentre P^+, we choose the longitude $\mu = +180°$ rather than $-180°$. Proposition 3.4.7 computes the longitude and latitude coordinates $\mu(\Lambda), \varphi(\Lambda)$ in terms of the projected invariant.

Proposition 3.4.7 (formulae for SPI, [32], Proposition 5.2)**.** *For any lattice* $\Lambda \subset \mathbb{R}^2$ *with* $\mathrm{PI}(\Lambda) = (x, y) \in \mathrm{QT}$*, if* $x \neq t = 1 - \dfrac{1}{\sqrt{2}}$*, then set* $\psi = \arctan \dfrac{y-t}{x-t}$*, otherwise* $\psi = \mathrm{sign}(y-t)90°$*.*

(3.4.7a) The longitude of the lattice Λ *is* $\mu(\Lambda) = \begin{cases} \psi + 22.5° \text{ if } x < t, \\ \psi - 157.5° \text{ if } x \geq t, \psi \geq -22.5°, \\ \psi + 202.5° \text{ if } x \geq t, \psi \leq -22.5°. \end{cases}$

(3.4.7b) The latitude is $\varphi(\Lambda) = \mathrm{sign}(\Lambda) \cdot \begin{cases} \frac{x\sqrt{2}}{\sqrt{2}-1} 90° \text{ if } \mu(\Lambda) \in [-45°, +67.5°], \\ \frac{y\sqrt{2}}{\sqrt{2}-1} 90° \text{ if } \mu(\Lambda) \in [+67.5°, +180°], \\ \frac{1-x-y}{\sqrt{2}-1} 90° \text{ if } \mu(\Lambda) \in [-180°, -45°]. \end{cases}$

The incentres $P^{\pm} \in \mathrm{QT}^{\pm}$ *have* $\psi = 0$ *and* $\mu = \pm 90°$*, respectively,* φ *is undefined.* ■

Proof. Let $(\mathrm{PI}(\Lambda) = (x, y)_\epsilon)$. Assume initially that $(x, y) \neq (t, t)$. The translation $(x, y) \mapsto (x - t, y - t)$ where $t = 1 - \frac{1}{\sqrt{2}}$ moves the incentre P to the origin. Denote by $\psi = \arctan(y-t)/(x-t)$ the anticlockwise angle in the range $[-90°, 90°]$ between the line ℓ from the origin to $(x - t, y - t)$ and the x axis, and by p the point at which this line meets the translated boundaries of the QT.

Longitude computations are then a matter of converting the relevant range of ψ to that of μ. If $x < t$ then $\psi \in [-90°, 90°]$ and $\mu(\Lambda) \in [-67.5, 112.5°] = \psi + 22.5°$. If $x \geq t$ then:

$$\begin{aligned} \psi \in [-90°, -22.5°] &\implies \mu(\Lambda) \in [112.5°, 180°] \\ \psi \in [-22.5°, 90°] &\implies \mu(\Lambda) \in [-180°, -67.5°] \end{aligned}$$

To compute latitude $\varphi(\Lambda)$, we parameterise the line $\ell_s = s(x, y) + (t, t), s \in \mathbb{R}$ such that $\ell_0 = (t, t) = P, \ell_1 = (x+t, y+t) = \mathrm{PI}^o(\Lambda)$ and determine the value of s for which ℓ_s intersects the QT boundary. Then $\psi(\Lambda) = \mathrm{sign}(\Lambda)\frac{90°}{s}$. The appropriate boundary line ℓ_b is determined by the longitude:

$$\begin{aligned} \mu(\Lambda) \in [-45°, 67.5°] &\implies \ell_b = \{(x, y) | x = 0\}, s = x/t \\ \mu(\Lambda) \in [-67.5°, 180°] &\implies \ell_b = \{(x, y) | y = 0\}, s = y/t \\ \mu(\Lambda) \in [-180°, = 45°] &\implies \ell_b = \{(x, y) | 1 - (x + y) = 0\}, s = (1 - x - y)/2t \end{aligned}$$

and one computes the explicit formulae of Proposition 3.4.7 from the above.

If $(x, y) = (t, t)$ then $s = 0$ and $\varphi(\Lambda)$ is undefined, as is μ. We wish to map the point to the north or south poles, depending on the sign of the lattice, and since P is not on a boundary $\mathrm{sign}(\Lambda) \neq 0$ and $\varphi = \mathrm{sign}(\Lambda)90°$. □

Example 3.4.8. *All mirror-symmetric lattices* $\Lambda \subset \mathbb{R}^2$ *have* $\operatorname{sign}(\Lambda) = 0$ *and* $\operatorname{SPI}(\Lambda) = (\mu(\Lambda), 0)$ *by (3.4.7b). All square lattices* Λ_4 *with* $\operatorname{PI}(\Lambda_{p4mm}) = (0,0)$ *have* $\operatorname{SPI}(\Lambda_{p4mm}) = (67.5°, 0)$ *by (3.4.7a). All hexagonal lattices* Λ_{p6mm} *with* $\operatorname{PI}(\Lambda_{p6mm}) = (0,1)$ *have* $\mu(\Lambda_{p6mm}) = \arctan\frac{1}{1-\sqrt{2}} + 22.5° = -45°$. *Any rectangular lattice* Λ *with* $\operatorname{PI}(\Lambda) = (1 - \frac{1}{\sqrt{2}}, 0)$ *has* $\mu(\Lambda) = -90° + 202.5° = 112.5°$. *A centered rectangular lattice* Λ *with* $\operatorname{PI}(\Lambda) = (\frac{1}{2}, \frac{1}{2})$ *at the midpoint of the diagonal of* QT *has* $\mu(\Lambda) = \arctan 1 - 157.5° = -112.5°$. *Any lattice* Λ_G *with* $\operatorname{PI}(\Lambda_G) = G = (0, \sqrt{2}-1)$ *has* $\mu(\Lambda_G) = \arctan\big(1-\sqrt{2}\big) + 22.5° = 0$, *lying at the 'Greenwich point'* $(0°, 0°)$. ■

This computation illustrates the following, implied but not directly stated in [80]:

Theorem 3.4.9. *The spherical projected invariant* $\operatorname{SPI}(\Lambda)$ *is a complete invariant of two dimensional lattices up to similarity.*

Proof. The explicit computation in the proof of Proposition 3.4.7 is both a one-to-one map between any projected invariant and a point in the punctured sphere, and by Theorem 3.3.16 this is a complete similarity invariant of a two dimensional lattice. □

Furthermore, inverse computation of a lattice from its spherical projected invariant is possible, as illustrated in Figure 3.8:

Example 3.4.10. *Let a lattice have* $SPI(\Lambda) = (15°, 65°)$. *Since it is in the upper hemisphere, it has positive sign. From* $\mu(\Lambda) = 15° \in [-45°, 67.5°]$ *we may compute*

$$\varphi(\Lambda) = 65° = 90\frac{x\sqrt{2}}{\sqrt{2}-1} \implies x = \frac{65(\sqrt{2}-1)}{90\sqrt{2}} \approx 0.212$$

Since $x \geq t$ *and* $\mu(\Lambda) \in [-67.5°, 112.5°]$, *set* $\psi = 67.5° - 22.5° = 42.5°$, *and for* $t = 1 - 1/\sqrt{2}$:

$$\tan(\psi) = \frac{y-t}{x-t} \implies y = (x-t)\tan\psi + t$$

and thus $y \approx 0.218$

From $PI^o(\Lambda) = (0.212, 0.218)_+$ *we may use the explicit computation of Theorem 3.3.15 to directly compute that for a lattice of size* σ

$$\frac{1}{\sigma}\operatorname{RI}^o(\Lambda) \approx (0.073, 0.285, 0.503)_+$$

If we let $\sigma = 1$, *then the application of Theorem 3.3.11 uniquely reconstructs the resulting lattice basis as*

$$v_1 \approx (0, 0.294), v_2 = (-0.297 - 0.444)$$

Thus, $\operatorname{RI}(\Lambda), \operatorname{PI}(\Lambda)$ and $\operatorname{SPI}(\Lambda)$ are complete and computationally invertible by Theorem 3.3.10, Corollary 3.3.16 and Theorem 3.3.11. Furthermore, the (oriented) root and projected invariants are continuous by Theorem 3.3.21, and thus are complete solutions to Problem 1.4.1.

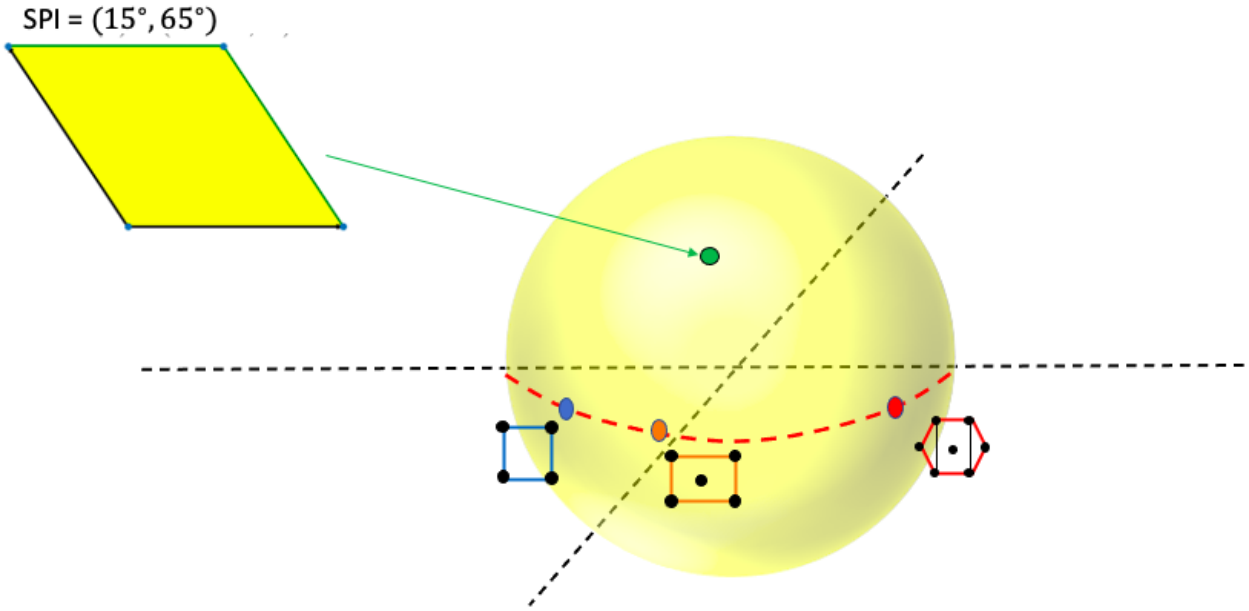

Figure 3.8: The inverse mapping from SPI(Λ) to a similarity class of lattices demonstrated in Example 3.4.10

.

3.5 Mapping 2D Lattices in the CSD

In this section we apply our map to a large database of two dimensional lattices generated from real world crystal structures, enabling us to examine how such structures occupy the space of all possible lattices.

For any periodic crystal from the Cambridge Structural Database (CSD), which has full geometric data of its lattice $\Lambda \subset \mathbb{R}^3$, we extract pairs of basis vector and angle parameters (a, b, γ), $(b, c, \alpha)$and (a, c, β) (see the note on lattice parameter notation in Chapter 1) and apply our invariants to the 2-dimensional lattices generated by these parameters.

Figure 3.9 shows all resulting 2.6 million lattices in the quotient square QS. To emphasise the symmetric nature of the gluing operation, we have shown primitive and centered rectangular lattices on the boundaries of both 'copies' of the QT glued together in the QS. Only about 55% of all lattices have Bravais classes with mirror symmetries. The remaining 45% of lattices are oblique, and occupy all areas of QS except those close to the vertex $(1, 0)$ where lattices become very flat and elongated. There appear to be no preferred geometric configurations overall.

After removing all non-oblique lattices represented by root invariants along the sides and the diagonal of QS, the map in Figure 3.10 shows a preference for positive lattices. This can be explained by the fact that in the CSD lattice parameters are ordered by length. Thus the vectors v_1, v_2 of the derived two dimensional lattice will already be ordered in size - if the basis is already part of an obtuse superbase then the sign of the lattice will be positive.

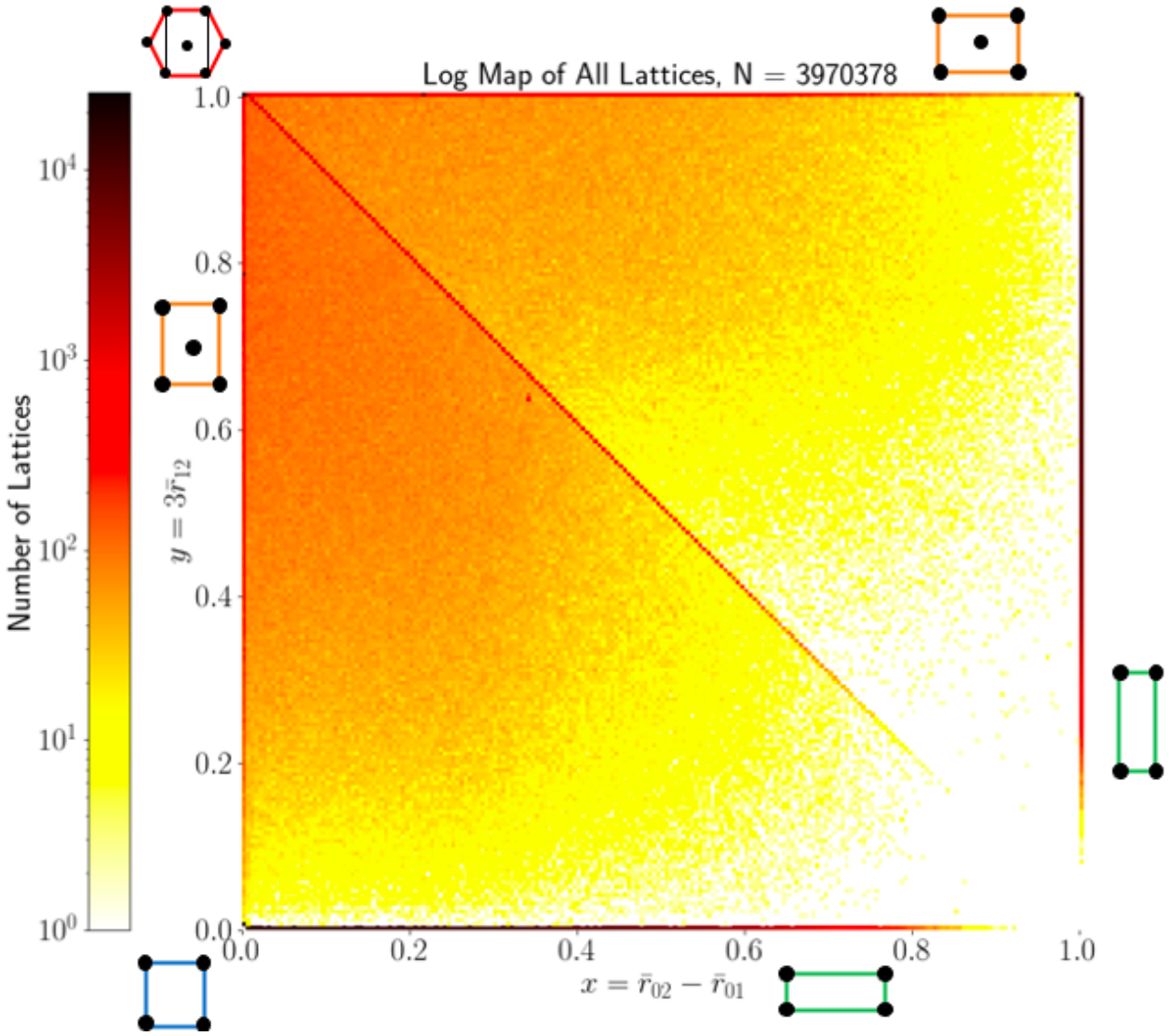

Figure 3.9: Density maps in QS of triplets of 2D lattices extracted from CSD crystals in the manner described in the text. Each pixel is of size 0.01×0.01 , and its colour indicates (on the logarithmic scale) the number of lattices whose projected invariant $\mathrm{PI}(\Lambda) = (x, y) = (\bar{r}_{02} - \bar{r}_{01}, 3\bar{r}_{12})$ belongs to this pixel. The darkest pixels represent rectangular lattices on the bottom and right edges of QS.

Another clearly visible feature is the dark spot near to the diagonal representing centered rectangular lattices at $\mathrm{PI}(\Lambda) \approx (0.4, 0.6)$. This arises from 386 near-identical primitive monoclinic crystals of α-oxalic acid dihydrate. This molecule has been used as a benchmark for the calculation of electron densities since its crystallographic properties were thoroughly documented in [95]. As a result, hundreds of publications have since generated and deposited refinements of its structural determination.

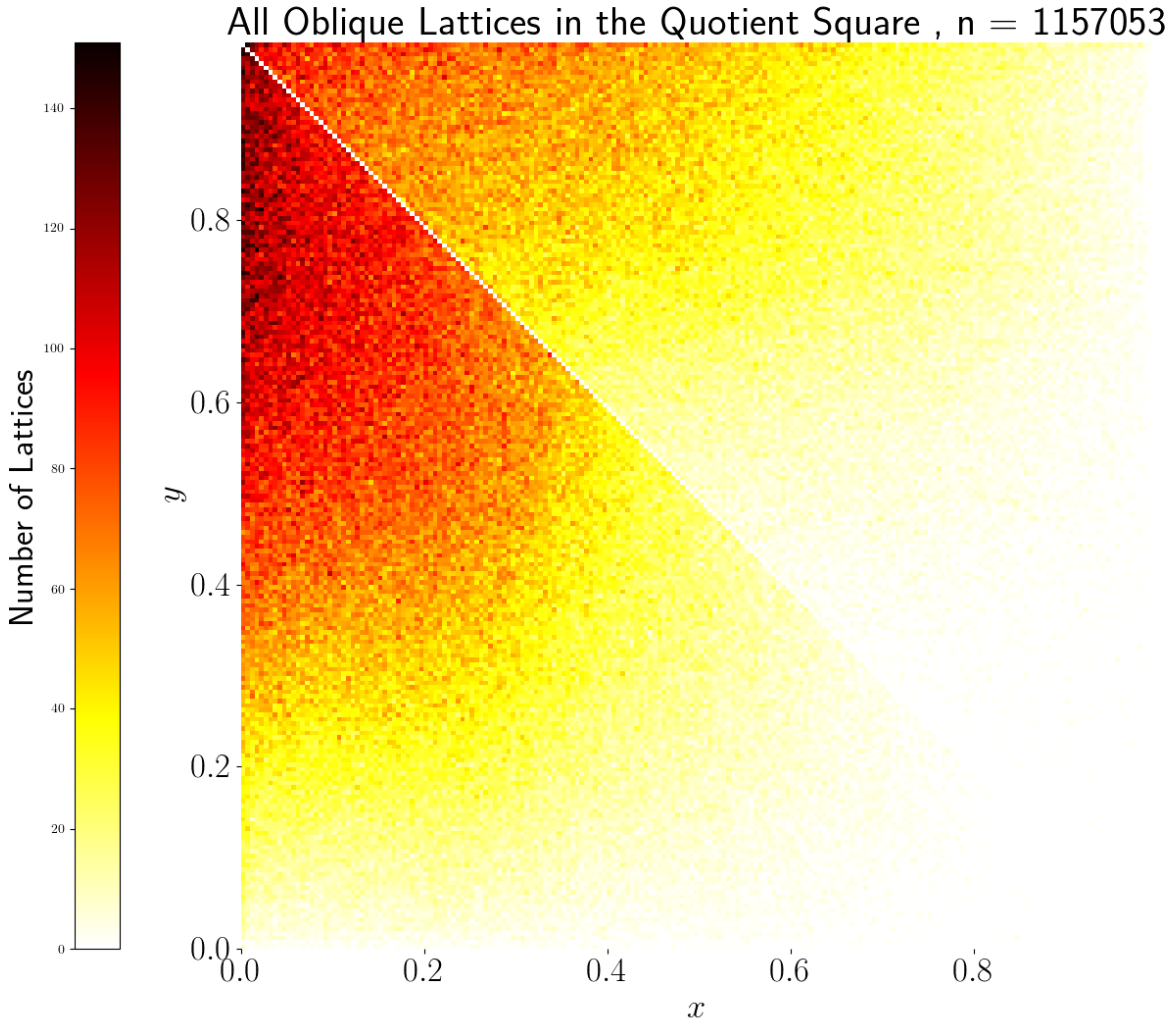

Figure 3.10: Normal density map of all 2D oblique lattices from CSD crystals in QS. After removing mirror-symmetric lattices on the boundary and diagonal of QS, we can better see the tendency towards hexagonal lattices at the top left corner $(0, 1) \in$ QS.

Some detail is lost in the QS map since we cannot see all parameters of higher symmetry lattices. Since there are only two distinct values of root product in the root invariant of we can, however, investigate a continuous map of just these two quantities. In the density map of primitive rectangular lattices in Figure 3.11 (right), the most prominent feature is the high-density area in the region where the shortest side length is between 2.5 and 5Å.

In Figure 3.11 (right) representing centered rectangular lattices, we see a visible line $b = \sqrt{2}a$ of high-density pixels. This line represents 2D lattices derived from body-centered cubic lattices, where the ratio of any pair of side lengths is $\sqrt{2}$.

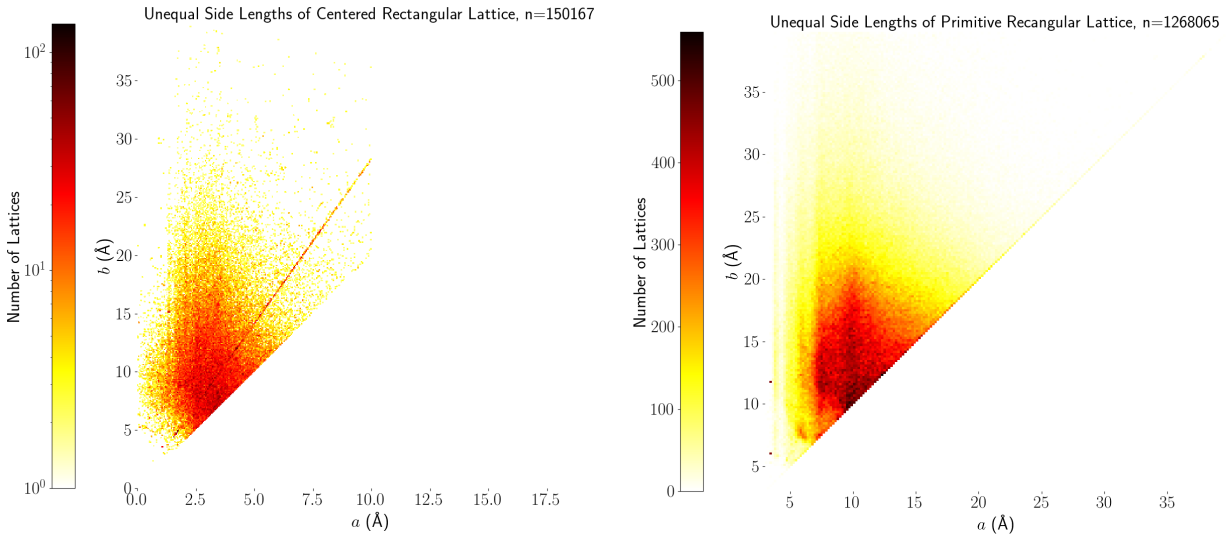

Figure 3.11: Density maps of parameters (a, b) in Å. **Left**: rectangular lattices with primitive unit cells $a \times b$ in $N = 1094109$ crystals in the CSD. **Right**: centred-rectangular lattices with conventional cells $2a \times 2b$ in $N = 147451$ crystals in the CSD.

A high density spot is visible representing 130 structures of a standard test molecule (hexamethylenetetramine), which has frequently been in the investigation of lattice vibrations [96]. The CSD thus also contains multiple depositions of the crystal structure of this molecule.

The single points at the vertices $(0, 0)$ and $(0, 1)$ representing square and hexagonal lattices respectively can be expanded into a continuous map simply by plotting a histogram of the single parameter which governs them (that is, their side length) as in Figure 3.12.

For square lattices we see what appears to be a continuous distribution of side lengths, skewed towards smaller structures although with a few very large lattices. It is notable that there are very few *precisely* hexagonal lattices in the dataset - not enough to draw a similar conclusion in that case. We conjecture that this is due to computation algorithms such as those discussed in the final section of Chapter 2 which assign lattices to particular Bravais types if their parameters are close to those of that type within a given tolerance. If a three dimensional lattice is shown to be close to primitive cubic, then all of its angle parameters will be automatically set to 90°.

Figures 3.13,3.14,3.15,3.16 show the density maps of 2D lattices from Figure 3.9 on the northern, southern, western, eastern hemispheres for the spherical map $\mathrm{SM} : \mathrm{QS} \to S^2$.

The north pole represents the incentre P^+ whose pixel contains 230 lattices in Figure 3.10 but appears sparsely populated in Figure 3.13 because this incentre pixel is split into many more 1×1 degree curved 'pixels' of a much lower density. The high density near the point representing hexagonal lattices is visible in Figures 3.13 and 3.14 as a concentration near the longitude $\mu = -45°$.

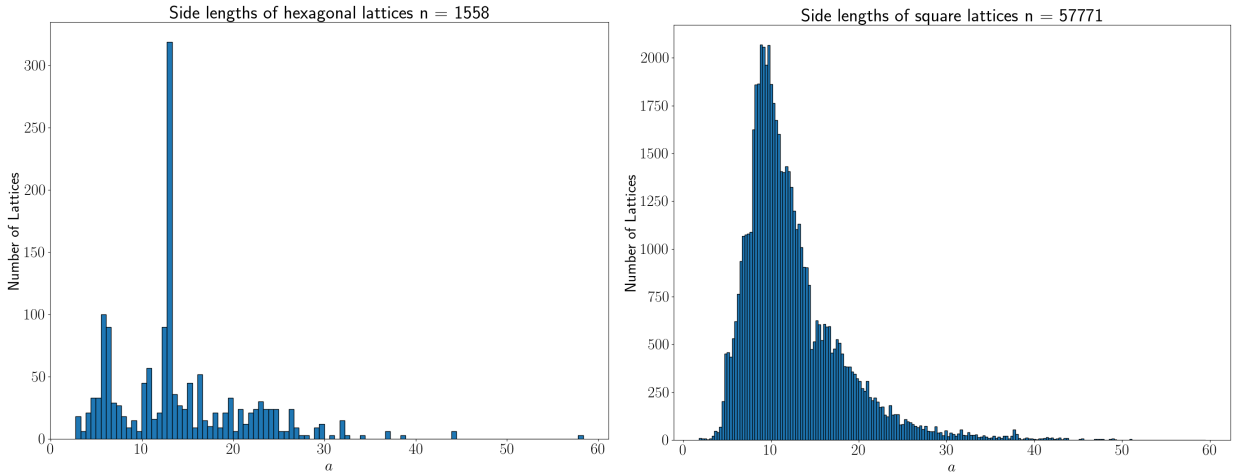

Figure 3.12: The histograms of minimum inter-point distances a in Angstroms. **Left**: all hexagonal 2D lattices in CSD crystals. **Right**: all square 2D lattices in CSD crystals.

Where non-oblique lattices are included, the concentrations of density along the borders of the QT can be seen, with primitive rectangular lattices appearing as a dense arc on the equator for $\mu \in [67.5°, 180°)$. The density maps show a hexagonal 'ridge' along the meridional arc at $\mu = -45°$ in Figures 3.13 and 3.14, which appears as a round arc in Figures 3.15 and 3.16. The density of exact square and rectangular lattices is even higher (dark pixels for the Bravais classes p4mm, p2mm, c2mm).

3.6 Conclusion and Discussion

In this chapter we have given a rigorous demonstration that the *root invariant* - the ordered pairwise inner products of the Selling-reduced (obtuse) superbase - is an isometry invariant for lattices in 2 dimensions which uniquely represents any such lattice as a point in a cone in the positive orthant of $\mathbb{R}^3$, and that the *projected invariant* derived from it is a similarity invariant. We have extended each invariant with the sign of the lattice to give its *orientation-aware* version, which is an isometry up to rigid motion. We have shown that these invariants satisfy key conditions of Problem 1.4.1 - they are complete up to the relevant equivalence relation, easily computable and fully invertible.

We have implemented the computation of each invariant, and used this to display what is to our knowledge the first complete, continuous map of two dimensional lattices arising from the Cambridge Structural Database - one of the largest databases of deposited crystal structures available. This map shows a strong preference for higher symmetry lattices with positive sign, although this is in part driven by the way that the lattices have been isolated from their parent lattice. The map shows that naturally occurring two dimensional lattices fill a large proportion of the space - justifying the need for a continuous classification of lattices in particular, and periodic structures in general.

In the next chapter we will impose metrics on the space of orientation-aware and unaware root and projected invariants, and demonstrate that they have the properties required of them by our research problem.

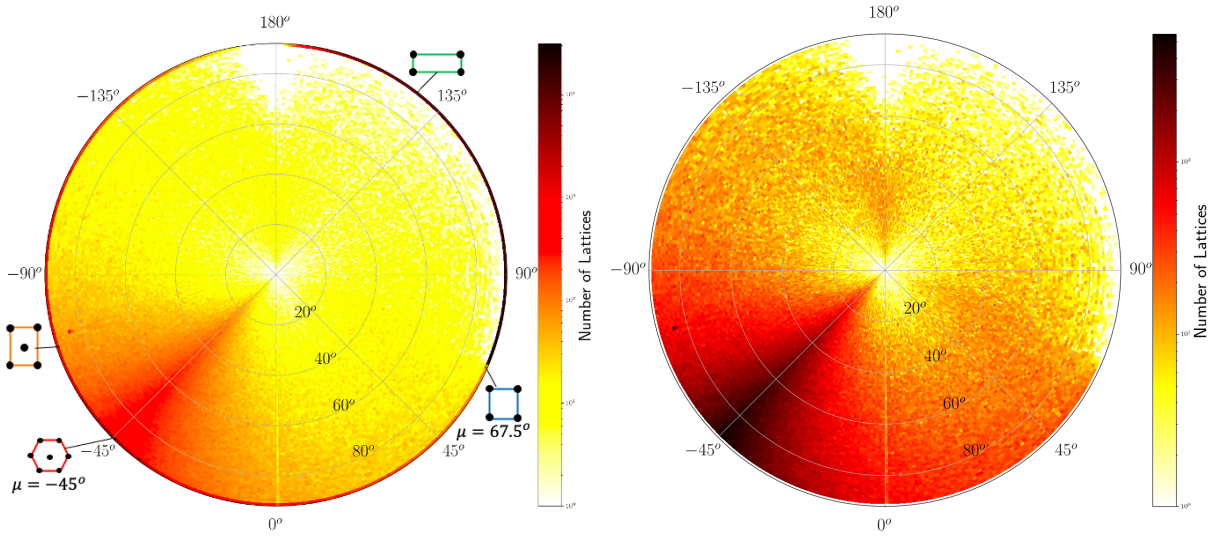

Figure 3.13: The density map of 2D lattices from CSD crystals on the northern hemisphere of the spherical map. The circumference (equator) is parameterised by the longitude $\mu \in (-180°, 180°]$. The radial distance is the latitude $\varphi \in [0°, 90°]$. **Left**: all $N = 2191887$ lattices with $\text{sign}(\Lambda) \geq 0$, $\varphi \geq 0$. **Right**: all $N = 741105$ oblique lattices with $\text{sign}(\Lambda) > 0$, $\varphi > 0$.

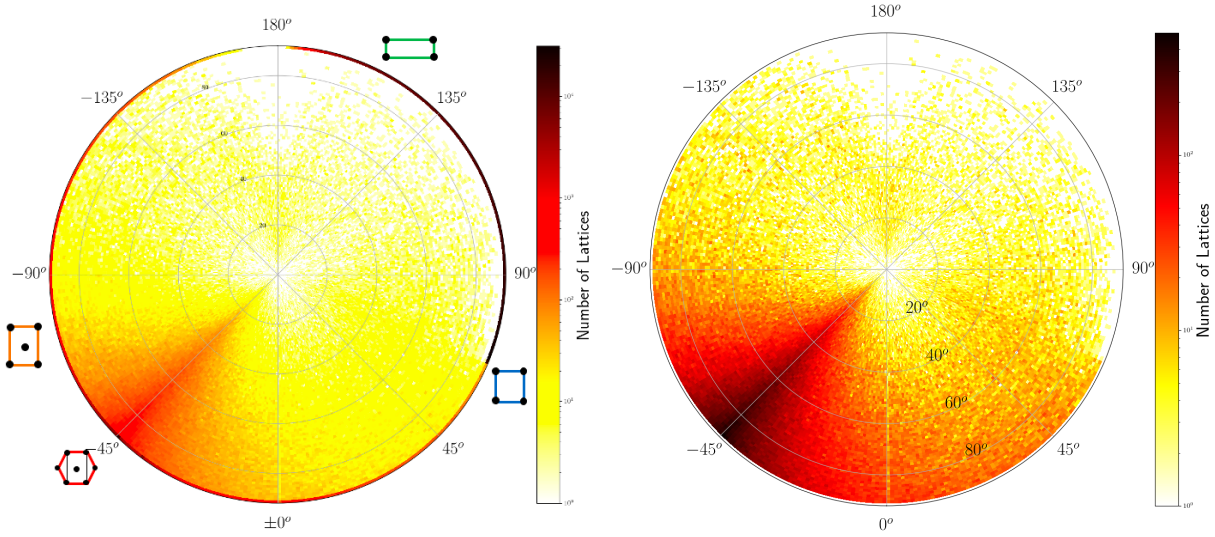

Figure 3.14: The density map of 2D lattices from CSD crystals on the southern hemisphere of the spherical map. The circumference (equator) is parameterised by the longitude $\mu \in (-180°, 180°]$. The radial distance is the latitude $\varphi \in [0°, 90°]$. **Left**: all $N = 1854209$ lattices with $\text{sign}(\Lambda) \leq 0$, $\varphi \leq 0$. **Right**: all $N = 406930$ oblique lattices with $\text{sign}(\Lambda) < 0$, $\varphi < 0$.

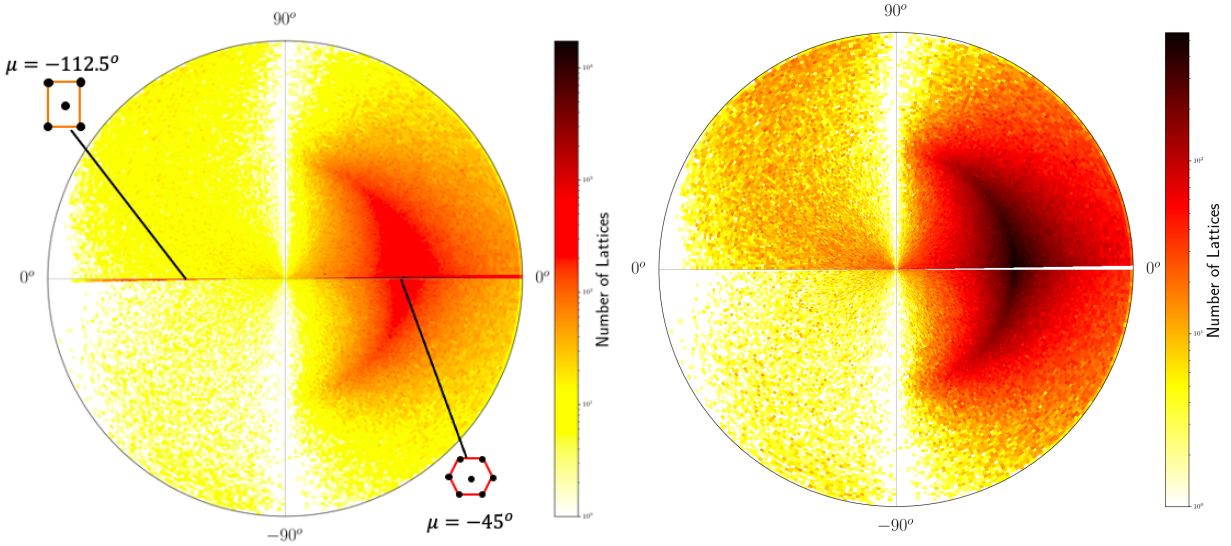

Figure 3.15: The density map of 2D lattices from CSD crystals on the western hemisphere of the spherical map ($\varphi \in [-90°, 90°], \mu \in (-180, 0]$). Angles on the circumference show the latitude $\varphi \in [-90°, 90°]$. **Left**: $N = 1100580$ lattices with $\mu \in (-180°, 0°]$. The hexagonal lattice at $\mu = -45°$ and the centered rectangular lattice at $\mu = -112.5°$ are marked on the horizontal arc (western half-equator). **Right**: all $N = 932626$ oblique lattices with $\mu \in (-180°, 0°]$ and $\varphi \neq 0$.

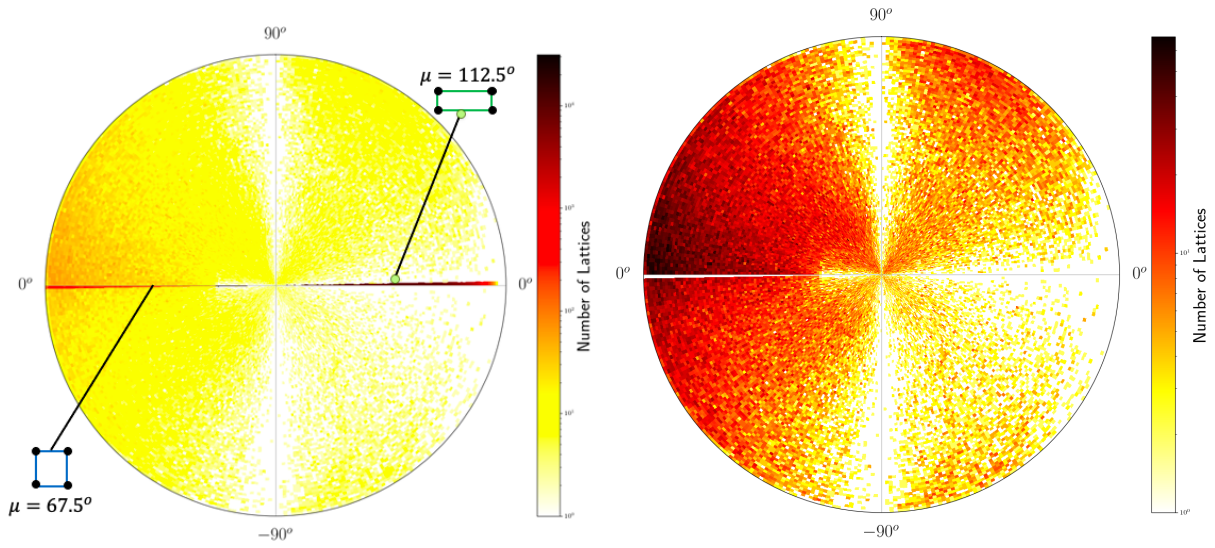

Figure 3.16: The density map of 2D lattices from CSD crystals on the eastern hemisphere. Angles on the circumference show the latitude $\varphi \in [-90°, 90°]$. **Left**: all $N = 1511307$ lattices with $\mu \in [0°, 180°)$, the square lattice point at $\mu = 67.5°$ and the rectangular lattice at $\mu = 112.5°$ are marked on the the horizontal arc (eastern half-equator). **Right**: all $N = 215409$ oblique lattices with $\mu \in [0°, 180°)$, $\varphi \neq 0$.

Chapter 4

Continuous Chiral Distances on 2D Lattices

4.1 Chapter Outline and Contribution

In the previous chapters, we demonstrated that both the *root invariant* (Definition 3.3.3)of a two dimensional lattice - the ordered triple consisting of the negative of the inner products of its unique (up to isometry or rigid motion) obtuse superbase - and the *projected invariant* (Definition 3.3.14) in their orientation-aware and orientation-unaware versions are not only complete invariants, but also vary continuously under small perturbations of the lattice. This led us to the notion of the *Root Invariant Space* (RIS - Definition 3.3.22 and, to show that the *Doubled Cone* (Definition 3.4.5), the *Quotient Square* (Definition 3.4.5) and the spherical projected invariant (Definition 3.4.6) are all representations of the space of isometry (or rigid motion) and similarity classes of lattices respectively.

To go further and actually *compare* lattices, we need to define an explicit metric on these spaces, and we will do so in this chapter. After a discussion of previous attempts to define the notion of chirality both discretely and continuously, the main theoretical work will be the definition of the general comparison metric and the proof that it follows all metric axioms of Definition 1.2.4, with an overview of definitions, proofs and computations from [86] and [80]. We will use this to derive a family of *chiral distances*, essentially minimising the distance between a point in RIS (or the QT) and some boundary subspace representing a particular (or any) lattice with mirror symmetry. As with isometry classification, the requirement for continuous distances between *periodic crystals* is motivated by the growing number of simulated and experimental structures being published.

The remainder of the chapter will be devoted to the application of chiral distances to real crystal structures. To demonstrate the efficiency of computation of chiral distances, we will compute distributions of these distances on the large dataset of 2.7 million $2D$ lattices mapped in the previous chapter. We will also demonstrate a more practical application of chiral distances by using them to investigate to large public databases of two dimensional materials.

4.2 Previous Work on Continuous Chirality

4.2.1 Discrete Chirality

The term *chirality* has for most of its history been used as a binary property of molecular structures. Almost all previous work on the chirality of periodic crystals [97] has studied discrete versions of chirality based on symmetry groups, which are discontinuous under perturbations.

Chiral molecules can have very different properties - the most well known case being that of the drug Thalidomide, which has distinct R- and S-chiral enantiomers. While the highly purified R-enantiomer proved to be an effective therapy for leprosy and other diseases, the presence of even small mounts of the S-chiral version can cause fetal malformation in pregnant women [98, 99].

In the crystallographic context the idea was initially defined informally by Lord Kelvin for a 'geometrical figure' or 'group of points' , which he said to be *chiral* if '...its mirror image, ideally realised, cannot be brought to coincide with itself.' [100]. In the same passage he defined the term *enantiomer* to describe the two mirror images of a chiral structure.

Definitions of this nature are generally applied to an embedding of a point set or other object in $\mathbb{R}^n$, but can be generalised to classes of object in any metric space [101]. We state the following formal definition for lattices:

Definition 4.2.1. *(Lattice Chirality) Two lattices have opposite chiralities if they are isometric but not related by rigid motion (see Definition 1.3.2).*

Thus, by Lemma 3.3.8, two lattices are enantiomers if their root invariants differ only in their sign (Definition 3.3.7). In three dimensions, chiral structures can arise in lattices of all Bravais types (see [102] for an overview of chiral symmetries in three dimensional lattices), and as with individual molecules, crystals built from distinct enantiomers have measurably different physical properties [103].

4.2.2 Continuous Chirality

Attempts to formally define a quantity which reflected 'how asymmetric' a molecule or other structure might be were being made in the 19th century [104], but the connection between the physical, chemical, and biological properties of materials and the extent to which their structures deviate from mirror symmetry [105] has seen a growing interest in the development of materials where this deviation can be practically measured and controlled [106], rather than characterised discretely.

A quantification of chirality for a very simple finite structure - the triangle - was developed by Buda [107] . A more general quanitification of chirality for finite molecules based on continuous atomic positions was proposed by Osipov et al [108]. The Osipov-Dunmur Pickup (OPD) index relies on an integral over some function of the positions of points of a molecule in space.

Its applicability is limited by computability issues - direct analytical expressions for the integral are only available for simple arrangements of small numbers of points. It has also been shown [109] that it was possible for any measure of this type to exhibit 'chiral zeroes' - that is, the OPD index may take a value of zero for a chiral molecule.

In a series of papers published in the late 90s [110, 111, 112, 113, 114], Zabrodsky, Avinr and Pinsky discuss an alternative approach to continuous symmetry measurement.

The general idea is to define a minimum deformation required to move a a given configuration of atoms to a configuration that is symmetric. As with the OPD index, it is more easily computable for small, finite configurations of molecules [115]. A key idea in this work which we explore in the lattice context is the notion that 'asymmetry' is not a single quantity - one might compute the deformation required to move to a configuration with *specific* symmetries. The quantification of 'chirality' could be considered as a minimisation of such deformations over all possible achiral configurations [112].

4.3 Root, Projected and Spherical Metrics

Instead of beginning with the idea of deviation from symmetry, the approach in this work is to define a more general metric between different lattices from distances in the various isometry spaces discussed in the previous chapter. As discussed in Chapter 3, previous quantified comparisons between lattices have not successfully been shown to satisfy the properties of a continuous metric.

Since we have mapped isometry classes of lattices to a subspace of $\mathbb{R}^3$, a metric between any two such classes can be defined by restricting any valid $\mathbb{R}^3$ metric to that subspace - for example, for the root invariant space we apply the metric to the triangular cone of Definition 3.4.1 since all root invariants will be within that space, while for projected invariants we apply it within the Quotient Triangle:

Definition 4.3.1 ([84], Definition 5.1)**.** *If L_q is the Minkowski metric of example 1.2.7, then the* root metric *between any two lattices Λ, Λ' is given by* $\mathrm{RM}_q(\Lambda, \Lambda') := L_q(\mathrm{RI}(\Lambda), \mathrm{RI}(\Lambda'))$.

Similarly, the projected metric *is given by* $\mathrm{PM}_q(\Lambda, \Lambda') := L_q(\mathrm{PI}(\Lambda), \mathrm{PI}(\Lambda')$.

Thus $\mathrm{RM}_2(\Lambda, \Lambda')$ and $\mathrm{PM}_2(\Lambda, \Lambda')$ is simply the straight line Euclidean distance between the two points in the TC and QT respectively, representing the lattices Λ and Λ'.

Example 4.3.2 (Computation of Root and Projected Metrics)**.** *Let Λ_1 be the square lattice $u_1 = (1, 0), u_2 = (0, 1)$ and Λ_2 a centered rectangular lattice $v_1 = (-1, 0.5), v_2 = (1, 0.5)$*

We compute $\mathrm{RI}(\Lambda_1) = (0, 1, 1)$ *and* $\mathrm{RI}(\Lambda_2) = (0.5, 0.5, 0.75)$*, and thus* $RM_2(\Lambda_1, \Lambda_2) = \sqrt{0.5^2 + 0.5^2 + 0.25^2} \approx 0.53$

Similarly, $\mathrm{PI}(\Lambda_1) = (0, 0)$ *and* $\mathrm{RI}(\Lambda_2) = (0.25, 0.75)$ *- as we would expect on the line $y = 1 - x$, and thus $PM_2(\Lambda_1, \Lambda_2) = \sqrt{10}/16 \approx 0.79$.*

It is more complex to define distances between classes of lattices up to rigid motion in the triangular cone or quotient square. Any continuous deformation between lattices of opposite sign will pass through some symmetric configuration represented by a point on the boundary of the space, and since our choice of representation of root and projected invariants up to rigid motion depended on gluing a second copy of the space along an arbitrary selection of one of those boundaries (see Defintions 3.4.2 and 3.4.5) we cannot simply restrict the straight line metric to the space they describe - potentially the distance between the two would be shorter had we made some other choice, as illustrated in Figure 4.1). This is captured by the definitions below.

Definition 4.3.3 ([84], Definition 5.5)**.** *Recalling the definition of the boundaries* $\partial^0_{TC}, \partial^1_{TC}, \partial^2_{TC}$ *of* TC*, the* orientation-aware *root metric is given by*

$$\mathrm{RM}^o_q(\Lambda, \Lambda') = \begin{cases} \mathrm{RM}_q(\Lambda, \Lambda') & \mathrm{sign}(\Lambda) = \mathrm{sign}(\Lambda') \\ \min\limits_{\mathrm{RI}(\Lambda_o) \in \partial^0_{TC} \cup \partial^1_{TC} \cup \partial^2_{TC}} \mathrm{RM}_q(\Lambda, \Lambda_o) + \mathrm{RM}_q(\Lambda_o, \Lambda') & \mathrm{sign}(\Lambda) \neq \mathrm{sign}(\Lambda') \end{cases}$$

Similarly, defining the boundaries of the QT as

$$\begin{aligned} \partial^0_{QT} &= \{(x, y) \in \mathbb{R}^2 | x = 0\} \\ \partial^1_{QT} &= \{((x, y) \in \mathbb{R}^2 | y = 0\} \\ \partial^2_{QT} &= \{((x, y) \in \mathbb{R}^2 | x + y = 1\} \end{aligned}$$

we define the orientation-aware projected metric *as*

$$\mathrm{PM}^o_q(\Lambda, \Lambda') = \begin{cases} \mathrm{PM}_q(\Lambda, \Lambda') & \mathrm{sign}(\Lambda) = \mathrm{sign}(\Lambda') \\ \min\limits_{\mathrm{PI}(\Lambda_o) \in \partial^0_{QT} \cup \partial^1_{QT} \cup \partial^2_{QT}} \mathrm{PM}_q(\Lambda, \Lambda_o) + \mathrm{PM}_q(\Lambda_o, \Lambda') & \mathrm{sign}(\Lambda) \neq \mathrm{sign}(\Lambda') \end{cases}$$

We now present proofs that all the metrics defined above have the properties we seek to solve Problem 1.4.1

Theorem 4.3.4 ([84] Lemma 5.2)**.** *The root and projected metrics in their orientation-aware and orientation-unaware forms satisfy all metric axioms.*

Proof. For the orientation-unaware metrics, or orientation-aware metrics sharing the same sign, symmetry and the triangle inequality are inherited from the L_q metric. Identity arises from the completeness of the root and projected invariants up to isometry and similarity respectively, proven in Theorem 3.3.10 and Corollary 3.3.16.

For the orientation-aware metrics with lattices of the opposite sign, symmetry is also inherited from the original metric. It remains only to demonstrate that the triangle inequality holds.

Let $\Lambda_1, \Lambda_2, \Lambda_3$ be three lattices such that $\mathrm{sign}(\Lambda_1) \neq \mathrm{sign}(\Lambda_3)$ and $\mathrm{sign}(\Lambda_i) \neq 0$ for all $i \in \{1, 2, 3\}$.

Now either $\text{sign}(\Lambda_2) = \text{sign}(\Lambda_1)$ or $\text{sign}(\Lambda_2) = \text{sign}(\Lambda_3)$.

In the first case, let us suppose that Λ' is the lattice with $\text{sign}(\Lambda') = 0$ such that $\text{RM}_q^o(\Lambda_2, \Lambda_3) = \text{RM}_q(\Lambda_2, \Lambda') + \text{RM}_q(\Lambda', \Lambda_3)$, and Λ'' the lattice with $\text{sign}(\Lambda'') = 0$ such that $\text{RM}_q^o(\Lambda_1, \Lambda_3 = \text{RM}_q(\Lambda_1, \Lambda'') + \text{RM}_q(\Lambda'', \Lambda_3)$. Then

$$\begin{aligned}\text{RM}_q^o(\Lambda_1, \Lambda_2) + \text{RM}_q^o(\Lambda_2, \Lambda_3) &= \text{RM}_q(\Lambda_1, \Lambda_2) + RM_q(\Lambda_2, \Lambda') + \text{RM}_q(\Lambda', \Lambda_3) \\ &\leq \text{RM}_q(\Lambda_1, \Lambda_2) + RM_q(\Lambda_2, \Lambda'') + \text{RM}_q(\Lambda'', \Lambda_3) \\ &\leq \text{RM}_q(\Lambda_1, \Lambda'') + \text{RM}_q(\Lambda'', \Lambda_3) = \text{RM}_q^o(\Lambda_1, \Lambda_3)\end{aligned}$$

For the second case, suppose Λ' is the lattice with $\text{sign}(\Lambda') = 0$ such that $\text{RM}_q^o(\Lambda_1, \Lambda_2) = \text{RM}_q(\Lambda_1, \Lambda') + \text{RM}_q(\Lambda', \Lambda_2)$. Then

$$\begin{aligned}\text{RM}_q^o(\Lambda_1, \Lambda_2) + \text{RM}_q^o(\Lambda_2, \Lambda_3) &= \text{RM}_q(\Lambda_1, \Lambda') + RM_q(\Lambda', \Lambda_2) + \text{RM}_q(\Lambda_2, \Lambda_3) \\ &\leq \text{RM}_q(\Lambda_1, \Lambda'') + RM_q(\Lambda'', \Lambda_2) + \text{RM}_q(\Lambda_2, \Lambda_3) \\ &\leq \text{RM}_q(\Lambda_1, \Lambda'') + \text{RM}_q(\Lambda'', \Lambda_3) = \text{RM}_q^o(\Lambda_1, \Lambda_3)\end{aligned}$$

□

We are now in a position to substitute the generalised continuity of Theorem 3.3.21 with a proper metric continuity for orientation-unaware root and projected metrics.

Theorem 4.3.5. *[[84], Theorem 7.7] Let Λ, Λ' have obtuse superbases B, B' such that $\text{SIM}(B, B') = \delta$ and l is the length of the longest vector among both superbases. Then for $q \in [1, \infty)$:*

$$\begin{aligned}RM_q(\Lambda, \Lambda') &\leq 3^{\frac{1}{q}}\sqrt{2l\delta} \\ PM_q(\Lambda, \Lambda') &\leq 2^{\frac{1}{q}}\sqrt{2\delta/l}\end{aligned}$$

Furthermore, both $\text{RM}_q^o(\Lambda, \Lambda')$ and $\text{PM}_q^o(\Lambda, \Lambda')$ go to 0 as $\delta \to 0$.

Proof. For the inequality of $\text{RM}_q(\Lambda, \Lambda')$, let $\text{RI}(\Lambda) = (r_{12}, r_{01}, r_{02})$. From Lemma 3.3.20, the absolute difference between any pair of root products in the root invariant is less than $\sqrt{2l\delta}$, and thus

$$\left(\sum_{i<j, i,j\in 0,1,2} |r_{ij} - s_{ij}|^q\right)^{\frac{1}{q}} \leq (3(2l\delta)^{\frac{q}{2}})^{\frac{1}{q}} = 3^{\frac{1}{q}}\sqrt{2l\delta}$$

Similarly, let $\text{PI}(\Lambda) = (x_1, y_1)$ and $\text{PI}(\Lambda') = (x_2, y_2)$. Then again by Lemma 3.3.21, noting that the absolute difference between any pair of values in the projected invariant is less than $\sqrt{2\delta/l}$,

$$(|x_1 - y_1|^q + |x_2 - y_2|^q)^{\frac{1}{q}} \leq (2(2\delta/l)^{\frac{1}{q}} = 2^{\frac{1}{q}}\sqrt{2\delta/l}$$

For the final statement, note that the spaces $\text{TC}/\{\partial_{TC}^0 \cup \partial_{TC}^1 \cup \partial_{TC}^2\}$ and $\text{QT}/\{\partial_{QT}^0 \cup \partial_{QT}^1 \cup \partial_{QT}^2\}$ (see Definition 4.3.3) are open subsets of $\mathbb{R}^3$ and $\mathbb{R}^2$ respectively. Thus as the perturbation $\delta \to 0$ there will be some value for which the two lattices Λ, Λ' have the same sign and, the orientation-aware and unaware root and projected metrics are equal. □

Remark 4.3.6. *Note that we have specifically shown that* RM_q *and* PM_q *satisfy* Hölder continuity *in the sense of Definition 1.2.10, with* $\varepsilon = 1/q$.

We have included practical computability among our requirements in Problem 1.4.1, and this can be expedited by deriving analytic expressions for metrics between lattices. For RM_q metrics this is non-trivial for $q \geq 3$, and since in the results shown below we use exclusively $q = 2$, we demonstrate specific analytic expressions for this value - more complex expressions for $q = \infty$ can be found in [86].

Proposition 4.3.7 ([84], Proposition 5.9)**.** *Let* $\Lambda_+\Lambda_-$ *be two lattice with root forms* $\mathrm{RI}^o(\Lambda) = (r_{12}, r_{01}, r_{02})_+$ *and* $\mathrm{RI}^o(\Lambda') = (s_{12}, s_{01}, s_{02})_-$ *of opposite signs, and* $\mathrm{PI}^o(\Lambda_+) = (x_1, y_1)_+$ *and* $\mathrm{PI}({}^o\Lambda_-) = (x_2, y_2)_-$ *Then*

$$\mathrm{RM}_2^o(\Lambda_+, \Lambda_-) = \min\{L_2(\mathrm{RI}(\Lambda_+), (-s_{12}, s_{01}, s_{02})), L_2(\mathrm{RI}(\Lambda_+)(s_{01}, s_{12}, s_{02})), L_2(\mathrm{RI}\Lambda_+), (s_{12}, s_{02}, s_{01})\}$$
$$\mathrm{PM}_2^o(\Lambda_+, \Lambda_-) = \min\{L_2(\mathrm{PI}(\Lambda_+), (x_2, -y_2)), L_2(\mathrm{PI}(\Lambda_+), (x_2, -y_2)), L_2(\mathrm{PI}(\Lambda_+), (1 - y_2, 1 - x_2))\}$$

Proof. Let Λ_o be the lattice with sign 0 such that

$$\mathrm{RM}^o(\Lambda_+, \Lambda_-) = \mathrm{RM}(\Lambda_+, \Lambda_0) + \mathrm{RM}(\Lambda_0, \Lambda_-)$$

By the Definition 3.4.1 of TC, this lattice lies in one of the boundary subspaces given by $\partial^0_{TC}, \partial^1_{TC}, \partial^2_{TC}$. Denote by $f_i(\mathrm{RI}(\Lambda_-))$ the function that gives the reflection of the point representing Λ_i in the TC in the boundary subspace ∂^i_{TC} containing the point representing Λ_0. Now

$$\mathrm{RM}(\Lambda +_, \Lambda_0) + \mathrm{RM}(\Lambda_0, \Lambda_-) = \mathrm{RM}(\Lambda_+, \Lambda_0) + L_2(\Lambda_0, f_i(\Lambda_-))$$

and using the triangle inequality, this is minimised for the Euclidean straight line distance L_2 exactly when Λ_0 lies in the line between Λ_- and $f(\Lambda_-)$ as illustrated in Figure 4.1. Thus

$$\mathrm{RM}^o(\Lambda_+, \Lambda_-) = \min_{i \in \{0,1,2\}} L_2(\Lambda +_, f_i(\mathrm{RI}(\Lambda_-)))$$

and we can directly compute all $f_i(\mathrm{RI}(\Lambda_-))$ as:

$$f_0(s_{12}, s_{01}, s_{02}) = (-s_{12}, s_{01}, s_{02})$$
$$f_1(s_{12}, s_{01}, s_{02}) = (s_{01}, s_{12}, s_{02})$$
$$f_2(s_{12}, s_{01}, s_{02}) = (s_{12}, s_{02}, s_{01}).$$

The proof for PM_2^o proceeds similarly. In this case the relevant boundaries are $\partial^0_{QT} = \{((x, y)|x = 0\}, \partial^1_{QT} = \{y = 0\}$ and $\partial^2_{QT} = \{(x, y)|x + y = 1\}$. The reflections $g_i(\mathrm{PI}(\Lambda_-))$ in each ∂'_i boundary are given by

$$g_0(x_2, y_2) = (-x_2, y_2)$$
$$g_0(x_2, y_2) = (x_2, -y_2)$$
$$g_0(x_2, y_2) = (1 - y_2, 1 - x_2),$$

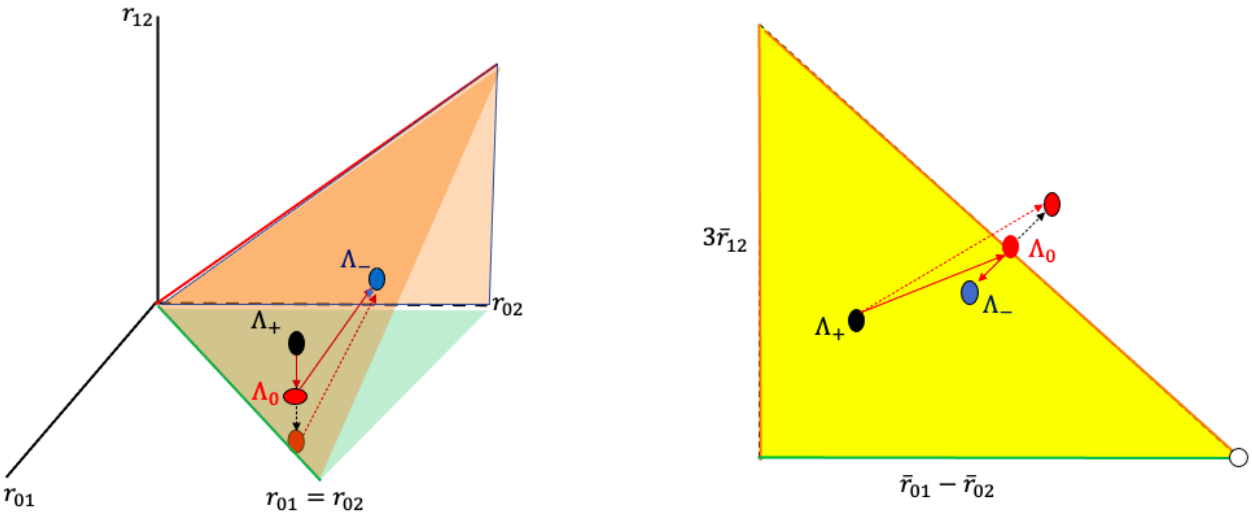

Figure 4.1: Illustration of the proof of Proposition 4.3.7: for lattices Λ_+, Λ_-, of opposite sign, the root and projected metrics with the L_2 distance are equivalent to the minimal straight line distance between the point representing Λ_+ in TC, QT respectively and the reflection of Λ_- in any boundary of the space.

and by the same argument as above

$$PM_2^o(\Lambda_+, \Lambda_-) = \min_{i\in\{0,1,2\}} L_2(\Lambda +, g_i(\mathrm{PI}(\Lambda_-)))$$

□

Example 4.3.8. *We consider the lattice Λ_1 of example 1.3.7 with Niggli-reduced basis $v_1 = (-1, 0)$ and $v_2 = (0.3, 0.7)$, and its mirror image Λ_2 given by $v_1' = (1, 0), v_2' = (-0.3, 0.7)$. As we would expect,*

$$\mathrm{RI}(\Lambda_1) = \mathrm{RI}(\Lambda_2) = (0.28, 0.3, 0.7)$$
$$\mathrm{PI}(\Lambda_1) = \mathrm{PI}(\Lambda_2) = (0.4, 0.84)$$

and their distance in the orientation unaware metrics defined in 4.3.1 is 0.

However, since they have opposite sign we may compute

$$\begin{aligned}\mathrm{RM}_2^o(\Lambda_1, \Lambda_2) &= \min(\sqrt{0.56^2}, \sqrt{0.2^2 + 0.02^2}, \sqrt{0.4^2 + 0.4^2}) \\ &\approx \min(0.56, 0.09, 0.57) = 0.09\end{aligned}$$

and similarly

$$\begin{aligned}\mathrm{PI}_2^o(\Lambda_1, \Lambda_2) &= min(0.8, 1.68, \sqrt{0.2^2 + 0.68^2}) \\ &\approx \min(0.8, 1.68, 0.71) = 0.71\end{aligned}$$

4.3.1 Spherical Metrics

We may also use the spherical projected invariant of Definition 3.4.6 to define an orientation-aware distance between similarity classes of lattices. This does not require the minimisation of Proposition 4.3.7 since points in the sphere already uniquely represent lattice classes up to rigid motion rather than isometry. Thus any quantity known to be a metric for points on the surface of S^2 will suffice. Thanks to the importance of this information for seafarers, this we may employ the well-known *haversine distance*.

Definition 4.3.9. *(Haversine distance) Denote by* $\text{hav}(\theta) := \sin^2 \frac{\theta}{2}$ *the* haversine function. *The* haversine distance *between two points of latitude and longitude* $(\mu_1, \varphi_1), (\mu_2, \varphi_2)$ *is then the minimum distance around a great circle [116] on* S^2*, given by*

$$h((\mu_1, \varphi_1), (\mu_2, \varphi_2)) = 2 \arcsin \sqrt{\text{hav}(\varphi_1 - \varphi_2) + \text{hav}(\mu_1 - \mu_2) \cos \varphi_1 \cos \varphi_2} \in [0°, 180°]$$

.

Tables of haversine distances have been used since the 19th century to approximate the distance between two points on the surface of the earth(see, for example, [116, 117]). Since the sphere of Definition 3.4.6 is defined to have radius 1, the haversine distance is in degrees.

Definition 4.3.10 ([80], Definition 2.7)**.** *Let* Λ_1, Λ_2 *be lattices with spherical invariant* $\text{SPI}(\Lambda_1) = (\mu_1, \psi_1)$ *and* $\text{SPI}(\Lambda_2) = (\mu_2, \psi_2)$.

The spherical projected metric *is given by the haversine distance between the two points on the sphere*

$$\text{SPM}(\Lambda_1, \Lambda_2) := h(\text{SPI}(\Lambda)1, \text{SPI}(\Lambda_2))$$

In fact, we may introduce invariants modulo rigid motion rather than similarity on the sphere by taking into account the size $\sigma(\Lambda) = r_{12} + r_{01} + r_{02}$ of Definition 3.3.12. The resulting chiral distances will be measured in the units of the original basis coordinates (such as Ångstroms) instead of degrees.

Definition 4.3.11 ([80], Definition 2.7)**.** *Let* Λ *be a lattice with root invariant* $\text{RI}(\Lambda) = (r_{12}, r_{01}, r_{02})$.

The spherical root invariant *is* $\text{SRI}(\Lambda) = (\mu, \varphi, \sigma)$*, where* $\text{SPI}(\Lambda) = (\mu, \varphi)$ *was introduced in Definition 3.4.6 and* σ *is the size of the lattice. Map the spherical coordinates* (μ, φ, σ) *to the standard Euclidean coordinates* $(x, y, z) = (\sigma \cos \varphi \cos \mu, \sigma \cos \varphi \sin \mu, \sigma \sin \varphi)$*. For any two lattices* $\Lambda_1, \Lambda_2 \subset \mathbb{R}^2$*, the* spherical root metric $\text{SRM}(\Lambda_1, \Lambda_2)$ *is the Euclidean distance between the points* $(x, y, z) \in \mathbb{R}^3$ *obtained from* $\text{SRI}(\Lambda_1), \text{SRI}(\Lambda_2)$ *as above. For a group* $G \in \{D_2, D_4, D_6\}$ *and any lattice* $\Lambda \subset \mathbb{R}^2$*, the* spherical root G-chiral distance $\text{SRC}[G](\Lambda)$ *is the minimum distance* $\text{SRM}(\Lambda, \Lambda')$ *for a lattice* Λ' *that has* $\sigma(\Lambda') = \sigma(\Lambda)$ *and the crystallographic group* G.

Since the spherical projected metric and the spherical root metric are related to the projected metric by a continuous homeomorphism (the gluing of the sides of the quotient square), they are also continuous.

4.4 Chiral Distances

Quantifications of chirality can be built on Definitions in 4.3.3, 4.3.10 and 4.3.11 by minimising the distance to the subspace of the Root or Projected Invariance Space (or the punctured sphere in the case of the spherical projected invariant) which contains all lattices with a particular symmetry.

Definition 4.4.1 ([80], Definition 2.7)**.** *Denote by* LIS_G *the subspace of* LIS *consisting of lattices with a symmetry group* $G \in \{D_2, D_4, D_6\}$*. Then the* root chiral distance *of a lattice* Λ *is given by:*

$$\mathrm{RC}_q[G](\Lambda) = \min_{\Lambda' \in \mathrm{LIS}_G} \mathrm{RM}_q(\Lambda, \Lambda')$$

and similarly we define the projected chiral distance *as*

$$\mathrm{PC}_q[G](\Lambda) = \min_{\Lambda' \in \mathrm{LIS}_G} \mathrm{PM}_q(\Lambda, \Lambda')$$

We can derive explicit computations for $q = 2$ as follows:

Proposition 4.4.2 ([84], Propositions 6.5, 6.6)**.** *Let* Λ *be a lattice such that* $\mathrm{RI}(\Lambda) = (r_{12}, r_{01}, r_{02})$ *and* $\mathrm{PI}(\Lambda) = (x, y)$*. Then*

$$\begin{aligned}
\mathrm{RC}_2[D_6] &= \sqrt{\frac{2}{3}(r_{12}^2 + r_{01}^2 + r_{02}^2 - ((r_{12}r_{01} + r_{01}r_{02} + r_{12}r_{02}))} \\
\mathrm{RC}_2[D_4] &= \sqrt{r_{12}^2 + \frac{1}{4}(r_{02} - r_{01})^2} \\
\mathrm{RC}_2[D_2] &= \min\left\{r_{12}, \frac{r_{01} - r_{12}}{\sqrt{2}}, \frac{r_{02} - r_{01}}{\sqrt{2}}\right\} \\
\mathrm{PC}_2[D_6] &= \sqrt{(1-x)^2 + (1-y)^2} \\
\mathrm{PC}_2[D_4] &= \sqrt{x^2 + y^2} \\
\mathrm{PC}_2[D_2] &= \min\left\{x, y, \frac{1 - x - y}{\sqrt{2}}\right\}
\end{aligned}$$

Proof. $\mathrm{RC}_2[D_6]$: the root invariant of any hexagonal lattice is given by (s, s, s) for some $s \in \mathbb{R}^+$. We are therefore aiming to minimise the quantity

$$l = \sqrt{((r_{12} - s)^2 + (r_{01} - s)^2 + (r_{02} - s)^2}$$

which we compute from

$$\frac{dl}{ds} = \frac{6s - 2(r_{12} + r_{01} + r_{02})}{\sqrt{((r_{12} - s)^2 + (r_{01} - s)^2 + (r_{02} - s)^2}} = 0 \implies s = \frac{1}{3}(r_{12} + r_{01} + r_{02})$$

and thus by substituting this value into l we compute

$$\begin{aligned} l_{min} &= \sqrt{\frac{1}{3}\left((2r_{12}-r_{01}-r_{02})^2+(2r_{01}-r_{02}-r_{02})^2+(2r_{02}-r_{12}-r_{01})^2\right)} \\ &= \sqrt{\frac{2}{3}(r_{12}^2+r_{01}^2+r_{02}^2-((r_{12}r_{01}+r_{01}r_{02}+r_{12}r_{02}))} \end{aligned}$$

$\mathrm{RC}_2[D_4]$: the root invariant of any square lattice is given by $(0,s,s)$ for some $s \in \mathbb{R}^+$. We are therefore aiming to minimise the quantity

$$l = \sqrt{r_{12}^2+(r_{01}-s)^2+(r_{02}-s)^2}$$

which we compute from

$$\frac{dl}{ds} = \frac{4s-2(r_{01}+r_{02})}{\sqrt{(r_{12}^2+(r_{01}-s)^2+(r_{02}-s)^2}} = 0 \implies s = \frac{1}{2}(r_{01}+r_{02})$$

and thus by substituting this value into l we compute

$$l_{min} = \sqrt{r_{12}^2+\frac{1}{2}(r_{01}-r_{02})^2}$$

$\mathrm{RC}_2[D_2]$: We wish to minimise the distance to the three boundaries of the TC - for $r_{12}=0$ this is simply r_{12} while for each of the the two boundaries $r_{ij}-r_{0j}, j \in \{1,2\}, i \neq j$ the relevant distance is given by $\sqrt{(r_{ij}+r_{0j})^2/2}$ as required

$\mathrm{PC}_2[D_6], \mathrm{PC}_2[D_4]$: the projected invariant of every hexagonal lattice is equal to $(0,1)$, and the projected invariant of every square lattice is equal to $(0,0)$ so we simply compute the L_2 Euclidean distance to these points

$\mathrm{PC}_2[D_2]$: We wish to find the minimal distance to any boundary of the QT. For the vertical and horizontal boundaries. This is simply x and y respectively, and for $x+y=1$ we compute the s which minimises the squared distance $l^2=(x-s)^2+(y-1+s)^2$

$$\frac{d(l^2)}{ds} = 4s-2x+2y-2 = 0 \implies s = \frac{(1+x-y)}{2}$$

which on substitution gives $l=(1-x-y)/\sqrt{2}$ as required. □

We may similarly define minimised distances to such subspaces in the spherical case:

Definition 4.4.3 ([80], Definition 2.7)**.** *For any lattice $\Lambda \subset \mathbb{R}^2$ and a group $G \in \{D_2, D_4, D_6\}$, the* spherical projected G-chiral distance *is given by*

$$\mathrm{SPC}[G](\Lambda) := \min_{\Lambda' \in \mathrm{LIS}_G} \mathrm{SPM}(\Lambda, \Lambda')$$

and similarly the spherical root G-chiral distance

$$\mathrm{SRC}[G](\Lambda) := \min_{\Lambda' \in \mathrm{LIS}_G} \mathrm{SRM}(\Lambda, \Lambda')$$

As with general distances between lattices, the definition and computation of chiral distances for spherical root invariants is more straightforward since it does not require minimisation over multiple reflections:

Proposition 4.4.4 ([80], Proposition 2.8)**.** *For a lattice* Λ *with* $\mathrm{SRI}(\Lambda) = (\mu, \varphi, \sigma)$*, the distances from Definition 4.4.3 can be computed as follows:*

$$\begin{aligned}
\mathrm{SPC}[D_2](\Lambda) &= |\varphi|, \\
\mathrm{SPC}[D_4](\Lambda) &= 2 \arcsin \sqrt{\mathrm{hav}(\varphi - 67.5^\circ) + \mathrm{hav}(\mu) \cos\varphi \cos 67.5^\circ} \\
\mathrm{SPC}[D_6](\Lambda) &= 2 \arcsin \sqrt{\mathrm{hav}(\varphi + 45^\circ) + \mathrm{hav}(\mu) \cos\varphi \cos 45^\circ},
\end{aligned}$$

where $\mathrm{hav}(\theta) = \sin^2 \frac{\theta}{2}$*, and*

$$\begin{aligned}
\mathrm{SRC}[D_2](\Lambda) &= 2\sigma |\sin \frac{\varphi}{2}| \\
\mathrm{SRC}[D_4](\Lambda) &= \sigma \sqrt{(\cos\varphi\cos\mu - \cos 67.5^\circ)^2 + (\cos\varphi \sin\mu - \sin 67.5^\circ)^2 + \sin^2\varphi} \\
\mathrm{SRC}[D_6](\Lambda) &= \sigma \sqrt{(\cos\varphi\cos\mu - \cos 67.5^\circ)^2 + (\cos\varphi \sin\mu + \sin 45^\circ)^2 + \sin^2\varphi}.
\end{aligned}$$

Proof. For a plane crystallographic group $G \in \{D_2, D_4, D_6\}$, Proposition 4.4.4 expresses the root spherical chiral G-distance $\mathrm{SRC}[G](\Lambda)$ and the projected spherical chiral G-distance $\mathrm{SPC}[G](\Lambda)$ of any 2D lattice $\Lambda \subset \mathbb{R}^2$ in terms of its spherical root invariant $\mathrm{SRI}(\Lambda) = (\mu, \varphi, \sigma)$.

Case of $\mathrm{SPC}[D_2]$. Any lattice that has the crystallographic group D_2 is mirror-symmetric (primitive or centred rectangular). Hence its spherical projected invariant $\mathrm{SPI} = (\mu, 0)$ lies on the equator of S^2 for some longitude $\mu \in (-180^\circ, 180]$. By Definition 4.3.10, for any other lattice Λ with $\mathrm{SPI} = (\mu, \varphi)$, the spherical projected D_2-chiral distance $\mathrm{SPC}[D_2](\Lambda)$ is equal to the haversine distance from (μ, φ) to the equator (minimal along the meridional arc where μ is constant): $\mathrm{SPC}[D_2](\Lambda) = h((\mu, \varphi), (\mu, 0)) = 2 \arcsin \sqrt{\mathrm{hav}(\varphi)} = 2 \arcsin \sqrt{\sin^2 \frac{\varphi}{2}} = |\varphi|$.

Cases of $\mathrm{SPC}[D_4]$ and $\mathrm{SPC}[D_6]$. By Definition 3.4.6 all square and hexagonal lattices are represented by the spherical projected invariants $(\mu, \varphi) = (67.5^\circ, 0)$ and $(\mu, \varphi) = (-45^\circ, 0)$, respectively, see Figure 3.7. By Definition 4.4.3 the spherical projected chiral distances are $\mathrm{SPC}[D_4] = h((\mu, \varphi), (67.5^\circ, 0^\circ))$ and $\mathrm{SPC}[D_6] = h((\mu, \varphi), (-45^\circ, 0^\circ))$, and the resulting formulae can be directly computed from the haversine distance formula of Definition 4.3.9

For any 2D lattice Λ with a spherical root invariant $\mathrm{SRI}(\Lambda) = (\mu, \varphi, \sigma)$, Definition 4.3.11 gives the Euclidean coordinates $(x, y, z) = \sigma(\cos\varphi\cos\mu, \cos\varphi\sin\mu, \sin\varphi) \in \mathbb{R}^3$ used below.

Case of $\mathrm{SRC}[D_2]$. In the spherical coordinates (μ, φ, σ), the subspace of all mirror-symmetric lattices, which have the crystallographic group D_2, is the equatorial plane $\varphi = 0$ or the horizontal plane $z = 0$ in the Euclidean coordinates $(x, y, z) = \sigma(\cos\varphi\cos\mu, \cos\varphi\sin\mu, \sin\varphi)$.

By Definition 4.3.11 for any 2D lattice Λ, the root spherical distance $\mathrm{SRC}[D_2](\Lambda)$ to a closest mirror symmetric lattice of the same size has the minimum Euclidean distance from the fixed point (x, y, z) to the equatorial circle $\sigma(\cos\mu', \sin\mu', 0)$ whose radius is fixed, but the longitude μ' is variable.

Ignoring the size factor σ^2 and noting that $\sin\varphi$ is fixed, we minimise the squared distance $s(\mu') = (\cos\varphi\cos\mu - \cos\mu')^2 + (\cos\varphi\sin\mu - \sin\mu')^2$ by differentiation:

$$\begin{aligned}\frac{ds}{d\mu'} &= 2\sin\mu'(\cos\varphi\cos\mu - \cos\mu') - 2\cos\mu'(cos\varphi\sin\mu - \sin\mu'),\\ &= 2\cos\varphi(\cos\mu\sin\mu' - \sin\mu\cos\mu') = 2\cos\varphi\sin(\mu' - \mu)\\ \frac{d^2s}{d\mu'^2} &= 2\cos\varphi\cos(\mu' - \mu).\end{aligned}$$

If $\dfrac{ds}{d\mu'} = 0$ for $\mu \in [-180°, 180°]$ then either $\cos\varphi = 0$ or $\sin(\mu' - \mu) = 0$, which implies that $\mu' - \mu = 180°n$ for $n \in \{-1, 0, 1\}$. If $\cos\varphi = 0$, then $\varphi = \pm 90°$ and $s = \cos^2\mu' + \sin^2\mu' = 1$ independent of μ, while $\sin\varphi = 1$ giving $\mathrm{SRC}_2[D_2](\Lambda) = \sqrt{2}\sigma$.

If $\mu' - \mu = 180n°$ and $n = \pm 1$ then $\frac{d^2s}{d\mu'^2} = \cos(\pm 180°) = -1$ and s has a maximum. In the remaining case $\frac{d^2s}{d\mu'^2} = \cos(\pm 0) = 1$ and, substituting μ' for μ we find that s achieves a minimum at $s = \cos^2\mu(\cos\varphi - 1)^2 + \sin^2\mu(\cos\varphi - 1)^2 = (1 - \cos\varphi)^2$, so

$$\begin{aligned}\mathrm{SRC}[D_2](\Lambda) &= \sigma\sqrt{(1 - \cos\varphi)^2 + \sin^2\varphi}\\ &= \sigma\sqrt{2 - 2\cos\varphi}\\ &= \sigma\sqrt{4\sin^2\frac{\varphi}{2}}\\ &= 2\sigma|\sin\frac{\varphi}{2}|\end{aligned}$$

Case of $\mathrm{SRC}[D_4]$. In the spherical coordinates (μ, φ, σ), the subspace of square lattices is defined by $\varphi = 0$, $\mu = 67.5°$, see Figure 3.7. The spherical root D_4-chiral distance $\mathrm{SRC}[D_4](\Lambda)$ equals the Euclidean distance from $(x, y, z) = \sigma(\cos\varphi\cos\mu, \cos\varphi\sin\mu, \sin\varphi)$ to the point $\mathrm{SRI}(\Lambda_4) = \sigma(\cos 67.5°, \sin 67.5°, 0)$, which represents the only square lattice Λ_4 of the same size σ, so $\mathrm{SRC}[D_4](\Lambda) = \sigma\sqrt{(\cos\varphi\cos\mu - \cos 67.5°)^2 + (\cos\varphi\sin\mu - \sin 67.5°)^2 + \sin^2\varphi}$.

Case of $\mathrm{SRC}[D_6]$. In the spherical coordinates, the subspace of hexagonal lattices is defined by $\varphi = 0$, $\mu = -45°$, see Figure 3.7. The spherical root D_6-chiral distance $\mathrm{SRC}[D_6](\Lambda)$ equals the Euclidean distance from $(x, y, z) = \sigma(\cos\varphi\cos\mu, \cos\varphi\sin\mu, \sin\varphi)$ to the point $\mathrm{SRI}(\Lambda_6) = \sigma(\cos 45°, -\sin 45°, 0)$, which represents the only hexagonal lattice Λ_6 of the same size σ, so $\mathrm{SRC}[D_6](\Lambda) = \sigma\sqrt{(\cos\varphi\cos\mu - \cos 45°)^2 + (\cos\varphi\sin\mu + \sin 45°)^2 + \sin^2\varphi}$.

□

The upper bound of any chiral distance in the sphere will be 90° (the distance to the equator), and any *root* chiral distance will not have any theoretical upper bound.

Proposition 4.4.5 (Kurlin [84]). *The value of $PC_2[D_2]$ has an upper bound of $\frac{1}{2+\sqrt{2}} \approx 0.29$.*

Proof. By proposition 4.4.2, $\mathrm{PC}_2[D_2] = \min\left\{x, y, \frac{1-x-y}{\sqrt{2}}\right\}$, which must be maximal when $x = y = \frac{1-x-y}{\sqrt{2}} \implies \frac{1-2(x+y)}{\sqrt{2}} = 0 \implies x = y = \frac{1}{2+\sqrt{2}}$. □

4.5 Maps of G-Chiral Distances in the CSD

This section illustrates the ease with which the chiral distances can be computed for very large datasets by visualising histograms of G-chiral distances from the millions of 2D lattices extracted from all 870+ thousand crystals in the Cambridge Structural Database in the manner described in Chapter 3. All plots were produced on a standard laptop in a few minutes by the code at `https://github.com/MattB-242/Lattice_Invariance`.

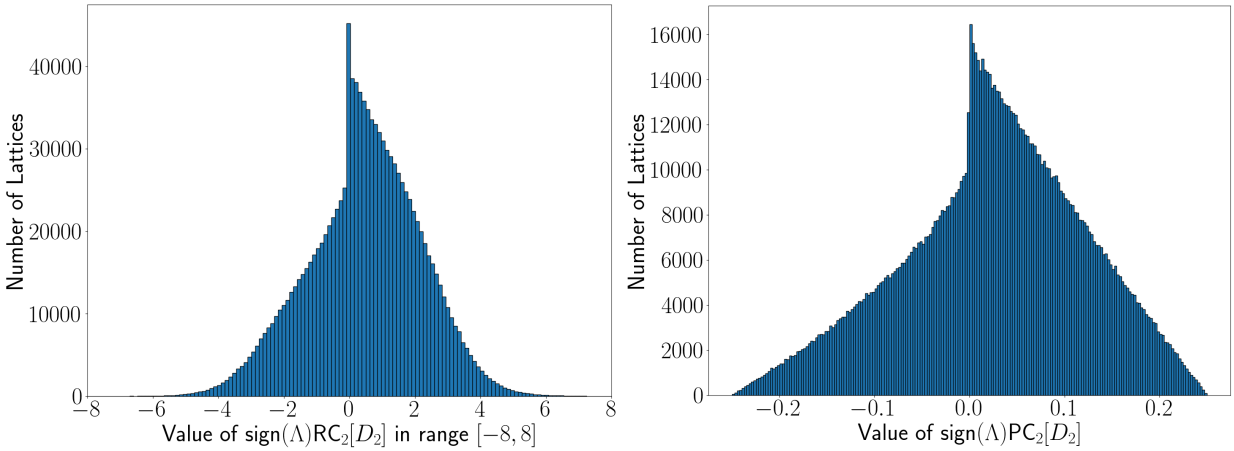

Figure 4.2: Signed D_2-chiral distances of all oblique 2D lattices found in the CSD, see Definition 4.4.1 **Left**: $\mathrm{sign}(\Lambda)\mathrm{RC}_2[D_2](\Lambda)$ in Ångstroms. **Right**: $\mathrm{sign}(\Lambda)\mathrm{PC}_2[D_2](\Lambda)$ is unitless.

Since any non-oblique (mirror-symmetric) 2D lattice has all D_2-chiral distances equal to zero, we first focus on oblique (non-mirror symmetric)lattices. The total number of these is 1177678, which is about 45% of all 2D lattices found in the CSD. Figure 4.2-4.4 show the histograms of the signed distances $\mathrm{sign}(\Lambda)\mathrm{RC}_2[G](\Lambda)$ and $\mathrm{sign}(\Lambda)\mathrm{PC}_2[G](\Lambda)$ for the point groups $G \in \{D_2, D_4, D_6\}$.

Figure 4.2 quantifies the continuous tendency towards non-oblique lattices, which have $\mathrm{RC}_2[D_2] = 0 = \mathrm{PC}_2[D_2]$. The preponderance of lattices of positive sign is explained by the ordering of lattice vectors, as discussed in the exploration of Figure 3.9 in Chapter 3. The fact that values of $PC_2[D_2]$ occupy almost the full range between the values $\pm\frac{1}{2+\sqrt{2}}$ of Proposition 4.4.5 indicates again that lattices in real crystals can adopt a wide range of geometric configurations. Since there is no theoretical upper bound on $\mathrm{RC}_2[D_2]$, it is notable that the vast majority of lattices (99.9%) occupy a fairly narrow range of signed chiral distances between ± 8.

In Figures 4.2-4.6, the histograms of all root G-chiral distances have the bin size 0.1Å, while the histograms of all projected G-chiral distances have the bin size of 0.01 (unitless). In all charts we omit any lattices with G-chiral distances equal to zero for the relevant symmetry group G. There are a number of structural elements to note in Figures 4.3 and 4.4 - in particular the differing size of the gaps around zero chirality and the well-defined peaks.

Figure 4.7 explains some of the features visible in these plots. The central density plot recalls the structure of the continuous map from the lattice invariance space, but confined to the quotient triangle QT of Definition 3.3.14. If we plot the number of $2D$ lattices extracted from the CSD in the QT, we observe a strong preference for higher symmetry structures (on the boundary) and a concentration of lattices towards the point $(0, 1)$ representing the hexagonal lattice, while the number decreases towards the point $(1, 0)$ representing infinitely long, thin cells, as seen in Chapter 3. Figure 4.7 (left) illustrates a geometric reason for this by showing how chiral distances change for the centred rectangular lattice Λ_θ with basis vectors of length 1 as its angle θ varies in $[90°, 120°]$. Close to 90°, $\mathrm{PC}_2[D_4](\Lambda_\theta)$ increases rapidly with a small change in angle - the rate of increase slows as we move closer to $\theta = 120°$. The plot thus concentrates lattices closer to the point $(0, 1)$ representing the hexagonal lattice, explaining the apparent rarity of lattices with low D_4-chiral distances compared to the plot for $\mathrm{PC}_2[D_6]$.

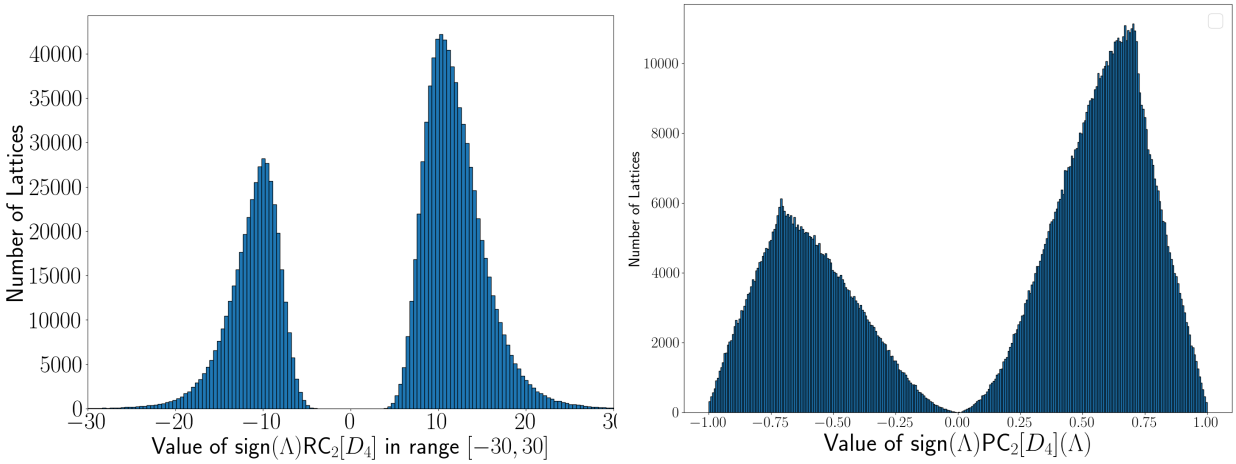

Figure 4.3: Signed D_4-chiral distances of 1,177,678 oblique 2D lattices in the CSD, see Definition 4.4.1 **Left**: $\mathrm{sign}(\Lambda)\mathrm{RC}_2[D_4](\Lambda)$ in Ångstroms. **Right**: $\mathrm{sign}(\Lambda)\mathrm{PC}_2[D_4](\Lambda)$ is unitless.

To explain the peaks of $\mathrm{PC}_2[D_4](\Lambda) \approx \frac{1}{\sqrt{2}}$ and $\mathrm{PC}_2[D_6] \approx \frac{1}{2}$, we observe the intersection of circles at the origin and the points $(0, 0)$ with the QT - see Figure 4.7 (right). We would expect the frequency of a particular chiral distance value to be a function of both the length of the intersection of the circle whose radius corresponds to that value and the density, in terms of CSD-derived 2D lattices, of the region through which the circle passes. The intersection of the circle at the origin of radius $\frac{1}{\sqrt{2}}$ with the QT gives a curve of maximal

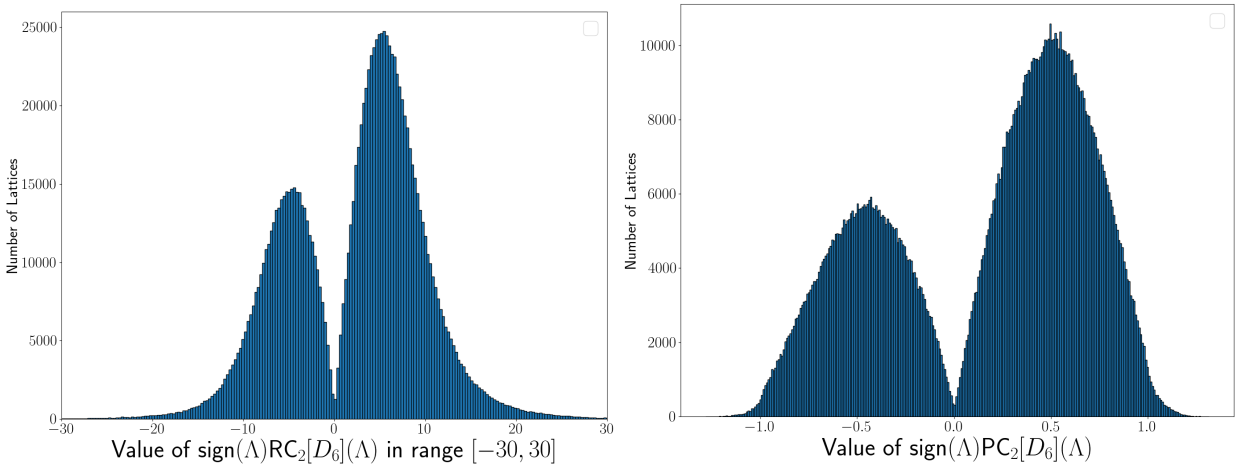

Figure 4.4: Signed D_6-chiral distances of 1,177,678 oblique 2D lattices in the CSD, see Definition 4.4.1. **Left**: $\text{sign}(\Lambda)\text{RC}_2[D_6](\Lambda)$ in Ångstroms. **Right**: $\text{sign}(\Lambda)\text{PC}_2[D_6](\Lambda)$ is unitless.

length. Thus a larger number of lattices in the plot in the centre will intersect with this curve.

The maximal length circle of radius 1 centred at the point $(1, 0)$ would pass mostly through a low-density area - as its radius decreases the density of lattices increases but the length of the intersection decreases - an optimum is evidently reached at radius $\frac{1}{2}$.

In Chapter 3 we discussed the single high density point representing multiple deposited structures of oxalic acid in the CSD. The two dimensional lattice Λ_{OX} derived from the single pair of non-orthogonal vectors in the primitive monoclinic parent lattice has parameters $a = 6.1143$Å, $b = 12.0109$Å, $\gamma = 106.1°$. Computation of chiral distances does indeed give the expected values $\text{PC}_2[D_4](\Lambda_{OX}) \approx \frac{1}{\sqrt{2}}$ and $\text{PC}_2[D_6](\Lambda_{OX}) \approx \frac{1}{2}$ - thus we do not see this structure as a separate peak since it occupies the most probable 2 dimensional configuration.

Figure 4.5 shows the spherical D_2-chiral distance on the complete dataset, exhibiting similar behaviour to the planar version. Any non-oblique lattice is either rectangular (primitive or centred) or has even higher symmetry (square or hexagonal).

Figure 4.6 shows the histograms of root distances from rectangular 2D lattices in the CSD to their closest square and hexagonal lattices. The high bar to about 6000 lattices in Figure 4.6 (right) indicates that the CSD has many centred rectangular lattices close to hexagonal ones and many fewer rectangular lattices close to square ones.

We can investigate the relationship between continuous chiral distances and chemical characteristics such as molecular weight by isolating the root and projected invariants of 2D lattices derived from the $50,000$ crystals whose constituent molecules had the highest molecular weight, and the $50,000$ of lowest molecular weight.

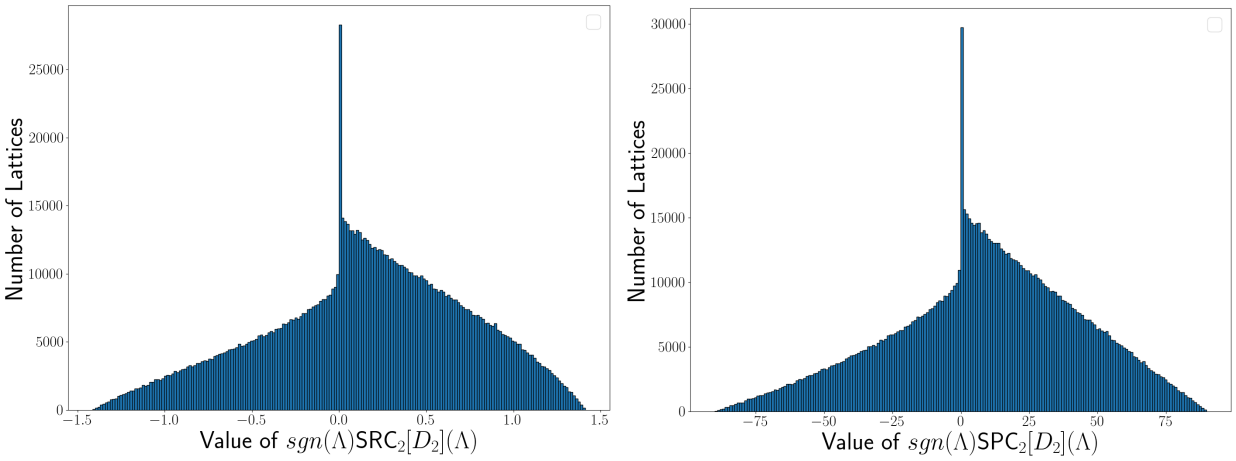

Figure 4.5: Histogram of signed spherical D_2-chiral distances of 2D lattices from all crystals in the CSD. **Left**: $\mathrm{SRC}[D_2](\Lambda)$ is in Ångstroms (Å). **Right**: $\mathrm{SPC}[D_2](\Lambda)$ is in degrees.

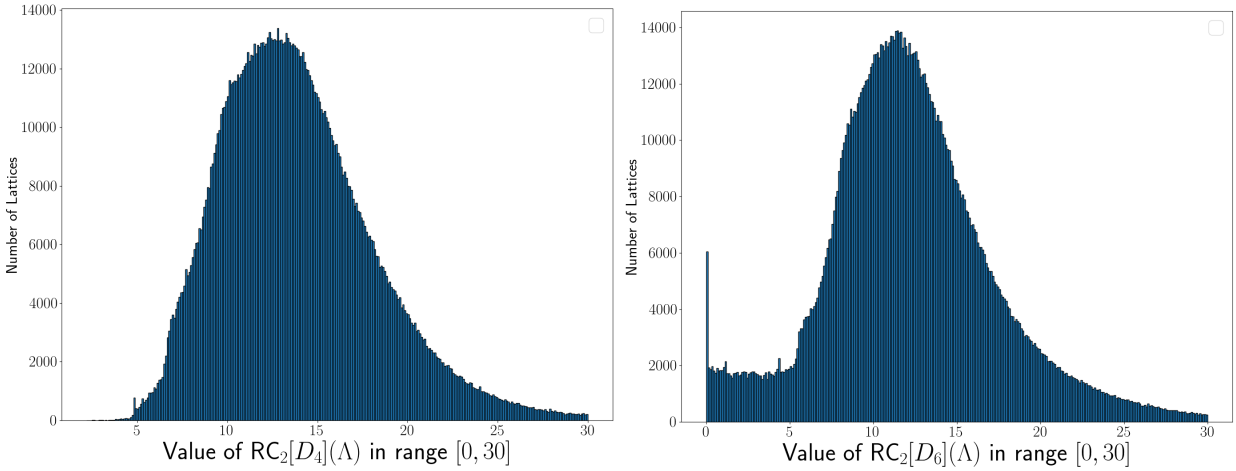

Figure 4.6: Distances (in Ångstroms) of rectangular (primitive and centred) 2D lattices. **Left**: $\mathrm{RC}_2[D_4](\Lambda)$ to a closest square lattice. **Right**: $\mathrm{RC}_2[D_6](\Lambda)$ to a closest hexagonal lattice.

A preliminary analysis shows that a slightly proportion (57%) of the lowest molecular weight molecules have $PC_2[D_2] = 0$. By this discrete analysis, we might say that crystals of lower-weight molecules tend to form a more symmetric lattice. Continuous analysis, reveals a more nuanced picture. Figure 4.8 compares the histograms of chiral distances for oblique 2D lattices extracted from crystals in the CSD whose main molecules have extreme (low or high) weight. The overall distribution of chiral distances for higher molecular weight molecules is slightly wider, indicating that higher molecular weight crystals tend to form lattices with more extreme chiral distances. There is a stronger preference towards negative sign for high-weight molecules which is more clearly visible when comparing values of $\mathrm{RC}_2[D_2]$.

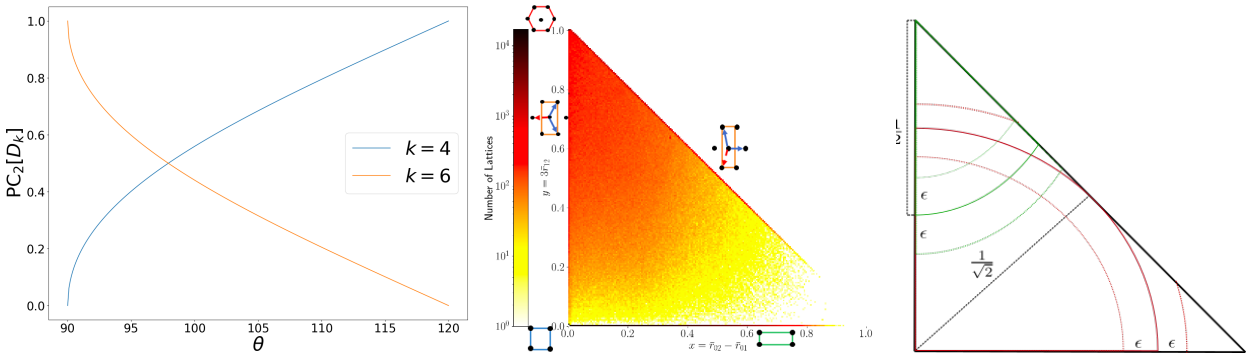

Figure 4.7: **Left**: values of $\mathrm{PC}_2[D_4]$ and $\mathrm{PC}_2[D_6]$ for a lattice with parameters $a = 1, b = 1$ and angle $\theta \in [90°, 120°]$ **Centre**: heat map of all 2D lattices in the quotient triangle, extracted from crystals in the CSD. **Right**: intersection of QT with red and green circles centred at the origin $(0, 0)$ and the vertex $(0, 1)$, respectively, of the radii $r_i = \frac{1}{2}$ and $r_i \pm \epsilon$ for $i = 1, 2$.

Organometallic crystals have unit cells containing an organic molecule non-covalently bonded to one or more metal ions. Their importance as new materials is illustrated by the fact that nearly half ($\sim 52\%$) of the deposited structures in the CSD which form oblique lattices are organometallic. They are often a target for materials design by crystal structure prediction experiments, and so there is a drive for methods that can help to categorise the outputs of such experiments [12].

In Figure 4.9, it appears that organometallic lattices have a stronger tendency to form crystals whose derived 2D lattices have negative signs, and from the histogram of $\mathrm{RC}_2[D_2]$ values we observe a wider distribution of distances overall.

The differences discussed above relatively small, but they illustrate the sort of analysis that can be done quickly to investigate possible differences between very large crystal datasets

4.6 G-Chiral Distances in 2D Materials

A more directly practical application of chiral distances is in the investigation of the geometry of 2D monolayers. This has been an area of great interest in chemistry since such materials are predicted to have many useful physical properties [118]. While the lattice parameters for 2D monolayers are very often close to those of high symmetry lattices (square or hexagonal), there is a growing interest in stable 2D structures with more generic lattice geometries [119]. Our chiral distances allow a more formal definition of this problem - we wish to find materials whose lattices have a high chiral distance, and whose projected invariants will thus occupy the interior of the QT.

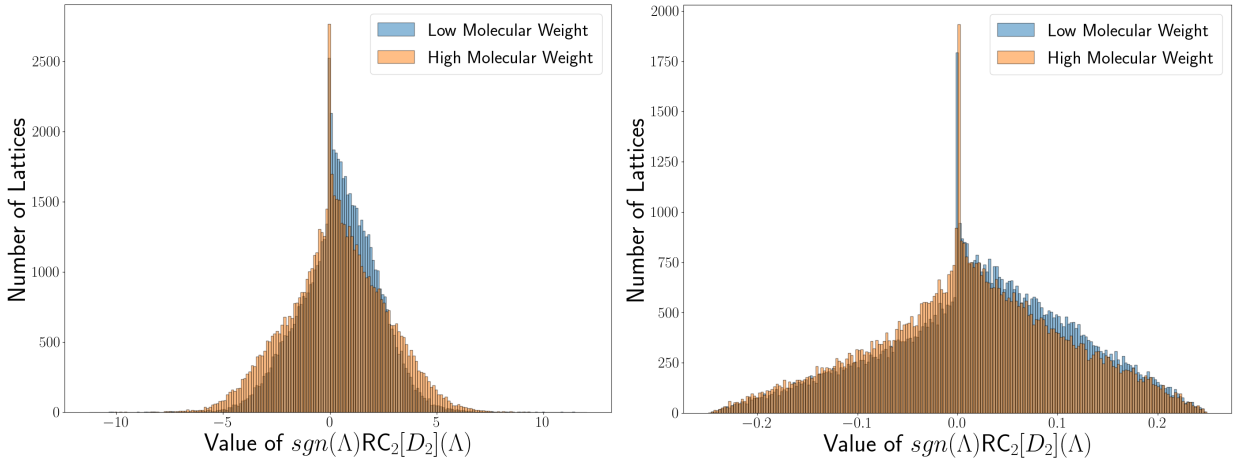

Figure 4.8: Histograms of $\mathrm{RC}_2[D_2]$ (**left**) and $\mathrm{PC}_2[D_2]$ (**right**) for oblique lattices in crystals whose molecular weight is among the the $50,000$ highest and lowest in the CSD.

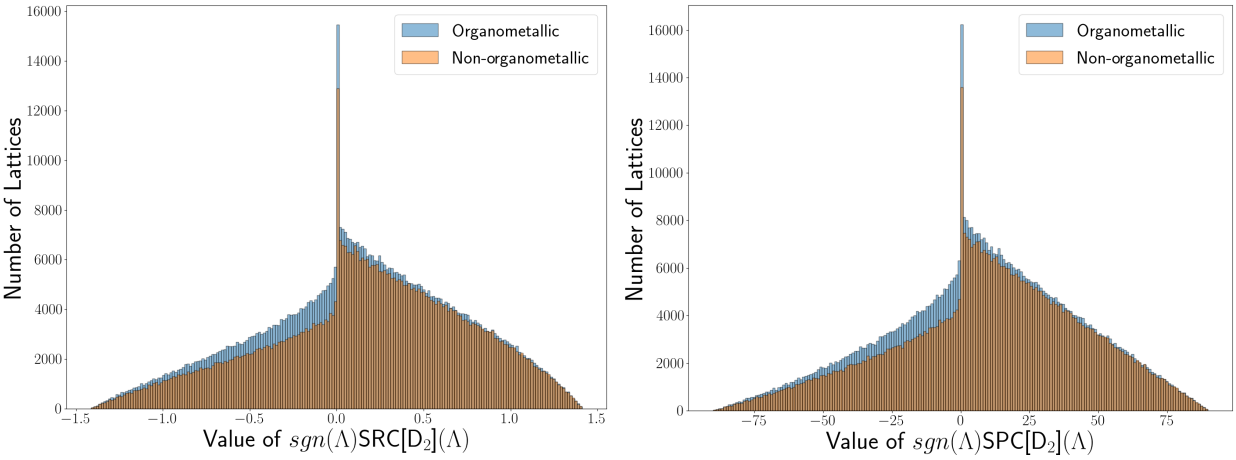

Figure 4.9: Histograms of spherical D_2-chiral distances of 2D lattices in the CSD, separated into organometallic and non-organometallic structures. **Left**: $\mathrm{SRC}[D_2]$. **Right**: $\mathrm{SPC}[D_2]$.

2DMatPedia [3] is one of the largest open-source databases of such materials available - currently containing $6,351$ crystal structures that have the potential to form monolayers. Of these, two were retrieved from existing literature, $2,940$ were found through a *layer detection* approach (referred to in the publication describing this data as a 'top-down' process), in which separable 2-dimensional features were detected from geometric data [120]. The remaining structures were then generated from this list by the *substitution* of atoms in the same group - the 'bottom-up' discovery process. Potential physical properties of the 2D structures are then simulated.

A natural first question is whether the database can tell us anything about the feasibility of synthesising 2D structures with oblique lattices. The database includes two quantities which determine this potential - the *decomposition energy*, which is the energy required to split a structure into its most stable components, and the *exfoliation energy*, which is the average energy per atom required to separate the modelled layer from its parent material. The former should be high, and the latter low, to guarantee stability - typically $0.2eV$ is considered an acceptable upper bound for exfoliation energy in 2D structures [121].

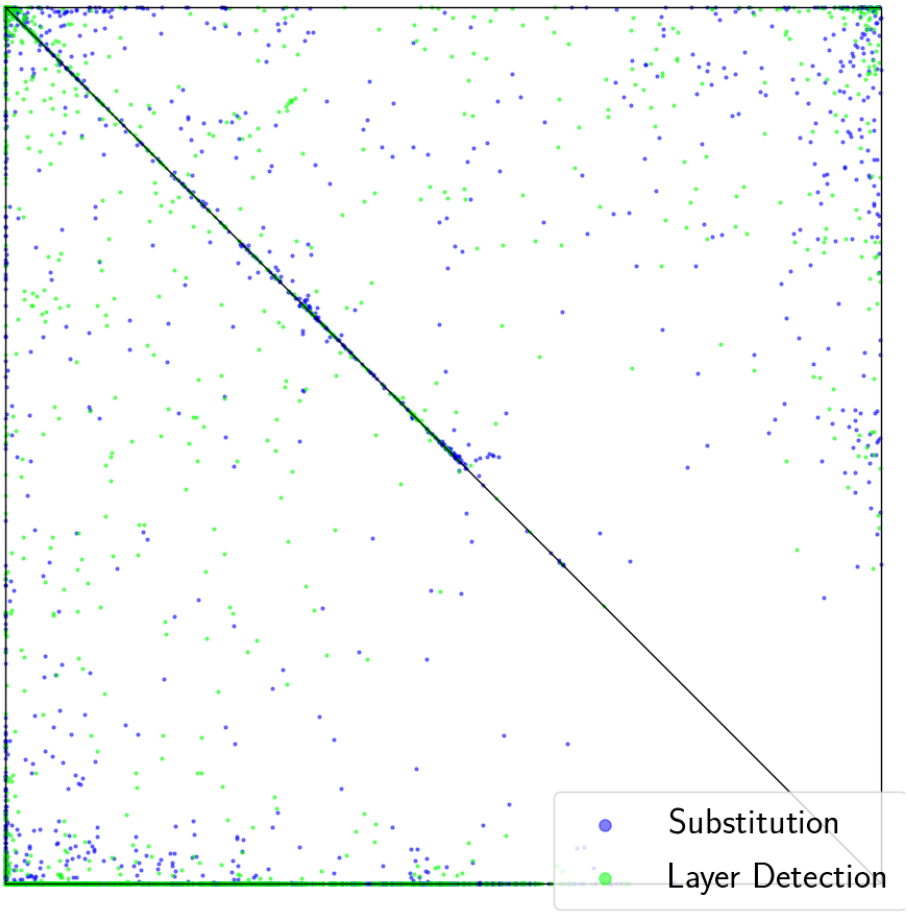

Figure 4.10: Invariants $\mathrm{PI}^o(\Lambda)$ in the square QS for 2D lattices of 6,351 monolayer structures [3] isolated from 3D crystals by layer detection or generated by atomic substitution.

Figure 4.10 shows the positions of the oriented projected invariants $\mathrm{PI}^o(\Lambda)$ (Definition 3.3.14), for 2D lattices of all structures in 2DMatPedia. It is clear that strongly oblique 2D lattices are relatively rare in this dataset. The majority of 2D lattices are non-oblique, with very few occupying the interior of the square: 66% of lattices in the database have sign 0, and 75% have extremely small D_2-chiral distances $\mathrm{RC}_2[D_2]$ less than 3×10^{-8}Å.

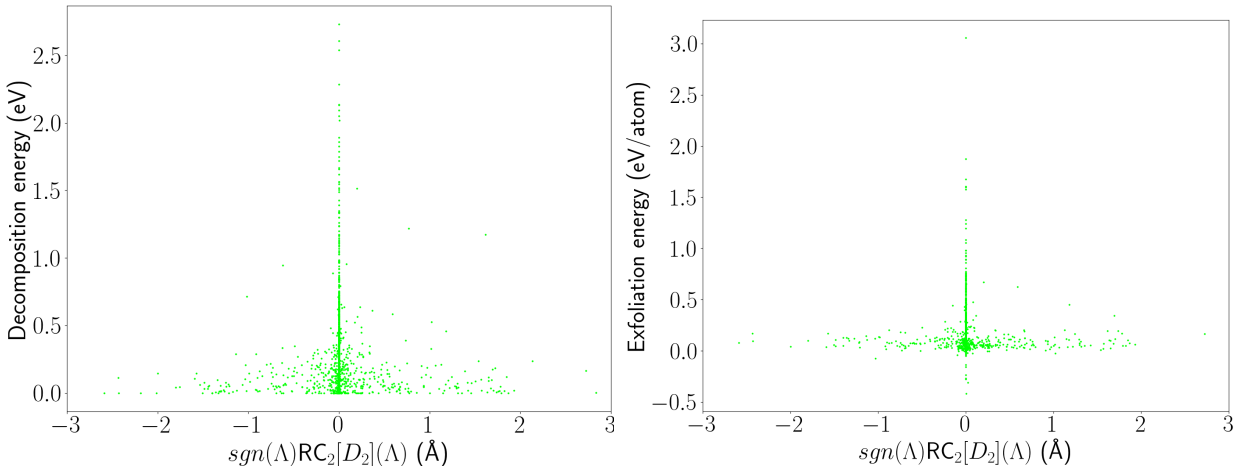

Figure 4.11: Scatter plot of physical properties of materials discovered by layer detection in 2DMatPedia vs sign(Λ)RC[D_2](Λ). **Left**: Decomposition energy in meV. **Right**: Exfoliation energy in meV per atom.

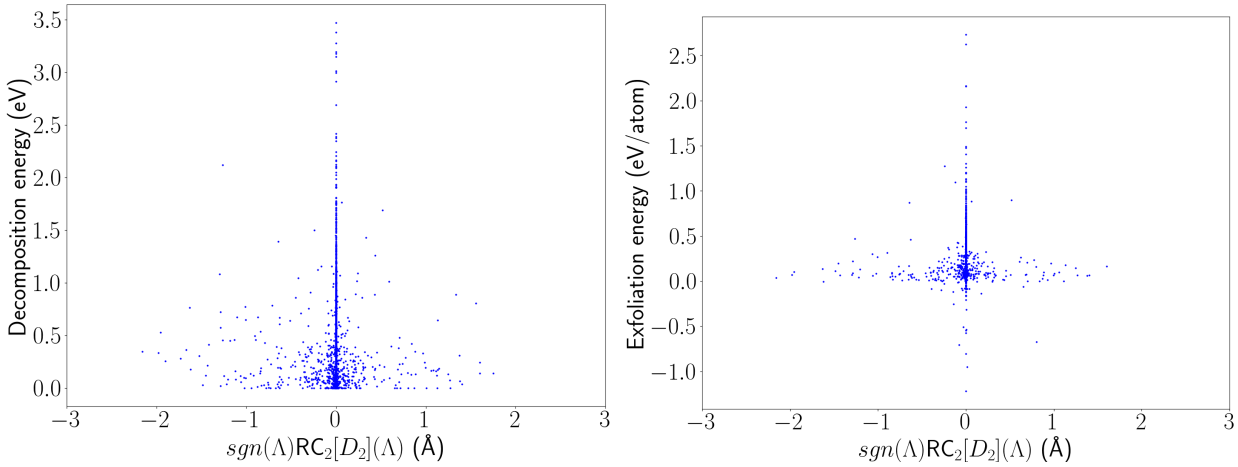

Figure 4.12: Scatter plot of physical properties of materials discovered by atomic substitution in 2DMatPedia vs sign(Λ)RC[D_2](Λ). **Left**: Decomposition energy in meV. **Right**: Exfoliation energy in meV per atom.

In Figures 4.11 and 4.12, we see the relationship between overall G-chiral distance (using the $\mathrm{RC}_2[D_2]$ metric) and both indicators of the feasibility of potential $2D$ materials. The most obvious thing to note is that the highest decomposition energies and lowest exfoliation energies occur with materials whose layers are non-oblique. It is also notable that the range of chiral distances overall is within $[-3, 3]$ - this less than half of the range of root chiral distances in lattices from the CSD shown in Figure 4.2. This suggests that oblique lattices are not structurally preferred or strongly stable in candidate 2D materials.

It is also interesting to note that on the whole atomic substitution gives rise to structures with lower chiral distances - lying in the range $[-2.1, 2.0]$ while structures found by identifying layers geometrically lie in the wider range of $[-2.5, 2.8]$.

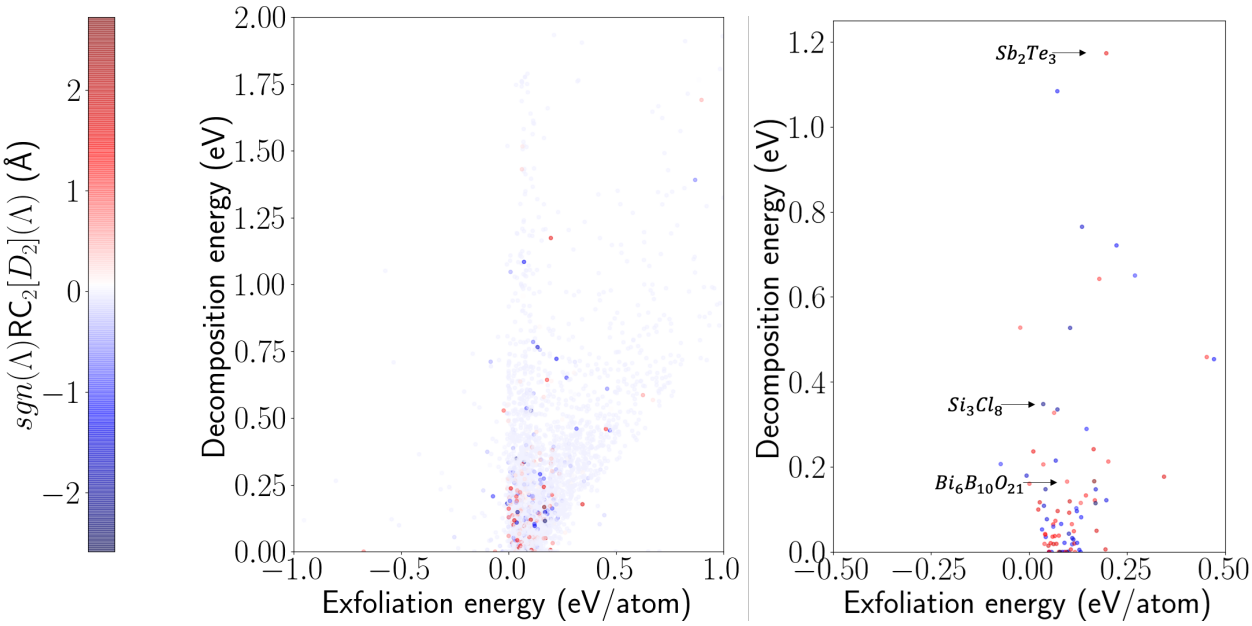

Figure 4.13: $2D$ scatter plot of exfoliation vs.decomposition energy, with G-chiral distance indicated by colour **Left**: All structures in 2DMatPedia. **Right**: Structures where $\mathrm{RC}_2[D_2] \geq 1$

In Figure 4.13 we try to isolate high G-chiral distance 2D structures that may feasibly be synthesised by plotting both exfoliation and decomposition energy on the same 2D plot. The right hand plot shows only those molecules with a D_2-chiral distance of an absolute value above 1, with three structures labelled that have low exfoliation and relatively high decomposition energy.

Of these three monolayer structures, only one, antimony telluride (Sb_2Te_3) has been reported in the literature. In its monolayer form, the structure of Sb_2Te_3 has been found to exhibit reversible state changes which switch its electrical resistance from low to high values [122]. The asymmetric geometry of its two dimensional structure means that it is one of a growing class of *Janus materials* [123, 124] with properties that are potentially useful in the field of quantum computing.

Of the other two structures, one - octachlorotrisilane(Si_3Cl_8) - has been reported in the chemical literature, where it has been used as a substrate for creating monolayers of Silicon Nitride [125], but not investigated as a potential $2D$ layer material in itself. The structure with formula $Bi_6B_{10}O_{21}$ exists only in simulated form, but as well as appearing in the database under investigation, it has an entry in the Materials Project [15], and in a database investigating materials with specific electronic transport properties [126].

We thus illustrate that our chiral distance measure successfully isolates existing asymmetric monolayer structures, and suggests potentially new targets for creating such structures.

The 2D materials database [4] is smaller than 2DMatPedia, containing only 1728 structures. It is of interest since of these structures, 183 were additionally 'relaxed': further DFT computations simulate the likely final 2D structures once isolated from the parent crystal. Our main analysis here investigates the effect of such relaxation on resulting G-chiral distances.

Figures 4.14 and 4.15 show the invariants PI(Λ) of 1726 original 2D lattices and 183 'relaxed' structures in the square QS with coordinates $(x, y) \in [0, 1]$, see Definition 3.4.5. The elemental structures (monolayers of a single element) are highlighted in red, the MX2 structures [127], where M is a metal and X is a halogen, are in green, and the transition metal dichalcogenide monolayers [128] (TMDC) are in blue. For illustration some of these have been labelled, although since several structures occupy higher symmetry lattice points at the vertics we have not labelled all of them. In Figure 4.15, the green dot at the top left vertex $(0, 1)$ of the square QS indicates the hexagonal crystal of Nb3Br8, whose monolayer form was recently discovered to have the long-sought-after property of acting as a superconducting diode [129].

The key observation in this analysis is that while candidate 2D structures in their parent crystal can be both oblique and non-oblique, nearly all such structures simulated in isolation become non-oblique. This suggests that candidate materials with even larger D_2-chiral distances such as those selected above from 2DMatpedia may, when isolated, revert to a mirror-symmetric state. We have labelled the three chiral molecules that retain non-zero D_2-chiral distances with the formula of their parent structure. AgNO2 has in fact been shown to form chiral monolayers [129], but we are not aware of any publications specifically concerning the other two structures.

4.7 Conclusion and Discussion

In this chapter, we have added metrics on the isometry, rigid motion and similarity invariants discussed in Chapter 3, and provided proofs that they obey all metric axioms. We have derived from this a continuous quantifications of the chirality of a lattice as its continuous distance from the subspace of lattices with a particular Bravais type within the metric space. By providing explicit closed formulae for these distances, we have demonstrated that as with the invariants themselves, the computability requirement of Problem 1.4.1 is satisfied.

Having implemented the computation of these chiral distances, we have applied them first to the large dataset of artificially generated lattices from the CSD in the previous chapter, demonstrating directly the strong preference even among oblique lattices for being as close as possible to a symmetric configuration.

More practically, we have shown that the metric can be used to investigate databases of actual two dimensional structures, helping to isolate those with lattice geometries which indicate they may have useful chemical properties.

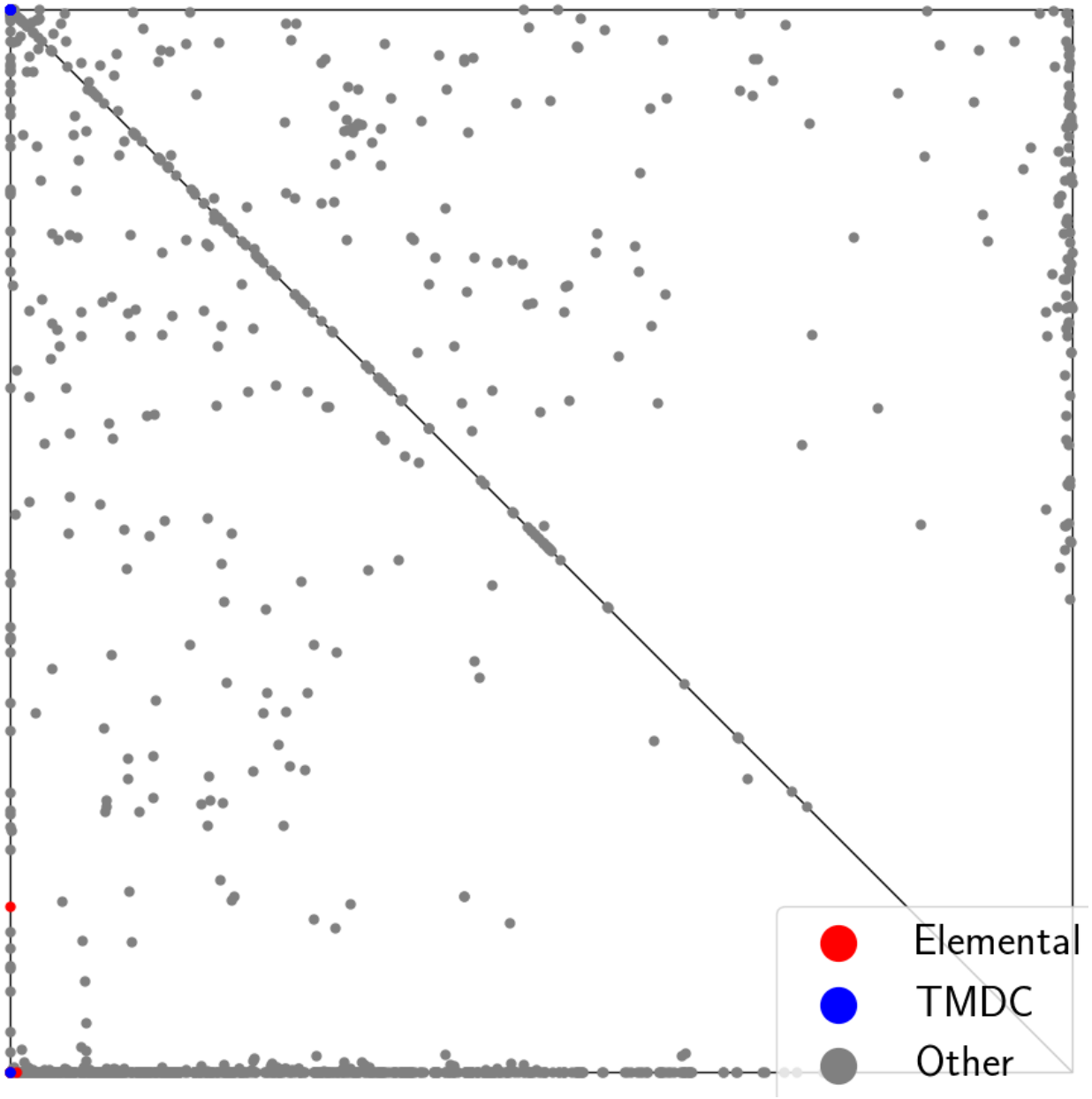

Figure 4.14: 2D lattices of 1726 monolayer structures [4] isolated from 3D crystals and shown by the invariants PI(Λ) in the quotient square (see Definition 3.4.5) and labels of structures in Figure 4.15.

In doing so, we have shown that it is possible to isolate materials from which layer structures with asymmetric lattices geometry may be derived, but also that there is liable to be a strong tendency for such layers to settle into a higher symmetry configuration when isolated.

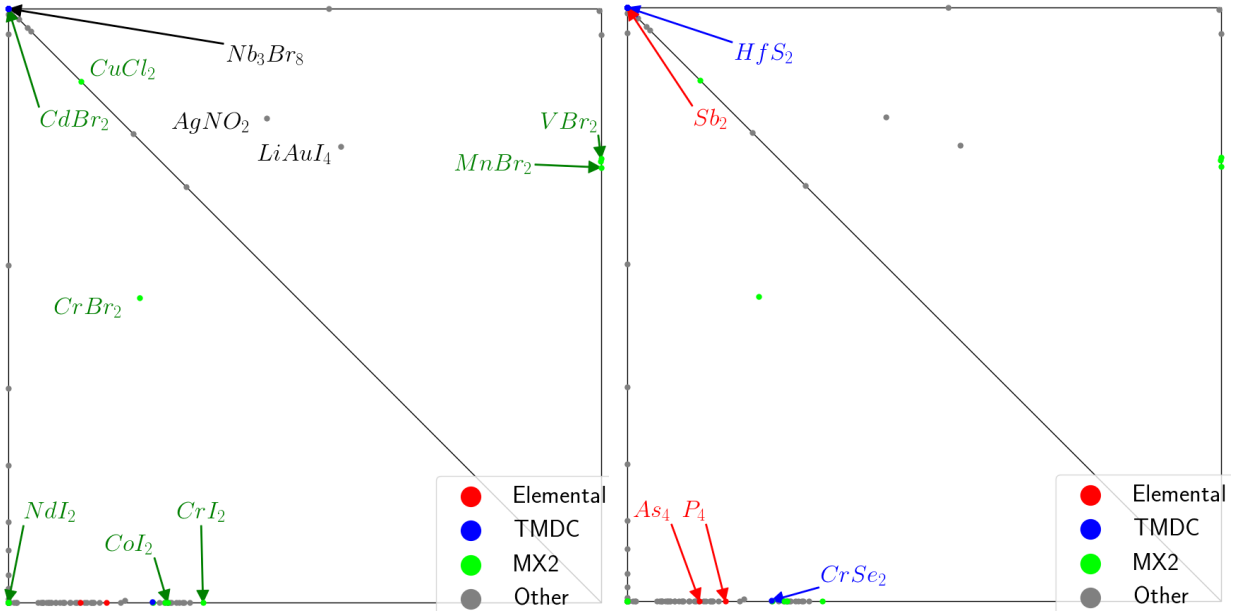

Figure 4.15: Projected invariants of 183 2D lattices simulated separately from their parent material in the QS- compare to the 1726 monolayer structures in Figure 4.14. **Left**: structures with oblique lattices and molecules of type MX2 are labelled in green. **Right**: elemental crystals and molecules of type TMDC are labelled in red and blue.

In the next chapter we will summarise the content of this thesis, and briefly discuss future work to extend the approach we have described to the three dimensional case.

Chapter 5

Conclusions and Future Work

5.1 Conclusions

In this section we briefly summarise the motivations behind this thesis and its key theoretical and applied contributions. We conclude by briefly discussing the extension of our work to three- and higher dimensional lattices.

5.1.1 Thesis Summary

The growth in crystal structure data can be illustrated by the fact that since the maps of Chapters 3 and 4 were generated in 2022, a recent download pursuant to future work on three dimensional lattices has indicated that over $10,000$ new crystal structures have been deposited in the Cambridge Crystallographic Structural database. Crystal Structure Prediction has become a standard tool of materials design, regularly producing datsets of many thousands of hypothetical structures explorable mainly through maps of their energy and density.

Since the geometry of a solid state material gives rise to many of its key properties, the ability to search through these large databases, or CSP landscapes, either to find materials with diverse geometries or to locate structures that have geometries similar to materials with known properties, is clearly beneficial. Current geometric descriptions, even at the most granular possible level, are certainly not complete invariants of the geometry of a crystal, since many structures with very different geometries as point sets can have the same space group. While the discrete classifications of classical crystallography discussed in Chapter 2 are an essential tool for broadly classifying these huge datasets, a continuous classification of the structures in them allow for a more fine-grained exploration of the relationship between their geometric structure and other properties of interest.

When considering any problem which requires a rigorous mathematical description, it is often beneficial to begin with the simplest non-trivial examples, in the hope that approaches which apply to them can be extended to more complex contexts. Since lattices are the fundamental building blocks of the description of any periodic material, this is where we

have begun in this thesis. In most cases, the mathematics of one dimensional lattices (sets of the form $\{ka : k \in \mathbb{Z}, a \in \mathbb{R}\}$ are too trivial to give rise to meaningful results, but lattices in two dimensions, as this thesis has shown, give rise to a rich mathematical structure.

In Chapter 1 we outlined in more detail the motivation behind this work and then developed the formal terminological machinery necessary to turn the broad aim of continuous classification defined about into an exact mathematical description of the problem for two dimensional lattices - ultimately leading to the full statement of Problem 1.4.1 which is addressed in the rest of the thesis.

In Chapter 2 we have discussed those elements of the long history of lattice geometry that are crucial to our approach to this problem. The proper selection of a lattice basis from among the infinite possible choices available to is a necessary first step, and we have discussed some of the approaches to these *lattice reductions*. Since we are aiming for a continuous classification of lattices, we have provided some historical detail on lattice classification, and the discrete approaches to the problem based on lattice symmetries. Finally in that section, we have discussed different approaches to continuous lattice comparison and how these fall short of the problem stated in Chapter 1

In Chapter 3 we develop part of the answer to this problem - the creation of a computable and easily invertible complete isometry invariant for two dimensional lattices. Ultimately, the correct lattice basis to approach this problem in two dimensions is given by the use of the obtuse superbase, of Definition 3.2.9. The crucial theoretical contribution, is summarised in Theorem 3.3.10, which states that the ordered inner products of the obtuse superbase of a two dimensional lattice are an isometry invariant which varies continuously with continuous deformation of the lattice itself. In addition, by defining the *size* of a lattice (Definition 3.3.12), we develop an additional invariant up to *similarity* - that is, isometry (or rigid motion) and scale. It follows from the proofs of completeness of the root invariant that this *projected invariant* (Definition 3.3.14) has the properties required by Problem 1.4.1 for similarity classes of lattice (see Corollary 3.3.16). By adding the *sign* of the lattice (Definition 1.3.4), we generate *orientation-aware* versions of both invariants which can be used to distinguish lattices up to rigid motion.

Our practical contribution is then the development of maps to visualise these invariants. The root invariant itself, and its orientation-aware version, map to the subsets of $\mathbb{R}^3$ given in definitions 3.4.1 and 3.4.2 respectively, while the projected invariant maps to subsets of $\mathbb{R}^2$ were given in Definition 3.3.14 and Definition 3.4.5 respectively. We also develop alternative maps of similarity classes of lattices to a punctured sphere in Definition 3.4.6, with an explicit mapping from the projected invariant to this space in Proposition 3.4.7.

Since the invariants discussed in Chapter 3 give rise to the *Root Invariant Space* of Definition 3.3.22, and the Projected Invariant Space of Definition 3.3.14, the natural next step to completing the problem is to construct an explicit metric on these spaces. In Chapter 4 we define such a metric for classes of lattices up to rigid motion or similarity mapped to the TC and QT respectively in Definition 4.3.3. We prove it is a metric in Theorem 4.3.4, and prove that this metric is continuous in Theorem 4.3.5.

For any given lattice, the minimal distance, in terms of these metrics, between that lattice and any of the lattices in a subspace representing all lattices with a particular point symmetry group G is defined as the *G-chiral distance*. Definitions 4.4.1 state this explicitly for root and projected invariants. Definition 4.4.3 applies the general definition to the spherical projected invariants, 3.4.6 and extends this to root projected invariants by adding the *size* of Definition 3.3.12 as a vertical height above the sphere in Definition 4.3.11.

As with the invariants themselves, our contribution in terms of application is the necessary code to compute all metrics and G-chiral distances, using the explicit closed forms of Propositions 4.3.7 4.4.2 and 4.4.4. We use this not only to look at symmetries within the same dataset of two dimensional lattices generated from the CSD as in the previous chapter, but at the geometries of real two dimensional monolayer materials. While these databases are somewhat smaller, we show that we are able to use chiral distances to isolate potential monolayer materials with highly asymmetric lattice geometries, and to quantify the modelled behaviour of such lattices when isolated as layers from their parent material, illustrating some of their potential use cases.

5.1.2 Extension to Higher Dimensons

The most obvious next step on the theoretical side is to extend our work to three dimensional lattices. A number of the theorems stated in chapters 3 and 4 are applicable to lattices in three or indeed any dimension. Theorems 3.2.8 and 3.2.12 allow us to characterise Voronoi vectors in any dimension, and theorem 3.2.10 of Delone gurantees that we can also find obtuse superbases for a three dimensional lattice.

The additional complication in three dimensions is based in the completeness proof of Theorem 3.3.10, which depends on the uniqueness of the obtuse superbase up to isometry proven in lemma 3.2.13, which in turn depends on the fact that that any obtuse superbase must consist of Voronoi vectors (Definition 3.2.6) proven in Theorem 3.2.12. Since for a lattice in general position (that is, without higher symmetry) there are only three pairs of Voronoi vectors (each pair related by a change of sign) there is only one possible choice of obtuse superbase up to inversion (that is, changing the sign of all superbase vectors).

A primitive rectangular $2D$ lattice has among its Voronoi vectors an orthogonal basis v_1, v_2, and another one given by $-v_1, v_2$ where v_1 is reflected in the line v_2. Thus the (non-strict) Voronoi vectors $\pm v_0 = \pm(v_1+v_2)$ and $\pm v_0' = \pm(v_1-v_2)$ complete the obtuse superbase - overall there are four rather than three pairs of Voronoi vectors, allowing for more than one superbase selection.

In the three-dimensional case, there are a maximum of seven pairs of Voronoi vectors for a lattice in general position (that is, with triclinic point group). However, as with the two dimensional case the presence of an orthogonal pair among these vectors gives rise to an additional pair of non-strict Voronoi vectors, but in this case we now have *eight* such pairs. This additional 'headroom' allows for the selection of obtuse superbases that are related by neither isometry nor rigid motion. We give an example of this below for the unit value primitive cubic lattice:

Example 5.1.1. *Let a cubic lattice be generated by the vectors* $v_1 = (1,0,0), v_2 = (0,1,0), v_3 = (0,0,1)$. *These vectors, along with* $v_0 = (-1,-1,-1)$, *form an obtuse superbase since for* $i, j \neq 0$, *the conorms (see Definition 3.3.1 are* $p_{ij} = 0, p_{0j} = 1$. *The vector lengths (vonorms) are* $v_1^2 = v_2^2 = v_3^2 = 1$ *and* $v_0^2 = 3$, *and thus an ordered list of lengths of the superbase vectors is given by* $(1,1,1,\sqrt{3})$.

We now consider the vectors

$$\begin{aligned} u_2 &= v_2 = (0,1,0) \\ u_3 &= -v_3 = (0,0,-1) \\ u_1 &= v_1 + v_3 = (1,0,1) \\ u_0 &= -(u_1 + u_2 + u_3) = -(v_1 + v_2) = (-1,-1,0) \end{aligned}$$

All vectors are in the quotient lattice $\Lambda/2\Lambda$ *and so by theorem 3.2.8 are Voronoi vectors. The coforms* $p_{23} = p_{12} = p_{03} = 0$ *and* $p_{13} = p_{01} = p_{02} = 1$ *indicate that the superbase is still obtuse, but in this case the vonorms are* $u_2^2 = u_3^2 = 1, u_1^2 = 2, u_0^2 = 2$ *- an ordered list of superbase vector lengths is given by* $(1,1,\sqrt{2},\sqrt{2})$. *We have constructed a second non-isometric obtuse superbase.*

In three dimensions, there are few enough Voronoi vectors that an exhaustive analysis of all possible obtuse superbases in each case can still bear fruit as a theoretical approach, since there will still be some sort of geometric relationship between all possible obtuse superbases in any given case. Note, for example, that in Example 5.1.1, an ordered list of conorm values is $(0,0,0,1,1,1)$ in both cases, with the only difference being that these values are assigned to conorms of different index.

Since Theorem 3.2.10 does not extend beyond Dimension 3, the approach to Problem 1.4.1 for 4 and higher dimensional lattices is likely to involve an entirely different theoretical approach. We are not aware of any such work in the current literature on lattice geometry.

Bibliography

[1] Qing Han, Zhong Li, Xiangming Liang, Yong Ding, and Shou-Tian Zheng. Synthesis of a 6-nm-long transition-metal rare-earth-containing polyoxometalate. *Inorganic Chemistry*, 58(19):12534–12537, 2019.

[2] A Pulido, L Chen, T Kaczorowski, D Holden, M Little, S Chong, B Slater, D McMahon, B Bonillo, C Stackhouse, A Stephenson, C Kane, R Clowes, T Hasell, A Cooper, and G Day. Functional materials discovery using energy–structure maps. *Nature*, 543: 657–664, 2017.

[3] J. Zhou, L. Shen, M.D Costa, and others. 2dmatpedia, an open computational database of two-dimensional materials from top-down and bottom-up approaches. *Scientific Data*, 86:669–684, 09 2019.

[4] Nicolas Mounet, Marco Gibertini, Philippe Schwaller, Davide Campi, Andrius Merkys, Antimo Marrazzo, Thibault Sohier, Ivano Eligio Castelli, Andrea Cepellotti, Giovanni Pizzi, et al. Two-dimensional materials from high-throughput computational exfoliation of experimentally known compounds. *Nature nanotechnology*, 13(3):246–252, 2018.

[5] D.T. Emerson. The work of Jagadish Chandra Bose: 100 years of mm wave research. *IEEE Transactions on Microwave Theory and Techniques*, 45(12):2267–2273, 1997.

[6] M. Eckert. Disputed discovery: the beginnings of X-ray diffraction in crystals in 1912 and its repercussions. *Acta Crystallographica A*, 68:30–39, 1997.

[7] J. Yoo, G. Seo, M.R. Chua, T.G. Park, Y. Lu, F. Rotermund, Y.K. Kim, C.S. Moon, N.J. Jeon, J.P. Correa-Baena, V. Bulović, S.S. Shin, M.G. Bawendi, and J. Seo. Efficient perovskite solar cells via improved carrier management. *Nature*, 7847:587–593, 2021.

[8] Zhong-Heng Fu, Xiang Chen, and Qiang Zhang. Review on the lithium transport mechanism in solid-state battery materials. *Wiley Interdisciplinary Reviews: Computational Molecular Science*, 13(1):e1621, 2023.

[9] Yingyi Zhang, Laihao Yu, Kunkun Cui, Hong Wang, and Tao Fu. Carbon capture and storage technology by steel-making slags: Recent progress and future challenges. *Chemical Engineering Journal*, 455:140552, 2023.

[10] Helen M. Berman, John Westbrook, Zukang Feng, Gary Gilliland, T. N. Bhat, Helge Weissig, Ilya N. Shindyalov, and Philip E. Bourne. The Protein Data Bank. *Nucleic Acids Research*, 28(1):235–242, 2000.

[11] Christopher J Cramer and Donald G Truhlar. Density functional theory for transition metals and transition metal chemistry. *Physical Chemistry Chemical Physics*, 11(46): 10757–10816, 2009.

[12] Alessandra Mattei, Richard S. Hong, Hanno Dietrich, Dzmitry Firaha, Julian Helfferich, Yifei Michelle Liu, Kiran Sasikumar, Nathan S. Abraham, Rajni Miglani Bhardwaj, Marcus A. Neumann, and Ahmad Y. Sheikh. Efficient crystal structure prediction for structurally related molecules with accurate and transferable tailor-made force fields. *Journal of Chemical Theory and Computation*, 18(9):583–621, 2022.

[13] Saulius Gražulis, Daniel Chateigner, Robert T. Downs, A. F. T. Yokochi, Miguel Quirós, Luca Lutterotti, Elena Manakova, Justas Butkus, Peter Moeck, and Armel Le Bail. Crystallography Open Database – an open-access collection of crystal structures. *Journal of Applied Crystallography*, 42(4):726–729, Aug 2009. doi: 10.1107/S0021889809016690. URL `http://dx.doi.org/10.1107/S0021889809016690`.

[14] D. Zagorac, H. Müller, S. Ruehl, J. Zagorac, and S. Rehme. Recent developments in the Inorganic Crystal Structure Database: theoretical crystal structure data and related features. *Journal of Applied Crystallography*, 52(5):918–925, 2019.

[15] Anubhav Jain, Shyue Ping Ong, Geoffroy Hautier, Wei Chen, William Davidson Richards, Stephen Dacek, Shreyas Cholia, Dan Gunter, David Skinner, Gerbrand Ceder, and Kristin A. Persson. Commentary: The Materials Project: A materials genome approach to accelerating materials innovation. *APL Materials*, 1(1):011002, 07 2013. ISSN 2166-532X. doi: 10.1063/1.4812323. URL `https://doi.org/10.1063/1.4812323`.

[16] Colin R Groom, Ian J Bruno, Matthew P Lightfoot, and Suzanna C Ward. The Cambridge Structural Database. *Acta Cryst B*, 72(2):171–179, 2016.

[17] I.D. Brown. CIF (Crystallographic Information File): A standard for crystallographic data interchange. *J Res Natl Inst Stand Technoll*, 101(3):341–346, 1996.

[18] Albert Musaelian, Simon Batzner, Anders Johansson, Lixin Sun, Cameron J Owen, Mordechai Kornbluth, and Boris Kozinsky. Learning local equivariant representations for large-scale atomistic dynamics. *Nature Communications*, 14(1):579, 2023.

[19] Felix Musil, Andrea Grisafi, Albert P Bartók, Christoph Ortner, Gábor Csányi, and Michele Ceriotti. Physics-inspired structural representations for molecules and materials. *Chemical Reviews*, 121(16):9759–9815, 2021.

[20] Gregory McColm. Automatically generated periodic graphs. *Zeitschrift für Kristallographie-Crystalline Materials*, 230(12):699–707, 2015.

[21] Alexander P Shevchenko, Aleksandr A Shabalin, Igor Yu Karpukhin, and Vladislav A Blatov. Topological representations of crystal structures: generation, analysis and implementation in the TopCryst system. *Science and Technology of Advanced Materials: Methods*, 2(1):250–265, 2022.

[22] Martin Grohe and Pascal Schweitzer. The graph isomorphism problem. *Communications of the ACM*, 63(11):128–134, 2020.

[23] Daniel Widdowson, Marco Mosca, Angeles Pulido, Vitaliy Kurlin, and Andrew Cooper. Average minimum distances of periodic point sets. *MATCH Communications in Mathematical and in Computer Chemistry*, 87:529–559, 2022.

[24] Daniel Widdowson and Vitaliy Kurlin. Resolving the data ambiguity for periodic crystals. *Advances in Neural Information Processing Systems (Proceedings of NeurIPS 2022)*, 35, 2022.

[25] Qiang Zhu, Daniel Widdowson Jay Johal, Zhongfu Pang, Boyu Li, Christopher Kane, Vitaliy Kurlin, Graeme Day, Marc Little, and Andrew Cooper. Analogy powered by prediction and structural invariants: Computationally-led discovery of a mesoporous hydrogen-bonded organic cage crystal. *Journal of the American Chemical Society*, 144: 9893–9901, 2022.

[26] R. Oishi-Tomiyasu. Positive-definite ternary quadratic forms with the same representations over $\mathbb{Z}$. *International Journal of Number Theory*, 16(7):1493–1534, 2020.

[27] Léo Ducas and Wessel van Woerden. On the lattice isomorphism problem, quadratic forms, remarkable lattices, and cryptography. In *Annual International Conference on the Theory and Applications of Cryptographic Techniques*, pages 643–673. Springer, 2022.

[28] N.J.A Sloane and J.H. Conway. *Sphere Packings, Lattices and Groups (3rd Ed.)*. Springer-Verlag, 1999.

[29] B. Zhilinskii. *Introduction to lattice geometry through group action*. EDP sciences, 2016.

[30] Pietro Sacchi, Matteo Lusi, Aurora J Cruz-Cabeza, Elisa Nauha, and Joel Bernstein. Same or different–that is the question: identification of crystal forms from crystal structure data. *Cryst Eng Comm*, 22(43):7170–7185, 2020.

[31] P. Niggli. Die topologische strukturanalyse II. *Zeitschrift für Crystallographie*, 65: 391–415, 1928.

[32] Matthew Bright, Andrew I Cooper, and Vitaliy Kurlin. Geographic-style maps for 2-dimensional lattices. *Acta Crystallographica Section A*, 79(1), 2023.

[33] Herbert Edelsbrunner, Teresa Heiss, Vitaliy Kurlin, Philip Smith, and Mathijs Wintraecken. The density fingerprint of a periodic point set. In *Proceedings of Symposium on Computational Geometry*, pages 32:1–32:16, 2021.

[34] Phil Smith and Vitaliy Kurlin. A practical algorithm for degree-k Voronoi domains of three-dimensional periodic point sets. In *Lecture Notes in Computer Science (Proceedings of ISVC)*, volume 13599, pages 377–391, 2022.

[35] Olga Anosova and Vitaliy Kurlin. Density functions of periodic sequences. In *Lecture Notes in Computer Science (Proceedings of DGMM)*, volume 13493, pages 395–408, 2022.

[36] Olga Anosova and Vitaliy Kurlin. Density functions of periodic sequences of continuous events. *Journal of Mathematical Imaging and Vision*, 65:689–701, 2023.

[37] Olga Anosova and Vitaliy Kurlin. An isometry classification of periodic point sets. In *Proceedings of Discrete Geometry and Mathematical Morphology*, pages 229–241, 2021.

[38] C. Gauss. *Disquisitiones Arithmeticae*. New York:Springer Verlag, 1896.

[39] Joseph Louis De Lagrange. Recherches d'arithmétique. *Nouveaux Mémoires de l'Académie de Berlin*, 1773.

[40] Jeremy Gray. *Lagrange's Theory of Quadratic Forms*, pages 23–36. Springer International Publishing, Cham, 2018.

[41] C. Hermite. Extraits de lettres de M. Ch. Hermite à M. Jacobi sur différents objects de la théorie des nombres. *Journal für die reine und angewandte Mathematik*, 40:261–277, 1850.

[42] Jacques Martinet. Hermite versus Minkowski. *arXiv pre-print*, 2014.

[43] Henry Cohn and Abhinav Kumar. The densest lattice in twenty-four dimensions. *Electronic Research Announcements of the American Mathematical Society*, 10(7):58–67, 2004.

[44] A. Korkine and G. Zolotareff. Sur les formes quadratiques positives. *Mathematische Annalen*, 11:242–292, 1877.

[45] Hermann Minkowski. Diskontinuitätsbereich für arithmetische Äquivalenz. *Journal für die reine und angewandte Mathematik*, 129:220–274, 1905.

[46] P. Niggli. *Krystallographische und strukturtheoretische Grundbegriffe*, volume 1. Akademische verlagsgesellschaft mbh, 1928.

[47] Lawrence C Andrews and Herbert J Bernstein. The geometry of Niggli reduction: BGAOL–embedding niggli reduction and analysis of boundaries. *J Applied Cryst.*, 47 (1):346–359, 2014.

[48] MJ Buerger. Note on reduced cells. *Zeitschrift für Kristallographie-Crystalline Materials*, 113(1-6):52–56, 1960.

[49] B. Gruber. The relationship between reduced cells in a general Bravais lattice. *Acta Crystallographica Section A*, 29(4):433–440, 1973.

[50] B Gruber. Reduced cells based on extremal principles. *Acta Cryst A*, 45(1):123–131, 1989.

[51] Phong Q Nguyen and Brigitte Vallée. *The LLL algorithm*. Springer, 2010.

[52] I Křivỳ and B Gruber. A unified algorithm for determining the reduced (Niggli) cell. *Acta Cryst. A*, 32(2):297–298, 1976.

[53] Leonid V Azaroff and Martin J. Buerger. *Powder method in X-ray crystalloraphy*. McGraw-Hill Book Company, New York, 1958.

[54] Ralf W Grosse-Kunstleve, Nicholas K Sauter, and Paul D Adams. Numerically stable algorithms for the computation of reduced unit cells. *Acta Crystallographica Section A: Foundations of Crystallography*, 60(1):1–6, 2004.

[55] Hong-Long Shi and Zi-An Li. Niggli reduction and Bravais lattice determination. *Journal of Applied Crystallography*, 55(1):204–210, 2022.

[56] Arjen K Lenstra, Hendrik Willem Lenstra, and László Lovász. Factoring polynomials with rational coefficients. *Mathematische annalen*, 261:515–534, 1982.

[57] LC Andrews, HJ Bernstein, and GA Pelletier. A perturbation stable cell comparison technique. *Acta Crystallographica Section A*, 36(2):248–252, 1980.

[58] Mois Ilia Aroyo. *International Tables for Crystallography*, volume A. Wiley Online Library, 2016.

[59] L Michel. Fundamental concepts for the study of crystal symmetry. *Physics Reports*, 341(1-6):265–336, 2001.

[60] L. Bieberbach. Über die bewegungsgruppen der Euklidischen räume, I. *Math. Ann*, 70:297–336, 1911.

[61] Peter Buser. A geometric proof of Bieberbach's theorems on crystallographic groups. *Enseignement Mathématique (2)*, 31:137–145, 1985.

[62] James Kuzmanovich and Andrey Pavlichenkov. Finite groups of matrices whose entries are integers. *The American Mathematical Monthly*, 109(2):173–186, 2002.

[63] A. Bravais. Mémoire sur les systèmes formés par les points distribués régulièrement sur un plan ou dans l'espace. *J. École Polytech.*, 19:1–128, 1850.

[64] H Burzlaff and H Zimmermann. Point-group symbols. *International Tables of Crystallography A*, 2006.

[65] Harold Brown, Rolf Bülow, Joachim Neubüser, Hans Wondratschek, and Hans Zassenhaus. *Crystallographic groups of four-dimensional space*. Wiley-Interscience [John Wiley & Sons], New York-Chichester-Brisbane, 1978. ISBN 0-471-03095-3.

[66] Wilhelm Plesken and Wilhelm Hanrath. The lattices of six-dimensional Euclidean space. *Mathematics of computation*, 43(168):573–587, 1984.

[67] P Niggli. *Handbuch der Experimentalphysike 7 Part 1*. Akademische Verlagsgesellschaft Leipzig, 1928.

[68] AD Mighell and JR Rodgers. Lattice symmetry determination. *Acta Crystallographica Section A: Crystal Physics, Diffraction, Theoretical and General Crystallography*, 36 (2):321–326, 1980.

[69] PM De Wolff and B Gruber. Niggli lattice characters: definition and graphical representation. *Acta Crystallographica Section A: Foundations of Crystallography*, 47(1): 29–36, 1991.

[70] Erik Nilsson, Julie Rowlett, and Felix Rydell. The isospectral problem for flat tori from three perspectives. *Bulletin of the American Mathematical Society*, 60(1):39–83, 2023.

[71] GL Watson. Determination of a binary quadratic form by its values at integer points. *Mathematika*, 26(1):72–75, 1979.

[72] John Horton Conway and Neil JA Sloane. Four-dimensional lattices with the same theta series. *International Mathematics Research Notices*, 1992(4):93–96, 1992.

[73] Alexander Schiemann. Ternary positive definite quadratic forms are determined by their theta series. *Mathematische Annalen*, 308:507–517, 1997.

[74] Herbert Bernstein and Lawrence Andrews. DC7 , a very efficient lattice comparison metric. *Acta Crystallographica Section A Foundations and Advances*, 77:C809–C809, 08 2021.

[75] Herbert J Bernstein, Lawrence C Andrews, and Mario Xerri. An invertible seven-dimensional Dirichlet cell characterization of lattices. *Acta Crystallographica Section A: Foundations and Advances*, 79(4), 2023.

[76] Lawrence C Andrews and Herbert J Bernstein. Lattices and reduced cells as points in 6-space and selection of Bravais lattice type by projections. *Acta Cryst. A*, 44(6): 1009–1018, 1988.

[77] Lawrence C Andrews, Herbert J Bernstein, and Nicholas K Sauter. Selling reduction versus Niggli reduction for crystallographic lattices. *Acta Cryst. A*, 75(1):115–120, 2019.

[78] Michele Catti. Calculation of elastic constants by the method of crystal static deformation. *Acta Crystallographica Section A: Foundations of Crystallography*, 41(5): 494–500, 1985.

[79] Gemma de la Flor, Danel Orobengoa, Emre Tasci, Juan Manuel Perez-Mato, and Mois I. Aroyo. Comparison of structures applying the tools available at the Bilbao Crystallographic Server. *Journal of Applied Crystallography*, 49(2):653–664, 2016.

[80] Matthew J Bright, Andrew I Cooper, and Vitaliy A Kurlin. Continuous chiral distances for two-dimensional lattices. *Chirality*, 2023. doi: 10.1002/chir.23598.

[81] J Lima-de Faria, E Hellner, F Liebau, E Makovicky, and E Parthé. Nomenclature of inorganic structure types. *Acta Cryst A*, 46(1):1–11, 1990.

[82] R Oishi-Tomiyasu. Rapid bravais-lattice determination algorithm for lattice parameters containing large observation errors. *Acta Crystallographica Section A: Foundations of Crystallography*, 68(5):525–535, 2012.

[83] John Horton Conway and Neil JA Sloane. Low-dimensional lattices. VI. Voronoi reduction of three-dimensional lattices. *Proceedings of the Royal Society A*, 436(1896): 55–68, 1992.

[84] Vitaliy A Kurlin. Mathematics of 2-dimensional lattices. *Foundations of Computational Mathematics*, 2022. doi: 10.1007/s10208-022-09601-8.

[85] B.N.Delone, N. Padurov, and A. Aleksandrov. *Mathematical Foundations of Structural Analysis of Crystals*. State Technical-Theoretical Press, USSR, 1934.

[86] Vitaliy Kurlin. A complete isometry classification of 3-dimensional lattices. *arxiv:2201.10543*, 2022.

[87] Marco Mosca and Vitaliy Kurlin. Voronoi-based similarity distances between arbitrary crystal lattices. *Crystal Research and Technology*, 55(5):1900197, 2020.

[88] Jakob Ropers, Marco M Mosca, Olga D Anosova, Vitaliy A Kurlin, and Andrew I Cooper. Fast predictions of lattice energies by continuous isometry invariants of crystal structures. In *International Conference on Data Analytics and Management in Data Intensive Domains*, pages 178–192, 2022.

[89] Evgraf S Fedorov. Elements of the study of figures. *Zap. Mineralog. Obsc.(2)*, 21(1): 279, 1885.

[90] Marjorie Senechal and Jean E. Taylor. Parallelohedra, old and new. *Acta Crystallographica Section A*, 79(3):273–279, 2023.

[91] Eduard Selling. Über die binären und ternären quadratischen formen. *Journal für die reine und angewandte Mathematik*, 77:143–229, 1874.

[92] LA Seeber. Versuch einer erklärung des inneren baus der festen körper [attempt to an explanation of the inner constitution of solid bodies]. *Gilberts Annalen der Physik*, 76 (4):349–372, 1824.

[93] Léon Charve. De la réduction des formes quadratiques quaternaires positives. *Annales scientifiques de l'Ecole nórmale supérieure*, 11:119–134, 1882.

[94] BN Delaunay, RV Galiulin, NP Dolbilin, VA Zalgaller, and MI Stogrin. On three successive minima of a three-dimensional lattice. In *Dokl. Akad. Nauk SSSR*, volume 209, pages 309–313, 1973.

[95] E.D. Stevens and P. Coppens. Experimental electron density distributions of hydrogen bonds. high resolution study of α-oxalic acid dihydrate at 1 100 k. *Acta. Cryst. B*, 36: 1864–1876, 1980.

[96] L N Becka and W J Cruickshank. The crystal structure of hexamethylenetetramine I. X-ray studies at 298, 100 and 34 k. *Proceedings of the Royal Society A*, 273:435–454, 1963.

[97] Howard D. Flack. Chiral and achiral crystal structures. *Helvetica Chimica Acta*, 86 (4):905–921, 2003.

[98] G von Blaschke, HP Kraft, K Fickentscher, and Ft Koehler. Chromatographic separation of racemic thalidomide and teratogenic activity of its enantiomers (author's transl). *Arzneimittel-forschung*, 29(10):1640–1642, 1979.

[99] Etsuko Tokunaga, Takeshi Yamamoto, Emi Ito, and Norio Shibata. Understanding the thalidomide chirality in biological processes by the self-disproportionation of enantiomers. *Scientific reports*, 8(1):17131, 2018.

[100] W. (Lord Kelvin) Thompson. *The Molecular Tactics of a Crystal*. Clarendon Press, 1894.

[101] Michel Petitjean. Chirality in affine spaces and in spacetime. *arXiv 2203.04066*, 2022.

[102] Gerhard H Fecher, Jürgen Kübler, and Claudia Felser. Chirality in the solid state: Chiral crystal structures in chiral and achiral space groups. *Materials*, 15(17):5812, 2022.

[103] Bowen Zhang, Xiaotong Sun, and Peng Du. Designing single chirality via crystallization method: spontaneous chiral symmetry breaking and deracemization. *Materials Today Chemistry*, 32:101636, 2023.

[104] Crum Brown. On the relation of optical activity to the character of the radicals united to the asymmetric carbon atom. *Proceedings of the Royal Society of Edinburgh*, 17: 181–185, 1891.

[105] Wei Ma, Liguang Xu, André F. de Moura, Xiaoling Wu, Hua Kuang, Chuanlai Xu, and Nicholas A. Kotov. Chiral inorganic nanostructures. *Chemical Reviews*, 117(12): 8041–8093, 2017.

[106] P. Kumar, T. Vo, M. Cha, A. Visheratina, J-Y. Kim, W. Xu, J. Schwartz, A. Simon, D. Katz, V.P. Nicu, E. Marino, W.J. Choi, M. Veksler, S. Chen, C. Murray, R. Hovden, S. Glotzer, and N.A. Kotov. Photonically active bowtie nanoasemblies with chirality continuum. *Nature*, 615(7952):418–424, 2023.

[107] Andrzej B Buda, Thomas PE Auf der Heyde, and Kurt Mislow. Geometric chirality products. *Journal of mathematical chemistry*, 6(1):243–253, 1991.

[108] Mikhail A. Osipov, Barry T. Pickup, and David A. Dunmur. A new twist to molecular chirality: intrinsic chirality indices. *Molecular Physics*, 84:1193–1206, 1995.

[109] Greg Millar, Noham Weinberg, and Kurt Mislow. On the Osipova-Pickup-Dunmur chirality index: why pseudoscalar functions are generally unsuitable to quantify chirality. *Molecular Physics*, 103(20):2769–2772, 2005.

[110] H. Zabrodsky, S. Peleg, and D. Avnir. Continuous symmetry measures. *J. Am. Chem. Soc*, 114:7843–7851, 1992.

[111] H. Zabrodsky, Peleg S., and D. Avnir. Continuous symmetry measures 2: Symmetry groups and the tetrahedron. *J. Am. Chem. Soc*, 115:8278–8289, 1992.

[112] H. Zabrodsky and D. Avnir. Continuous symmetry measures 4: Chirality. *J. Am. Chem. Soc*, 117:462–473, 1995.

[113] Mark Pinsky and David Avnir. Continuous symmetry measures. 5. the classical polyhedra. *Inorganic chemistry*, 37(21):5575–5582, 1998.

[114] D. Pinsky, K. Lipkowitz, and D. Avnir. Continuous symmetry measures 6: The relations between polyhedral point group/sub group symmetries. *J. Math. Chem.*, 30(1): 109–120, 2001.

[115] I. Tuvi-Arad, G. Alon, and D. Avnir. Cosym. `http://csm.ouproj.org.il`. Accessed: 2022-05-26.

[116] K. Gade. A non-singular horizontal position representation. *Journal of Navigation*, 63:395–417, 2010.

[117] James Inman. *Navigation and Nautical Astronomy for the Use of British Seamen.* C and J Rivington, 1835.

[118] Pere Miró, Martha Audiffred, and Thomas Heine. An atlas of two-dimensional materials. *Chem. Soc. Rev.*, 43:6537–6554, 2014.

[119] H. Tian, J. Rice, R. Fei, V. Tran, X. Yan, L. Yang, and H. Wang. Low-symmetry two-dimensional materials for electronic and photonic applications. *Nano Today*, 11 (6):763–777, 2016.

[120] Michael Ashton, Joshua Paul, Susan B. Sinnott, and Richard G. Hennig. Topology-scaling identification of layered solids and stable exfoliated 2d materials. *Phys. Rev. Lett.*, 118:106101, Mar 2017. doi: 10.1103/PhysRevLett.118.106101.

[121] Tom Barnowsky, Arkady V. Krasheninnikov, and Rico Friedrich. A new group of 2d non-van der Waals materials with ultra low exfoliation energies. *Advanced Electronic Materials*, 2022.

[122] Robin B Jacobs-Gedrim, Michael T Murphy, Fan Yang, Nikhil Jain, Mariyappan Shanmugam, Eui Sang Song, Yudhister Kandel, Parham Hesamaddin, Hong Yu Yu, MP Anantram, et al. Reversible phase-change behavior in two-dimensional antimony telluride (Sb2Te3) nanosheets. *Applied Physics Letters*, 112(13):133101, 2018.

[123] Wen-Jin Yin, Hua-Jian Tan, Pei-Jia Ding, Bo Wen, Xi-Bo Li, Gilberto Teobaldi, and Li-Min Liu. Recent advances in low-dimensional janus materials: theoretical and simulation perspectives. *Materials Advances*, 2(23):7543–7558, 2021.

[124] Lei Zhang, Yuantong Gu, and Aijun Du. Two-dimensional janus antimony selenium telluride with large rashba spin splitting and high electron mobility. *ACS omega*, 6 (47):31919–31925, 2021.

[125] Stefan Riedel, Jonas Sundqvist, and Thomas Gumprecht. Low temperature deposition of silicon nitride using Si3Cl8. *Thin Solid Films*, 577:114–118, 2015.

[126] Francesco Ricci, Wei Chen, Umut Aydemir, G Jeffrey Snyder, Gian-Marco Rignanese, Anubhav Jain, and Geoffroy Hautier. An ab initio electronic transport database for inorganic materials. *Scientific Data*, 4(1):1–13, 2017.

[127] V. Kulish and Y. Huang. Single-layer metal halides (MX2, X = Cl, Br, I): stability and tunable magnetism from first principles and monte carlo simulations. *J. Mater. Chem A*, 5:8734–8741, 2017.

[128] A. Eftekhari. Tungsten dichalcogenides (WS_2, WSe_2, and WTe_2): materials chemistry and applications. *J. Mater. Chem A*, 5:18299–18325, 2017.

[129] H. Wu, Y. Wang, Y. Xu, P.K. Sivakumar, C. Pasco, U. Filippozzi, S.S.P. Parkin, Y-J. Zeng, McQueen T., and Ali M.N. The field-free Josephson diode in a van der waals heterostructure. *Nature*, 604:653–656, 2022.